CZECH TECHNICAL
UNIVERSITY IN PRAGUE

FACULTY OF CIVIL
ENGINEERING

# MASTER'S THESIS

2020

MARTIN
JONÁŠ

**ČESKÉ VYSOKÉ UČENÍ TECHNICKÉ V PRAZE**
**Fakulta stavební**
Thákurova 7, 166 29 Praha 6

# ZADÁNÍ DIPLOMOVÉ PRÁCE

## I. OSOBNÍ A STUDIJNÍ ÚDAJE

Příjmení: Jonáš Jméno: Martin Osobní číslo: 459018

Zadávající katedra: 11210 Experimetnální centrum

Studijní program: Stavební inženýrství

Studijní obor: Konstrukce a dopravní stavby

## II. ÚDAJE K DIPLOMOVÉ PRÁCI

Název diplomové práce: Návrh a instalace stacionární měřicí linky na mostě ev. č. 27-117

Název diplomové práce anglicky: Design and installation of stationary measurement system on bridge No. 27-117

Pokyny pro vypracování:
V rámci teoretické části práce na základě projektové dokumentace mostu navrhnout rozmístění snímačů teploty a dalších fyzikálních veličin (vlhkost, přetvoření) na konstrukci nově budovaného mostu 27-117 v Alžbětíně za účelem ověření normových předpokladů průběhu teploty v mostní konstrukci, definovaných v ČSN EN 1991-1-5. V rámci experimentální části provést osazení těchto snímačů do budované konstrukce a provést experimentální ověření termofyzikálních parametrů reálného materiálu v konstrukci na vyrobených zkušebních tělesech. V rámci časového harmonogramu prací na mostě není možné v termínu odevzdání diplomové práce sebrat a vyhodnotit teplotní data, v závěru práce ale připravit návrh metodiky jejich zpracování.

Seznam doporučené literatury:
Normy ČSN EN 1991-2: Zatížení mostů dopravou, ČSN EN 1991-1-5: Zatížení konstrukcí - zatížení teplotou

Jméno vedoucího diplomové práce: Ing. Jan Zatloukal, Ph.D.

Datum zadání diplomové práce: 22.9.2020 Termín odevzdání diplomové práce: 4.1.2021
*Údaj uveďte v souladu s datem v časovém plánu příslušného ak. roku*

Podpis vedoucího práce Podpis vedoucího katedry

## III. PŘEVZETÍ ZADÁNÍ

*Beru na vědomí, že jsem povinen vypracovat diplomovou práci samostatně, bez cizí pomoci, s výjimkou poskytnutých konzultací. Seznam použité literatury, jiných pramenů a jmen konzultantů je nutné uvést v diplomové práci a při citování postupovat v souladu s metodickou příručkou ČVUT „Jak psát vysokoškolské závěrečné práce" a metodickým pokynem ČVUT „O dodržování etických principů při přípravě vysokoškolských závěrečných prací".*

23 -09- 2020

Datum převzetí zadání Podpis studenta(ky)

CZECH TECHNICAL UNIVERSITY
IN PRAGUE

Faculty of Civil Engineering

Experimental centre

# MASTER'S THESIS

## Design and installation of stationary measurement system on the bridge No. 27-117

Bc. Martin Jonáš

2020

Thesis advisor: Ing. Jan Zatloukal, Ph.D.

# Declaration

I hereby declare that thesis was written separately only under academic guidance of thesis advisor Ing. Jan Zatloukal, Ph.D.

I hereby declare that all used materials have been fully cited in list of used literature.

In Prague, 31.12.2020

……

Bc. Martin Jonáš

# Acknowledgements

I would like to acknowledge Ing. Jan Zatloukal, Ph.D. for his versatile support, extensive practical assistance and given knowledge during preparation of this thesis.

I would like to thank Bc. Jakub Veselý for his willing help with heat transfer models.

I would also like to thank doc. Ing. Eva Vejmelková, Ph.D. And Ing. Vojtěch Pommer for their help with measurement of thermal parameters of concrete.

# Design and installation of stationary measurement system on the bridge No. 27-117

# Návrh a instalace stacionární měřicí linky na mostě ev. č. 27-117

31.12. 2020

# Abstract

Newly constructed bridge No. 27-117 is instrumented by stationary measurement system. This system is designed to allow monitoring of temperature in five profiles and provides accessory measurement of strain and humidity. Subject of the thesis was design, preparing and installation of system on construction site. Purpose of temperature monitoring in this integral bridge with filler beam deck is verification of standard assumptions and extension of available information about thermal actions on bridges with accent to abutments of integral bridges. For purpose of future measurement verification, heat transfer models in finite elements software were created. These models created background for expectations from measurement, which will be launched in the beginning of year 2021. First evaluation of measurement will be processed after one-year period of operation.



# Keywords

thermal actions, integral bridge, filler beam deck, thermal monitoring, thermometer, heat transfer models, finite element method, numerical analysis

# Abstrakt

Nově vybudovaný most ev. č. 27-117 je vybaven stacionární měřicí linkou. Tato linka je navržena za účelem monitorování teploty v pěti vybraných profilech a poskytování přidružených měření přetvoření a vlhkosti. Předmětem práce byl návrh, příprava a instalace měřicí linky na stavbě mostu. Účelem teplotního monitoringu v tomto mostě s nosnou konstrukcí ze zabetonovaných nosníků je ověření normových předpokladů a rozšíření dostupných podkladů k tématu teplotního zatížení mostů s důrazem na opěry integrovaných mostů. Za účelem verifikace budoucího měření byly vytvořeny modely vedení tepla v programu využívajícího metodu konečných prvků. Tyto modely poskytly podklady pro realistické očekávání od měření, které bude spuštěno začátkem roku 2021. První vyhodnocení měření bude zpracováno po jednom roce provozu měřicí linky.

# Klíčová slova

zatížení teplotou, integrovaný most, zabetonované nosníky, teplotní monitoring, teploměr, modely vedení tepla, metoda konečných prvků, numerická analýza

# Contents


1 Introduction ... 1
2 Thermal actions on bridges ... 3
2.1 Thermal actions according to EN 1991-1-5 ... 3
2.1.1 Temperature changes in bridges ... 4
2.1.2 National annex ČSN EN 1991-1-5 ... 9
3 Bridge No. 27-117 ... 11
3.1 Location ... 11
3.1.1 Climate ... 12
3.2 Structure ... 13
4 Used sensors ... 16
4.1 Thermometers ... 16
4.1.1 Resistance thermometer PT 1000 ... 16
4.2 Strain gauges ... 17
4.2.1 Resistance strain gauge HBM LY11-10/120 ... 17
4.3 Moisture meters ... 19
4.3.1 Capacitive Soil Moisture Sensor ... 19
4.3.2 Resistive Soil Moisture Sensor ... 21
5 Stationary measurement system ... 22
5.1 ŘSD requirements ... 22
5.2 Expectations ... 25
5.3 Description of system parts ... 27
5.3.1 Sensor deployment ... 27
5.3.2 Wiring ... 34
5.3.3 Switchboard ... 38
5.4 Preparation ... 39
5.4.1 Thermometer HPC casings ... 39
5.4.2 Concrete casing beams ... 40
5.4.3 Strain gauges preparation ... 44
5.4.4 Further preparation of sensors ... 44
5.5 Installation ... 46
5.6 Data evaluation ... 50
5.6.1 Uniform temperature ... 50
5.6.2 Non-linear vertical temperature difference ... 50

5.6.3 Linear vertical temperature difference ..... 51
5.6.4 Strain ..... 52
5.6.5 Humidity ..... 52
6 Thermal FEM models ..... 53
6.1 Concrete parameters measurements ..... 53
6.2 Abutment shaft model ..... 54
6.2.1 Model description ..... 54
6.2.2 Minimal temperature ..... 55
6.2.3 Maximal temperature ..... 58
6.2.4 Maximal temperature fluctuation ..... 60
6.3 Bridge deck model – under traffic lane ..... 62
6.3.1 Model description ..... 62
6.3.2 Minimal temperature ..... 63
6.3.3 Maximal temperature ..... 66
6.3.4 Maximal temperature fluctuation ..... 69
6.4 Bridge deck model – under pavement ..... 72
6.4.1 Model description ..... 72
6.4.2 Minimal temperature ..... 74
6.4.3 Maximal temperature ..... 77
6.4.4 Maximal temperature fluctuation ..... 80
6.5 Comparison of thermal effects on structure model ..... 83
6.5.1 Model ..... 83
6.5.2 Heating ..... 85
6.5.3 Cooling ..... 86
7 Conclusion ..... 88
Literature ..... 89
List of figures ..... 92
List of charts ..... 97

# List of used symbols

| | |
|---|---|
| $A$ | regression coefficient |
| $A_c$ | area of capacitor plates |
| $B$ | regression coefficient |
| $C$ | regression coefficient |
| $c$ | specific heat capacity |
| $C_c$ | capacitor capacity |
| $d$ | distance between capacitor plates |
| $\Delta T_E$ | non-linear temperature difference component |
| $\Delta T_{M,cool}$ | equivalent linear temperature difference component |
| $\Delta T_{M,heat}$ | equivalent linear temperature difference component |
| $\Delta T_{My}$ | linearly varying temperature difference component |
| $\Delta T_{Mz}$ | linearly varying temperature difference component |
| $\Delta T_N$ | overall range of the uniform bridge temperature component |
| $\Delta T_{N,con}$ | contraction range of the uniform temperature component |
| $\Delta T_{N,exp}$ | expansion range of the uniform temperature component |
| $\Delta T_u$ | uniform temperature component |
| $\gamma$ | specific weight |
| $E$ | modulus of elasticity |
| $\varepsilon$ | material emissivity |
| $\varepsilon_0$ | vacuum permittivity |
| $\varepsilon_m$ | permittivity of medium |
| $\varepsilon_0$ | vacuum permittivity |
| $\varepsilon^*_r$ | complex relative permittivity |

| | |
|---|---|
| $\varepsilon'_r$ | real part of the permittivity |
| $\varepsilon''_r$ | imaginary part of the permittivity |
| $\varepsilon''_{relax}$ | molecular relaxation contribution |
| $\varepsilon_x$ | strain in direction of axis x |
| $f$ | frequency |
| $h$ | height of profile |
| $H$ | Heaviside function |
| $j$ | imaginary number $\sqrt{-1}$ |
| $k$ | gage factor |
| $k_{sur}$ | factor different with varying roadway thickness |
| $l$ | cable length |
| $\lambda$ | thermal conductivity |
| $Q(t)$ | heat flow function |
| $R_0$ | resistance at temperature 0 °C |
| $R_{add}$ | additional resistance of cable |
| $R_{core}$ | resistance of one cable core per meter |
| $R_t$ | resistance at temperature t |
| $\sigma_{dc}$ | electrical conductivity |
| $\sigma_x$ | tensile stress in direction of axis x |
| $t$ | time |
| $t(t)$ | time-temperature function |
| $T_0$ | initial temperature (during structure construction) |
| $T_{e,max}$ | maximum uniform bridge temperature component |
| $T_{e,min}$ | minimum uniform bridge temperature component |

| | |
|---|---|
| $T_{max}$ | maximum shade air temperature |
| $T_{min}$ | minimum shade air temperature |
| $\omega_M$ | simultaneity coefficient |
| $\omega_N$ | simultaneity coefficient |

# 1 Introduction

In last years, integral bridges are becoming more popular in construction praxis as structures used for short span bridging. Main difference between standard and integral bridges is absence on bearings between bridge supports and bridge deck. Deck and abutments are rigidly connected together. In some cases, concrete hinges are designed to enable rotation and therefore reduce bending moment in frame corner.

While integral bridges do not allow free temperature dilatation of bridge deck, these shifts are transferred into abutments and therefore into surrounding soil. This is the reason, why proper investigation of interaction between soil and structure is necessary.

Soil-structure interaction problem of integral bridges is widely described in literature. Very good materials are also available for thermal actions on bridge decks and effects bound with them. In case of temperature loading of abutments is the situation weaker. Overall influence of lack of more accurate approach to temperature loading of abutments might not be very significant. However, in some cases it might be suitable to consider distribution of temperature in the structure more precisely.

Due to these reasons, Ředitelství silnic a dálnic (ŘSD, Management company of roads and highways in Czech Republic) prepared project of temperature measurement on integral bridge. Contractor of this project became Experimental centre at the Faculty of Civil Engineering of the Czech Technical University in Prague (FCE CTU or FSV ČVUT in Czech).

Requirements of ŘSD were to prepare automatic measurement system which would enable long term temperature measurement and other physical values monitoring. These data should be available in real time for one year with opportunity to prolong measurement for extended period of time and should allow for evaluation of extreme thermal loading situations on the bridge. Other feature is to allow monitoring of structure degradation by the use of humidity meters and strain gauges. These are not dedicated for precise stress or humidity monitoring, but may provide alert in cases of extreme mechanical loading, abnormal humidity changes caused by insulation defects or rising content of ions by the combination of resistive and capacitive humidity measurement.

This master's thesis is dedicated to preparation of automatic measurement system, its installation on site and preparation of measured data evaluation. Software and electrotechnical parts of system are not subject of this work and are provided by the other party. Design and preparation of system parts were realized during summer of year 2020, further works on system were performed in autumn and rest of work will be finished in the end of year 2020 and in the beginning of year 2021.

Design of measurement system is based on given requirements and further work of Ing. Jan Zatloukal, PhD. and the thesis author. All the initial assumptions had to be accomplished and subsequently supplemented with our requirements to system and necessary features needed for proper operation of system. Specific emphasis was given to robustness and proper functionality of used sensors and other components built-in bridge structure.

Thesis discusses also some parts, which are not its primary task like switchboard, additional wiring resistances, etc. However, for the illustration of working principle of measurement system it is suitable to briefly describe these system parts, which are necessary for its proper functionality.

Reality of year 2020 delayed commissioning of system, at the due date of thesis, it is still not in operation. Due to this reason, heat transfer models were only prepared and not compared to measured data. These models should show, what is possible to expect during measurement in extreme climate situation. Main purpose of these models is however different. When the operation of system will be started, models will be used for verification of measurement.

These models are representing three different spots in structure and they consider three different climate situations for each model. The three climate situations are the same for all models. In result, nine models were evaluated and results were compared with standard.

For better comparison of modelled thermal situations and loading situations given by standard, simplified structure model was created, loaded by thermal effect and evaluated. Results showing internal forces are compared and discussed.

# 2 Thermal actions on bridges

There are multiple actions, which evoke force effects on structures and influence bearing capacity of system. In the first place, force actions act. Quantity of kinds of force actions have to be considered such as own weight, traffic load, snow, wind, etc. However, not only forces itself might evoke stress in structures. Most common types of non-forceful or also called indirect actions are thermal actions and displacement actions.

Non-forceful action play role only in case of statically indeterminate systems. Statically determinate systems can compensate changes caused by indirect actions by their free deformation without any stress change in all the elements, which the system consists of. However, if we load statically indeterminate system with indirect actions, free deformation of structure is prevented. Over again, in this case deformation also occurs, but now stress change is evoked. Stress changes are dependent to system or element stiffness. If the system/element is rigid, even small prevented deformation causes very high stress change. Therefore, bearing capacity might be reached in critical elements of system much sooner than it is acceptable.

Due to these matters of facts, influence of thermal actions to strain of whole structure has to be precisely examined, especially in case of stiff structures, like integral bridges. Approaches of European and national standards are described further.

## 2.1 Thermal actions according to EN 1991-1-5

Basic standards used for design of structures are European standards EN 1990 – EN 1999 also being marked as Eurocodes 1-9. Each standard represents specific category relevant for structure design. Actions on structures are described in Eurocode 1 (EN 1991) and specific types of actions are divided into standard parts. Part 1-5 is dedicated to thermal actions.

Standard generalizes all phenomenon, that influence temperature distribution in structure. According to EN 1991-1-5 daily and seasonal changes in shade air temperature, solar radiation, re-radiation, etc. will result in variations of the temperature distribution within individual elements of a structure. (1) Magnitude of thermal effects is dependent on local climate conditions, orientation of structure, its overall mass and finishes. (1) The temperature distribution within an individual structural element may be split into the following four essential constituent components (1)

- $\Delta T_u$ is uniform temperature component.
- $\Delta T_{My}$ is linearly varying temperature difference component about the *z-z* axis.
- $\Delta T_{Mz}$ is linearly varying temperature difference component about the *y-y* axis.
- $\Delta T_E$ is non-linear temperature difference component. This results in a system of self-equilibrated stresses which produce no net load effect on the element

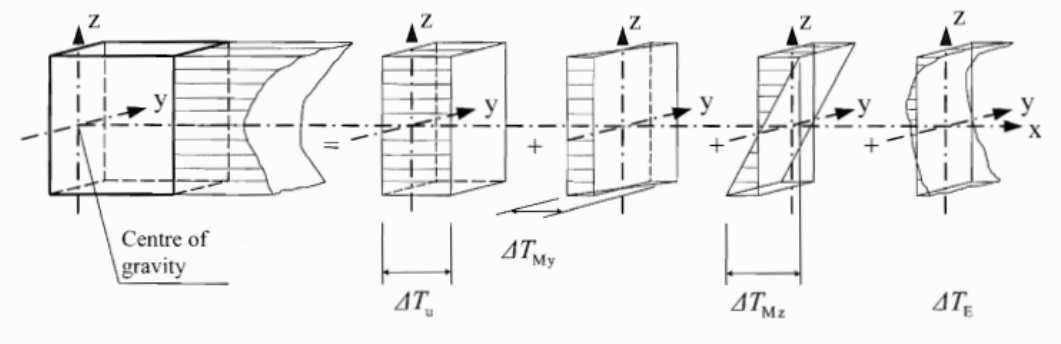


*Figure 1 Diagrammatic representation of constituent components of a temperature profile (1)*

Strains and stresses are dependent on the geometry, boundary conditions and physical properties of used material. Coefficient of linear expansion for a specific material should be used. (1)

### 2.1.1 Temperature changes in bridges

For purpose of specification of temperature changes in bridges, different approach is set according to bridge part and part type. Bridge decks have more complexly determined method of setting temperature distribution than other parts as piers, abutments, etc. According to their type, bridge decks are grouped as follows (1)

| | |
|---|---|
| Type 1 | Steel deck: steel box girder; steel truss or plate girder |
| Type 2 | Composite deck |
| Type 3 | Concrete deck: concrete slab; beam; box girder |

Representative values of thermal actions should be assessed by the uniform temperature component and the temperature difference components. (1) The uniform temperature component depends on the minimum and maximum temperature which a bridge will achieve. This results in a range of uniform temperature changes which, in an unrestrained structure would result in a change in element length.

Minimum shade air temperature $T_{min}$ and maximum shade air temperature $T_{max}$ for the site shall be derived from isotherms available in national annex, usually using temperature map of state. Subsequently the minimum and maximum uniform bridge temperature components $T_{e.min}$ and $T_{e.max}$ should be determined, national annex may define them differently.

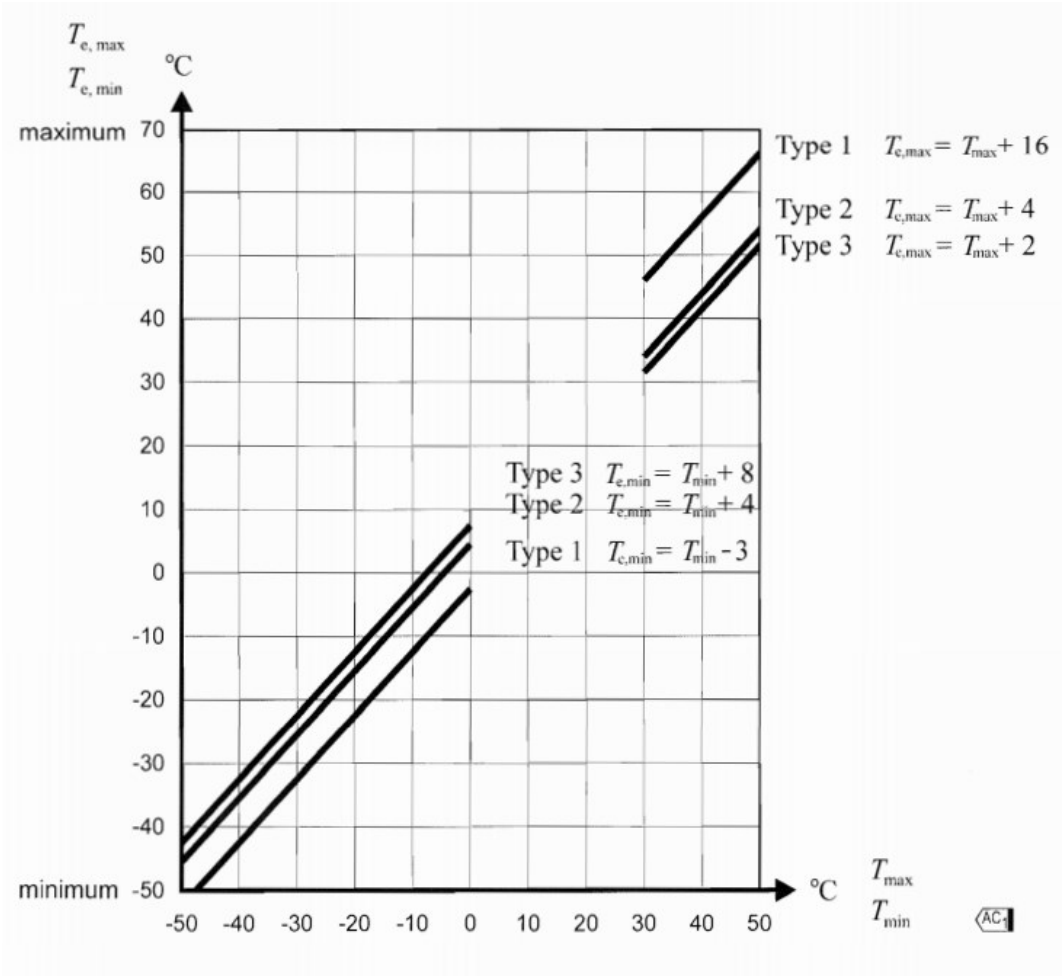


*Figure 2 Correlation between minimum/maximum shade air temperature ($T_{min}/T_{max}$) and minimum/maximum uniform bridge temperature component ($T_{e.min}/T_{e.max}$) (1)*

Next thermal characteristic necessary for thermal analysis of bridge deck is determination of range of uniform bridge temperature component. Range is dependent to minimum and maximum uniform bridge temperature components and initial temperature during construction.

The characteristic value of the maximum contraction range of the uniform bridge temperature component, $\Delta T_{N,con}$ should be taken as

$$\Delta T_{N,con} = T_0 - T_{e,min}$$

and the characteristic value of the maximum expansion range of the uniform bridge temperature component, $\Delta T_{N,exp}$ should be taken as

$$\Delta T_{N,exp} = T_{e,max} - T_0$$

The overall range of the uniform bridge temperature component is

$$\Delta T_N = T_{e,max} - T_{e,min}$$

National annex may specify maximum contraction and expansion range the uniform bridge temperature component. The recommended values are ($\Delta T_{N,con}$ + 20) °C and ($\Delta T_{N,con}$ + 20) °C. If the temperature at which the bearings and expansion joints, are set is specified, then the recommended values are ($\Delta T_{N,con}$ + 10) °C and ($\Delta T_{N,con}$ + 10) °C. (1)

Other step in determination of thermal action on bridge deck is setting the temperature difference components. These occurs in case of maximum cooling and maximum heating over a period of time. Horizontal and vertical components have to be set. Usually only vertical component plays role, but it is important not to neglect influence of horizontal component. (1)

The effect of vertical temperature differences should be considered by usage of vertical linear component or vertical components with non-linear effects. Depends on situation, which approach is more suitable for each case. It is necessary to properly consider which approach has to be chosen.

First approach, vertical linear component considers only thermal changes on the top and bottom of deck, course of temperature change on the height of deck is linear. Equivalent linear temperature difference components $\Delta T_{M,heat}$ and $\Delta T_{M,cool}$ are applied (according to situation), both are setting temperature difference between top and bottom of deck. Values of these components are specified in Table 1 and should be applied between the top and the bottom of the bridge deck. (1)

*Table 1 Recommended values of linear temperature difference component for different types of bridge decks for road, foot and railway bridges (1)*

| Type of Deck | Top warmer than bottom | Bottom warmer than top |
|---|---|---|
| | $\Delta T_{M,heat}$ (°C) | $\Delta T_{M,cool}$ (°C) |
| Type 1: Steel deck | 18 | 13 |
| Type 2: Composite deck | 15 | 18 |
| Type 1: Concrete deck | | |
| - concrete box girder | 10 | 5 |
| - concrete beam | 15 | 8 |
| - concrete slab | 15 | 8 |

The values given in the table are based on a depth of surfacing of 50 mm for road and railway bridges. For other depths of surfacing these values should be multiplied by the factor $k_{sur}$. Recommended values for the factor $k_{sur}$ are given in Table 2. (1)

*Table 2 Recommended values of $k_{sur}$ to account for different surfacing thickness (1)*

| Road, foot and railway bridges | | | | | | |
|---|---|---|---|---|---|---|
| Surface thickness | Type 1 | | Type 2 | | Type 3 | |
| | Top warmer than bottom | Bottom warmer than top | Top warmer than bottom | Bottom warmer than top | Top warmer than bottom | Bottom warmer than top |
| [mm] | $k_{sur}$ | $k_{sur}$ | $k_{sur}$ | $k_{sur}$ | $k_{sur}$ | $k_{sur}$ |
| unsurfaced | 0,7 | 0,9 | 0,9 | 1,0 | 0,8 | 1,1 |
| waterproofed | 1,6 | 0,6 | 1,1 | 0,9 | 1,5 | 1,0 |
| 50 | 1,0 | 1,0 | 1,0 | 1,0 | 1,0 | 1,0 |
| 100 | 0,7 | 1,2 | 1,0 | 1,0 | 0,7 | 1,0 |
| 150 | 0,7 | 1,2 | 1,0 | 1,0 | 0,5 | 1,0 |
| ballast (750 mm) | 0,6 | 1,4 | 0,8 | 1,2 | 0,6 | 1,0 |

Second approach considers non-linear distribution of thermal change on the height of deck. Shape of thermal changes in deck is multiple linear with given values in breaks of shape. Values are given by the standard in following figures. These values are valid for surface thickness of 40 mm for decks of Type 1 and 100 mm for decks of Type 2 and 3. Values for different surface thicknesses are specified in tables B.1-B.3 in standard. (1)

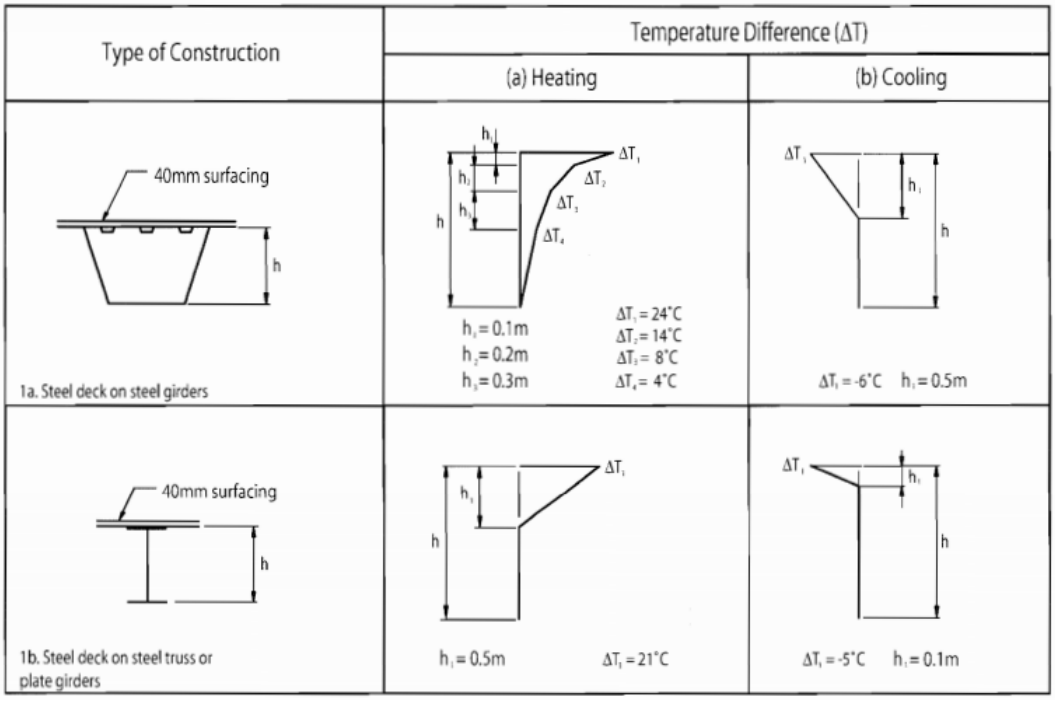


*Figure 3 Temperature differences for bridge decks Type 1: Steel Decks (1)*

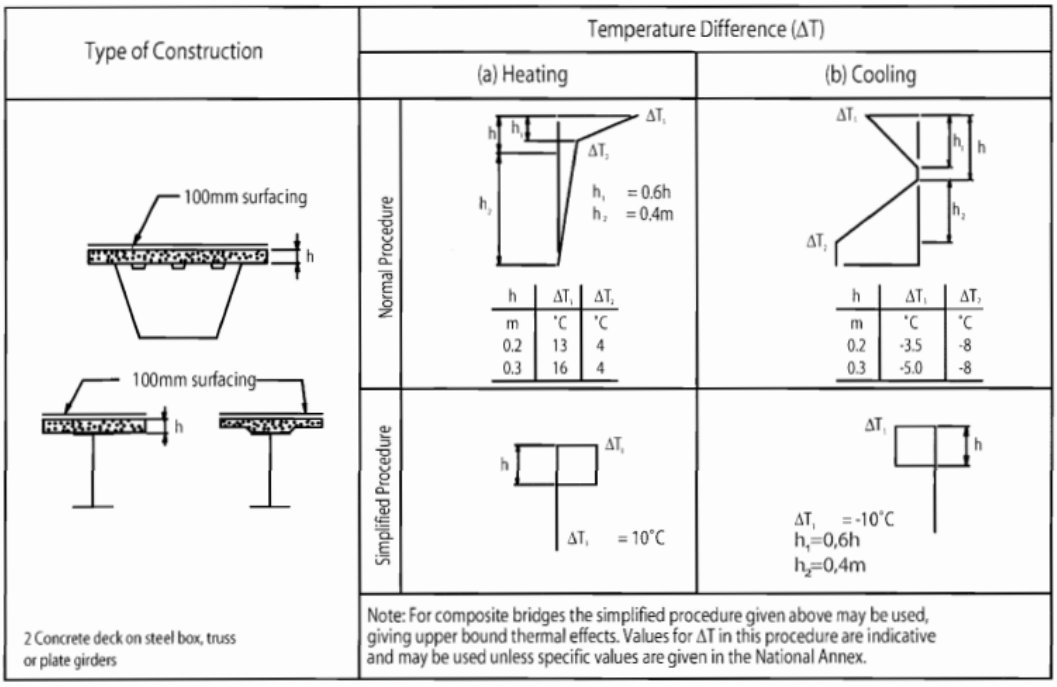


*Figure 4 Temperature differences for bridge decks -Type 2: Composite Decks (1)*

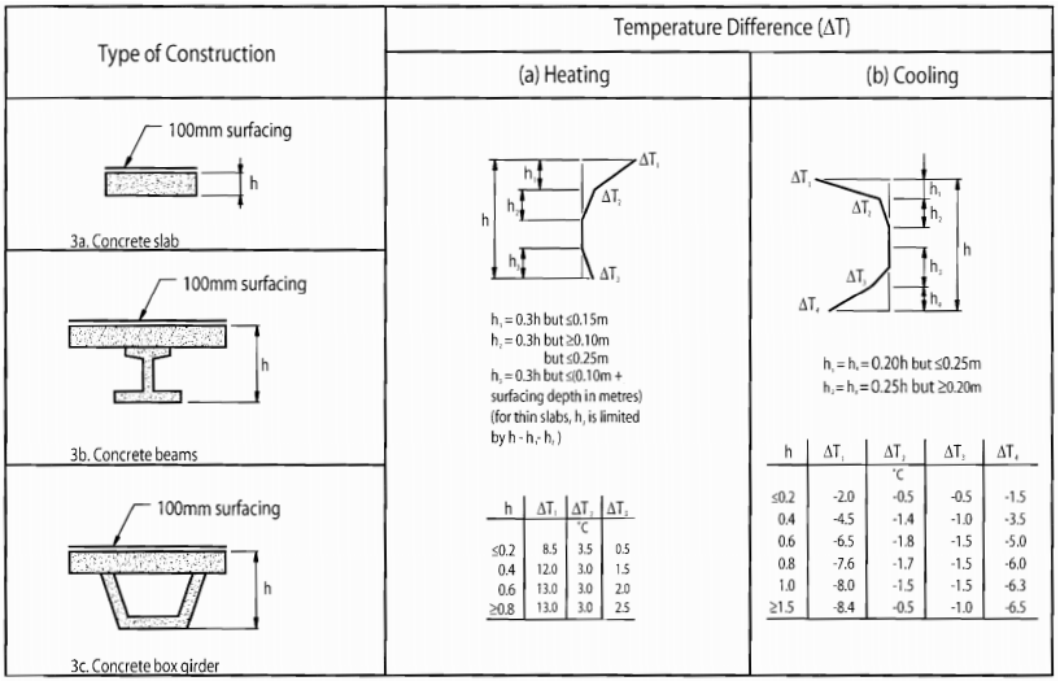


*Figure 5 Temperature differences for bridge decks -Type 3: Concrete Decks (1)*

In general, the temperature difference component need only be considered in the vertical direction. In particular cases however (for example when the orientation or configuration of the bridge results in one side being more highly exposed to sunlight than the other side), a horizontal temperature difference component should be considered. Standard does not specify exact effects of horizontal thermal changes however it offers recommendation of 5 °C temperature change between outer edges of structure with linear course, independent to deck width. (1)

In other specific cases, simultaneity of uniform and temperature difference components might need to be considered. Therefore, standard offers relations of common effect of simultaneity to cover this situation. Most adverse effect is chosen. (1)

$$\Delta T_{M,heat} + \omega_N \Delta T_{N,exp}$$

$$\Delta T_{M,cool} + \omega_N \Delta T_{N,con}$$

$$\omega_M \Delta T_{M,heat} + \Delta T_{N,exp}$$

$$\omega_M \Delta T_{M,cool} + \Delta T_{N,con}$$

$\omega_M$=0,75 recommended value of coefficient $\omega_M$ (1)
$\omega_N$=0,35 recommended value of coefficient $\omega_N$ (1)

Thermal differences between different structural elements have to be included too, while they can evoke additional adverse stresses and other load effects. Thermal difference of 15 °C is recommended between main structural parts and 10 °C for light colours or 20 °C for dark colours between deck and suspensions. (1)

Last, also thermal actions on bridge piers have to be considered in design. In the case of piers, standard is not very specific. Only values for concrete piers and walls are recommended. Linear temperature differences with value of 5 °C for concrete piers and 15 °C for walls are specified. (1)

### 2.1.2 National annex ČSN EN 1991-1-5

Czech standard ČSN EN 1991-1-5 is an extension of European standard EN 1991-1-5. Changes from the basic standard are very minor, they are listed in following paragraphs.

First change comes for paragraph 6.1.3, where relations for $T_{e,max}$ and $T_{e,min}$ are determined using other temperature constants. Relations according to Czech standard are following.

$$30\ °C \leq T_{max} \leq 50\ °C \begin{cases} Type\ 1\text{:}\ T_{e,max} = T_{max} + 16\ °C \\ Type\ 2\text{:}\ T_{e,max} = T_{max} + 4{,}5\ °C \\ Type\ 3\text{:}\ T_{e,max} = T_{max} + 1{,}5\ °C \end{cases}$$

$$-50\ °C \leq T_{min} \leq 0\ °C \begin{cases} Type\ 1\text{:}\ T_{e,min} = T_{min} - 3{,}0\ °C \\ Type\ 2\text{:}\ T_{e,min} = T_{min} + 4{,}5\ °C \\ Type\ 3\text{:}\ T_{e,min} = T_{min} + 8{,}0\ °C \end{cases}$$

Standard also sets, that in case of constructions on sites with specific climate conditions, that additional temperature data have to be considered in design. (2)

Other guidance is specified for paragraph 6.1.4, where Czech standard sets second approach of vertical temperature difference determination. Non-linear vertical thermal change is therefore used. (2)

Last but not least, most important part of Czech standard are national maps of isotherms. Maps of maximal and minimal shade temperatures are available.

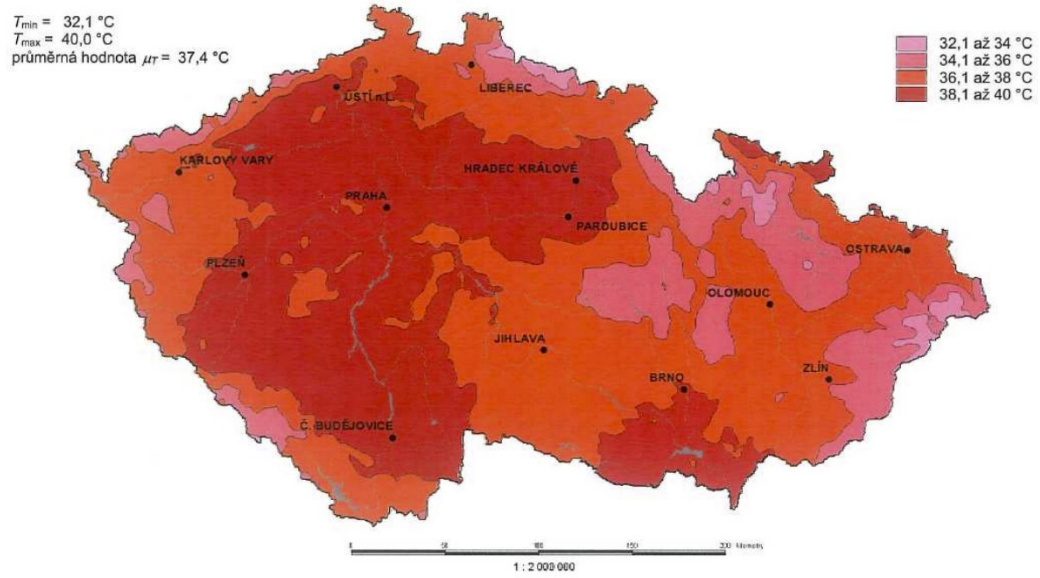


*Figure 6 Map of maximal shade temperature, which is exceeded by annual maximum with probability of 0,02 (2)*

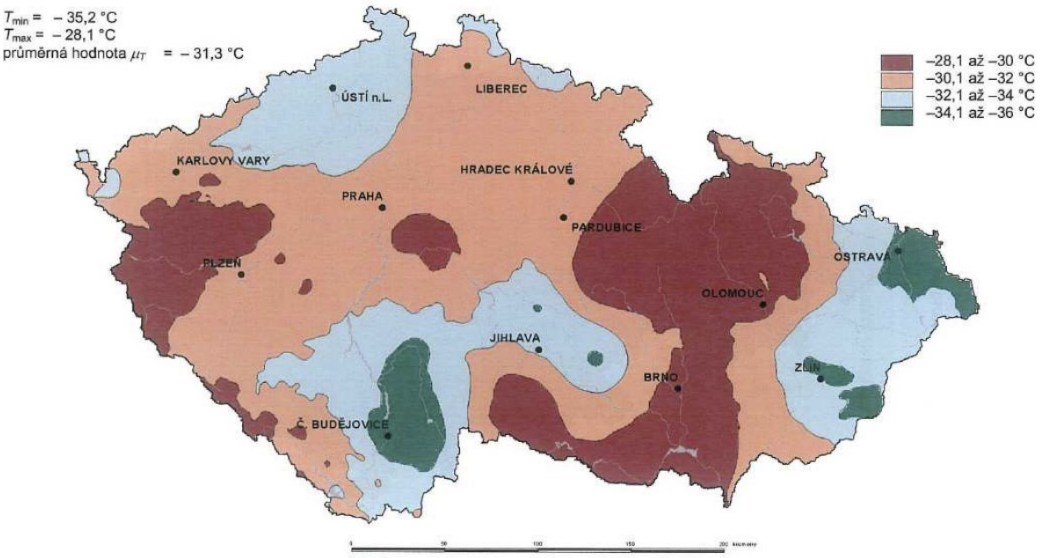


*Figure 7 Map of minimal shade air temperature, which is exceeded by annual minimum with probability of 0,02 (2)*

# 3 Bridge No. 27-117

Selection of appropriate structure was specified in requirements made by ŘSD. Bridge No. 27-117 was selected for its suitable locality, type of structure and modest construction.

Bridge is constructed at the place of previous bridge, built in 1990s. The previous bridge, despite of its low age, was in poor technical condition. Concrete parts were corroded thanks to defrosting salts, chlorides and freeze-thaw deterioration. Due its condition, decision of demolition and construction of new bridge came.

## 3.1 Location

Bridge is located in Alžbětín, city district of Železná Ruda town in Šumava mountains. Bridge carries traffic of road I/27 and concurrently E53. Road I/27 leads from Most through Žatec, Pilsen and Klatovy to state border with Germany. European road E53 leads from Pilsen (CZ) through Klatovy (CZ), Deggendorf (DE) and Landshut (DE) to Munich (DE).

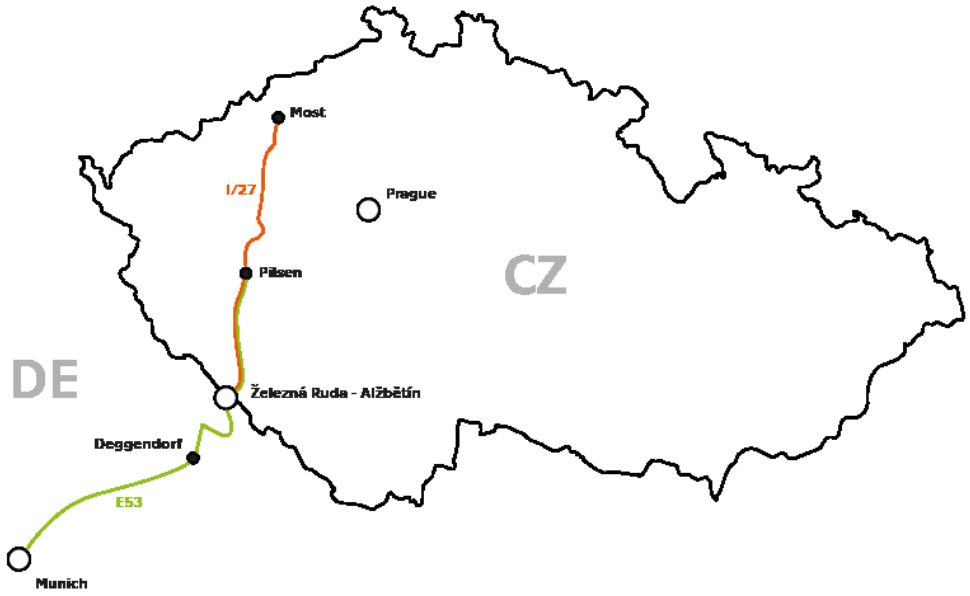


*Figure 8 Location of bridge in Czech Republic (background map from www.freevectormaps.com/czech-republic/CZ-EPS-01-0003)*

Bridge lays on the Czech side of border, however it is only about 20 meters from border line. It overcomes Svarožná stream, which mouths into the Řezná (Großer Regen) river about 60 meters down the stream from the bridge. Altitude of bridge is 710 meters AMSL.

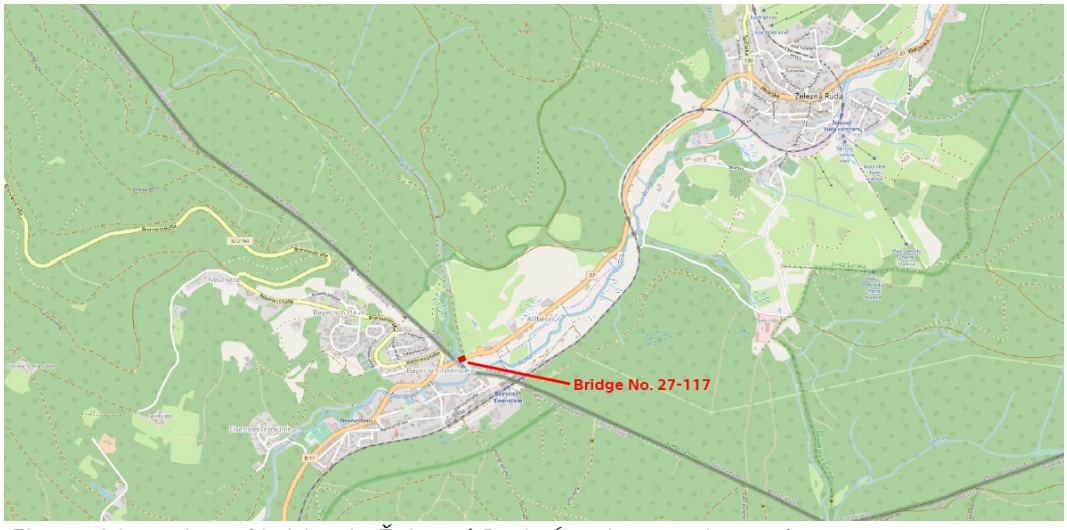


*Figure 9 Location of bridge in Železná Ruda (background map from www.openstreetmap.org)*

### 3.1.1 Climate

Železná Ruda is located in Šumava mountains (Bayerischer Wald on the German side of border), where mountain climate prevails. Long winters with low temperatures and high snow cover and short summers are for this location typical. Bridge lays in the valley of Řezná river, surrounded by numerous mountain summits of Šumava, e. g. Großer Arber (1456 m AMSL, highest peak of whole sierra, lays in Germany), Jezerní hora (1344 m AMSL) and Polom (1295 m AMSL). (3) (4)

*Figure 10 Großer Arber, 1456 m, from Bayerisch Eisenstein*

Czech Hydrometeorological Institute (CHMI) operates hydrometeorological station in Hojsova Stráž, part of Železná Ruda town, about 9,5 km from bridge site. Quantity of solid meteorological data is therefore available to use in thermal model and other expectations for this project. Mainly information about minimal and maximal air temperature and extreme sunshine time during day will be used. These data are available in their daily or monthly values from 1989 till 2019.

According to data from CHMI, annual mean temperature in Železná Ruda is 6-7 °C and annual sum of precipitation is above 1200 mm, what ranks this locality to four most rainy localities in whole republic (Krkonoše, Šumava, Moravskoslezské beskydy, Orlické hory). Lowest temperature reached in last 30 years was -22,0 °C and highest 34,8 °C. (5)

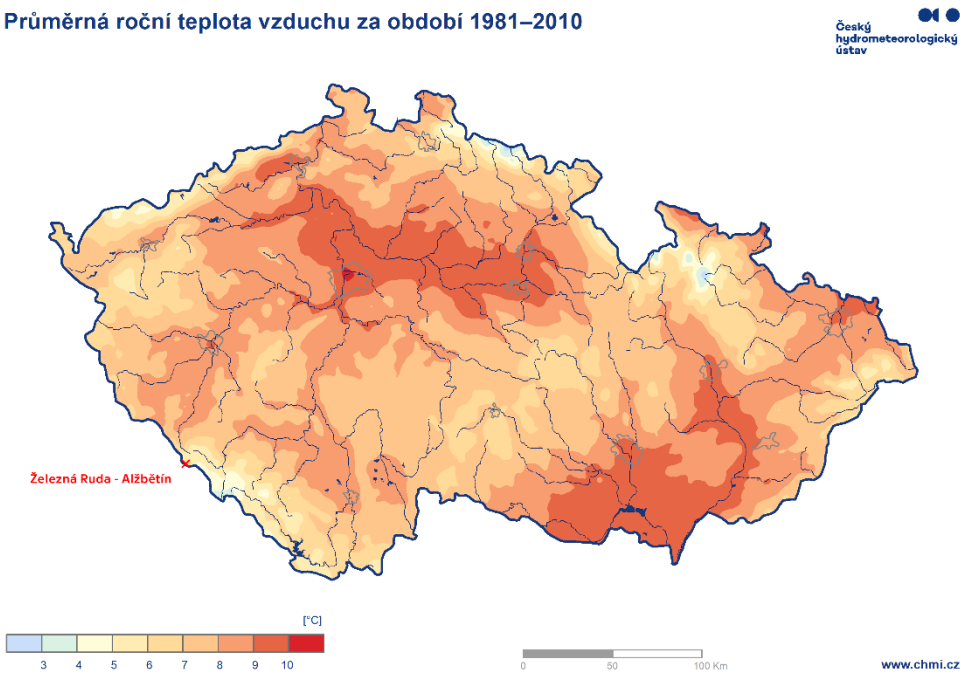


*Figure 11 Annual mean air temperature in Czech Republic*
*CHMI, Průměrná roční teplota vzduchu za období 1981-2010 [online]. [image]. [Accessed 27 October 2020]. Available from: http://portal.chmi.cz/files/portal/docs/meteo/ok/images/T8110.gif*

## 3.2 Structure

Bridge No. 27-117 is a skewed integral reinforced concrete structure with filler beam deck. Its span is 8,6 m, length is 9,64 m, bridging length is 8 m, width is 20,6 m, free height is 2,6 m and skewing angle is 85,05°. Filler beam deck is integrated with abutments, made of reinforced concrete, by usage of concrete hinges. (6)

Technology of filler beam deck provides high stiffness and carrying capacity and very good durability connected with low deck height. Main disadvantage of this type of structure is high steel consumption, however today, with lower prices of steel is this disadvantage more minor. (7)

Reinforced concrete abutments of width 600 mm are made of C 30/37 concrete and set on a monolithic lashing, which is founded on micropiles. Foundation soil consists of alluvial sandy silts and sandy gravels (disintegration of gneisses and granites of surroundings massif). (6) (8)

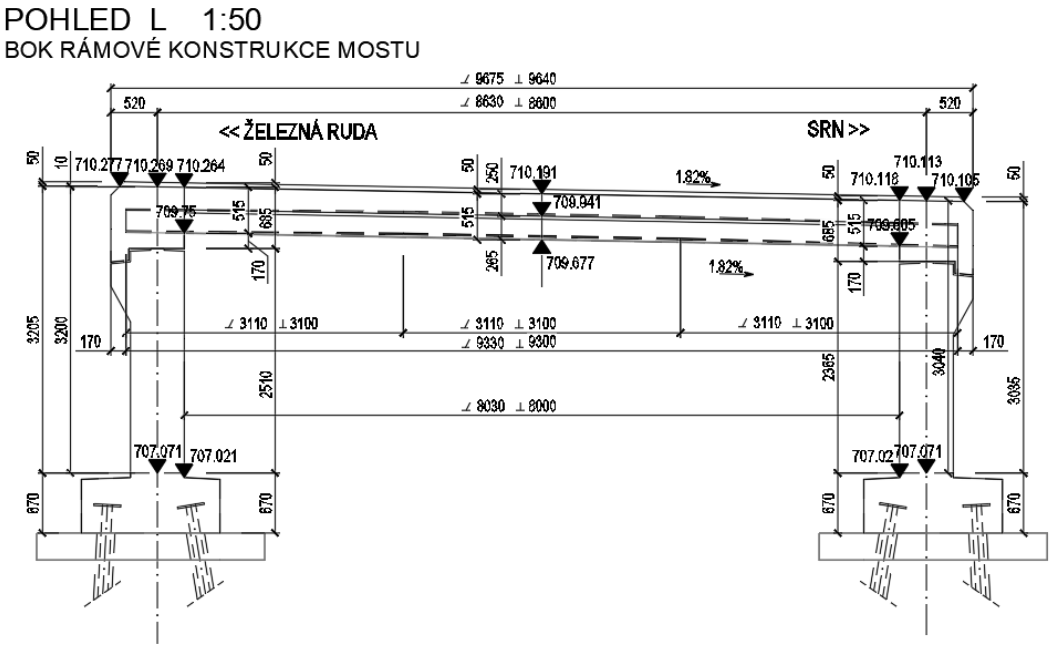


*Figure 12 Side view from north (6)*

Height of deck cross-section is variable. Therefore, more filler beams profiles are used. HEA and HEB steel beams are used. From HEA beams, HEA 300 and HEA 340 are used and from HEB beams, only HEB 240 is used. All the filler beams are with narrowed top flange, what is reached by welding of two various profiles together. In the webs of beams, holes for reinforcement bars are cut. Beams are made of S355 J2G3 steel. Filler beam deck is also reinforced by classic reinforcement steel bars (B500B). Lost formwork is used between filler beams to bear load of wet concrete. For this purpose, CETRIS plates are used. Concrete class chosen for deck is C 35/45. (6)

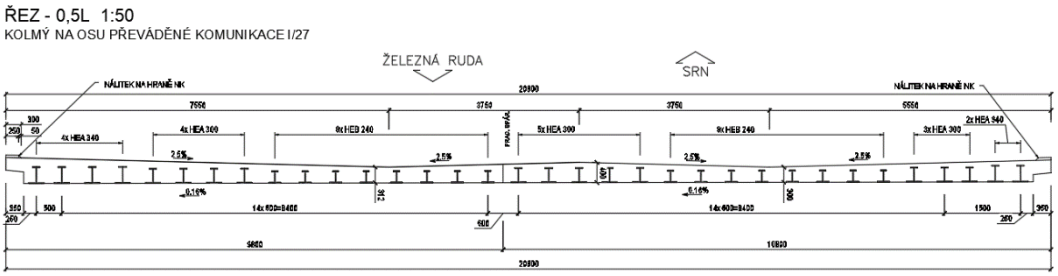


*Figure 13 Cross-section of bridge deck (6)*

Concrete hinge is reinforced by 32 mm bars and should provide joint behaviour of connection between abutments and deck. Concrete hinge should therefore be able to transfer vertical and horizontal forces from deck to abutment and vice versa. However, in case of bending moment, concrete neck of hinge should crack and little rotation should be allowed by deformation of reinforcement bars. (6)


*Figure 14 Bridge No. 27-117 under construction (picture: P. Švecová)*

Static scheme of bridge in longitudinal section may be considered as rod model (1D elements). Abutment rod is laid into elastic environment with parameters suitable for Winkler-Pasternak's model. Deck rod is connected to abutment rods by simple joints. However, this model is very simple, and not very suitable for this short and wide bridge, where spatial effects should be considered. More suitable and specific would be usage of slab model with 2D elements in programme using finite elements method (FEM). (7)

*Figure 15 Static scheme of integral bridge with concrete hinges with 1D elements*

# 4 Used sensors

## 4.1 Thermometers

Thermometers are basic sensors used in this monitoring system. Selection of specific type of thermometer was based mainly on mechanic robustness and reliability of measurement in extended period of time. Therefore PT 1000 thermometer type was selected.

### 4.1.1 Resistance thermometer PT 1000

PT 1000 thermometers work on very simple principle which is based on changes of electric resistance with varying temperature of platinum element. Platinum thermistor is placed in tip of probe and connected to wires. Electric current passes through the platinum thermistor and voltage is measured. It is determined by the amount of electric current and electric resistance of platinum thermistor and connecting wires. (9)

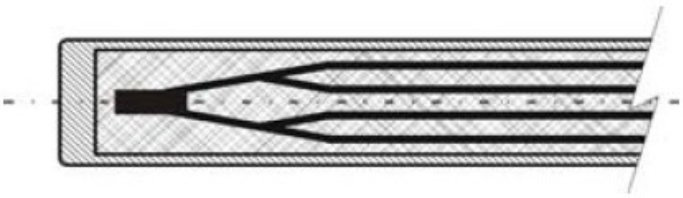

*Figure 16 Cross-section of sensor probe (10)*

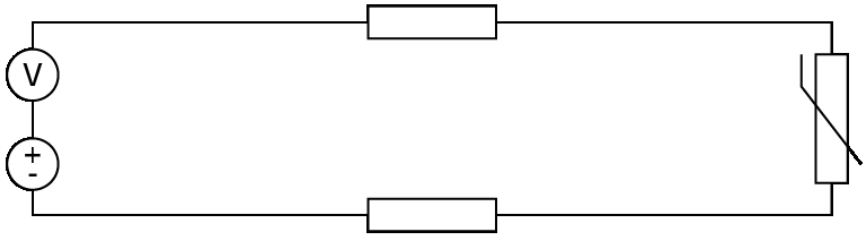


*Figure 17 2-wire configuration of PT 1000 sensor*

Platinum thermistor in PT 1000 thermometer has electric resistance of 1000 Ω at 0 °C. Increase of resistance with rising temperature is 4 Ω per 1 °C. Temperature resistance function of PT 1000 sensor is

$$R_t = R_0(1 + A * t + B * t^2 + C * (t - 100) * t^3)$$

$R_t$ is resistance at temperature t
$R_0$ is resistance at temperature 0 °C
$R_0 = 1000\ \Omega$
$A = 3.9803*10^{-3}$
$B = -5.775*10^{-7}$
$C = -4.183*10^{-12}$ for t < 0 °C
$C = 0$ for t > 0 °C

It is necessary to consider also electric resistance of wires, despite it is an order of magnitude lower than this platinum thermistor. Using standard wiring, error might be around 0.04 °C per meter of wire. This error is affecting measurement in case of 2-wire configuration. In 4-wire configuration it is easily corrected by usage of second branch of wires of same length without platinum thermistor. Second branch of wires determines resistance of wires itself and difference between resistance of branch with thermistor and without it determines resistance of thermistor itself.

While using 2-wire configuration, correction has to be made otherwise. Easiest method of correction is usage of constant resistance of used wiring, only needed value is resistance per meter of used wire. More accurate method uses temperature resistance function of used wiring. However, temperature of wiring would have to be measured, which brings other complication. In this case, also varying temperature of wiring (due to different conditions in bridge abutment and deck slab) would have be monitored. Consideration of possibilities led to selection of constant resistance of wire, despite it brought bigger error of measurement. (11) (12)

*Figure 18 PT1000 Thermometer used in measurement system*

## 4.2 Strain gauges

Other supplementary measurement in structure is monitoring of strain in concrete part of deck slab. Due to its low importance, sensors were used from available sources, in this case resistance strain gauge HBM LY11–10/120. This sensor, suitable for application on steel surfaces, was placed on steel adapter to make it suitable for application in concrete.

### 4.2.1 Resistance strain gauge HBM LY11-10/120

Resistance strain gauges are most commonly used sensor for monitoring of strain in materials. Thanks to their reliability and low price are suitable for wide applications in construction. Principle of these sensors is very simple, based on electric resistance changes with stretching or compressing fine wiring in sensor.

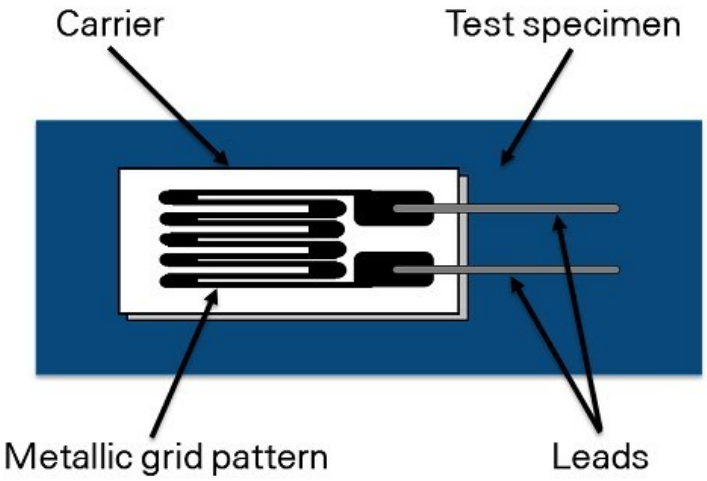


*Figure 19 Scheme of resistive strain gauge parts. NATIONAL INSTRUMENTS, 2020, Resistance strain gauge [online]. [image]. 2020. [Accessed 14 October 2020]. Available from: https://ni.scene7.com/is/image/ni/Strain_Gauge_Diagram2?scl=1*

Pivotal part of strain gauge is metallic grid made of very fine constantan wire. Metallic grid is embedded in carrier made of plastic foil, which secures uniform transfer of strain from material of sample to measuring grid. Bond between body of strain gauge and sample is usually made by suitable adhesive, for example HBM X 60 glue. Metallic grid is connected to metallic contacts, which are designed to connect wires or the strain gauge is made also with input and output leads. (13)

Metallic grid has very precisely determined resistance while it is not stretched. When the sample with strain gauge is stretched or compressed, metallic grid is stretched or compressed too. With this change, also electric resistance of grid changes. Increment of resistance is correlating with the increment of strain in tested material. Gage factor is used to convert the change of resistance to strain. (14) (15)

This type of sensor (HBM LY11-10/120) has linear grid, therefore it is dedicated for measuring strain in one direction. Length of grid is 10 mm, what is suitable for steel, but for this measuring system it is adjusted for measuring in concrete by using steel spreading adapter applied in concrete slab. Basic resistance of strain gauge is 120 Ω and gage factor is k=2.08.

Usually more useful for evaluation of measurement than strain is monitoring of stress changes in material. In this case, fundamental relation is used. It is Hooke's law and its equation is

$$\sigma_x = \varepsilon_x * E$$

$\sigma_x$ is tensile stress in direction of axis x
$\varepsilon_x$ is strain in direction of axis x
E is modulus of elasticity

However, some problems occur also for strain gauges. The problem of wiring additive resistance may be corrected relatively easily like in case of thermometers. Second problem occurs with varying temperature of measured sample or spot in structure. Thermal expansion of material causes volumetric changes of structures and therefore it also provokes change of measured strain. In case of monitoring system of bridge, this problem has to be solved. Thanks to wide usage of thermometers in the system, strain measurement may be corrected with usage of temperature measurement next to spot of strain measurement. Coefficient of thermal expansion of certain material is used to evaluate real strain change in material. (14)

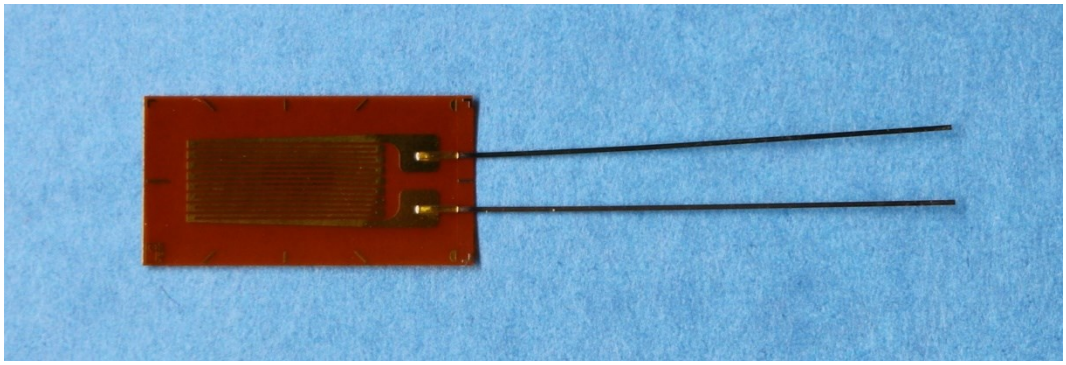

*Figure 20 Strain Gauge HBM LY11-10/120*

## 4.3 Moisture meters

Last category of sensors used in system on bridge are moisture meters. These sensors are used to monitor humidity in 2 spots in deck slab of bridge. Humidity is monitored due to its negative effects on durability of structure. It may lead to corrosion of steel beams and reinforcement and degradation of concrete slab.

Two types of moisture meters were used, capacitance moisture meter and resistance moisture meter. Both are primary dedicated for soil humidity measurement. Like soils, concrete is also three-phase spectrum, only it is bound, therefore usage of these sensors is possible in concrete. However, sufficient distance from electric conductors (beams, reinforcement) has to be managed.

### 4.3.1 Capacitive Soil Moisture Sensor

Capacitive moisture sensor uses permittivity changes of medium caused by changing amount of water diffused in medium. Concrete, soil, or similar mediums are dielectrics, which means, that they are insulants until they are ionized enough to electrical breakdown can occur. Permittivity of dielectric expresses resistance to conduction of electric current. While air and solid phase of medium has very high permittivity, water has significantly lower. Therefore, permittivity of whole medium is considerably affected by the content of water. (16)

This measurement is proceeded by the capacitor built in sensor. Capacitor capacity is proportional to permittivity of medium between positive and negative plate of capacitor. Permittivity of medium is affected by water content, porosity and ionic content. Relation between capacity and permittivity is given by equation

$$C_c = \varepsilon_m \frac{A_c}{d}$$

C is the capacity of capacitor
$\varepsilon_m$ is the permittivity of medium
A is the area of one capacitor plate
d is the distance between capacitor plates

Permittivity of medium has complex relation between more parameters, which affects resultant permittivity. Complex relative permittivity is given by relation

$$\varepsilon^*{}_r = \varepsilon'{}_r - j\varepsilon''{}_r = \varepsilon'{}_r - j\left(\varepsilon''{}_{relax} + \frac{\sigma_{dc}}{2\pi f \varepsilon_0}\right)$$

$\varepsilon^*{}_r$ is the complex relative permittivity
$\varepsilon'{}_r$ is the real part of the permittivity
$\varepsilon''{}_r$ is the imaginary part of the permittivity
$\varepsilon''{}_{relax}$ is the molecular relaxation contribution
j is the imaginary number $\sqrt{-1}$
$\sigma_{dc}$ is the electrical conductivity
f is the frequency
$\varepsilon_0$ is the vacuum permittivity

Sensor itself is flat capacitor, which has its plates in one plane. Plates are covered by hygroscopic dielectric foil, which protects the plates from corrosion. However, major function of hygroscopic layer is to be the dielectric between capacitor plates. Relative permittivity of dielectric foil rises sensitively with increasing humidity of material. In the other side of sensor is evaluation part, which converts analog measurement into digital signal. (16) (17)

Measurement is performed by the measurement of capacitor capacitance. Using known relation between capacity, area of plate and distance between them, permittivity of hygroscopic foil is evaluated. Humidity of medium is obtained by using known calibration relations between foil permittivity and material volumetric water content. (18)

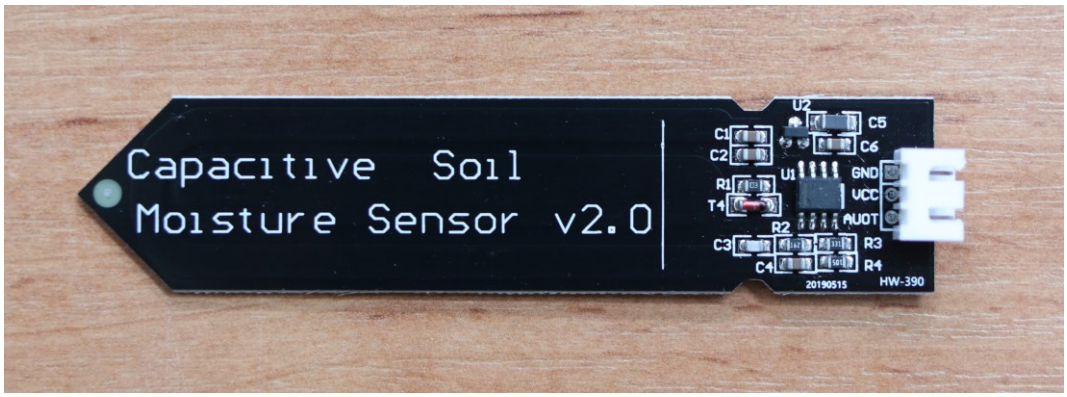


*Figure 21 Capacitive moisture sensor*

### 4.3.2 Resistive Soil Moisture Sensor

In contrast with capacitive moisture sensor which uses changes of dielectric constant of material, resistive sensors are based on conductivity changes of material. Soil, concrete, or other similar materials are poor conductors of electric current, because solid and gas phase of medium is almost insulant. However, if the content of water in these material rises, resistance of medium decreases. It is caused mainly by ionic content in water, which is scattered in material. (19) (18)

Resistive moisture sensor has two probes made of material with very good conductivity. Between these two probes, measured material should conduct the electric current. Resistance of this medium is measured and humidity is than evaluated. Like in the case of capacitance sensor, resistive sensor has also the part, which converts analog measurement into digital signal. (19)

Most common problem of these sensors is corrosion of probes. Not only caused by material moisture, also the electrolysis effect with usage of DC current occurs. Using AC current would help, however, for measurement is DC current more suitable. Other problem occurs with rising temperature, which can also affect measurement. (18)

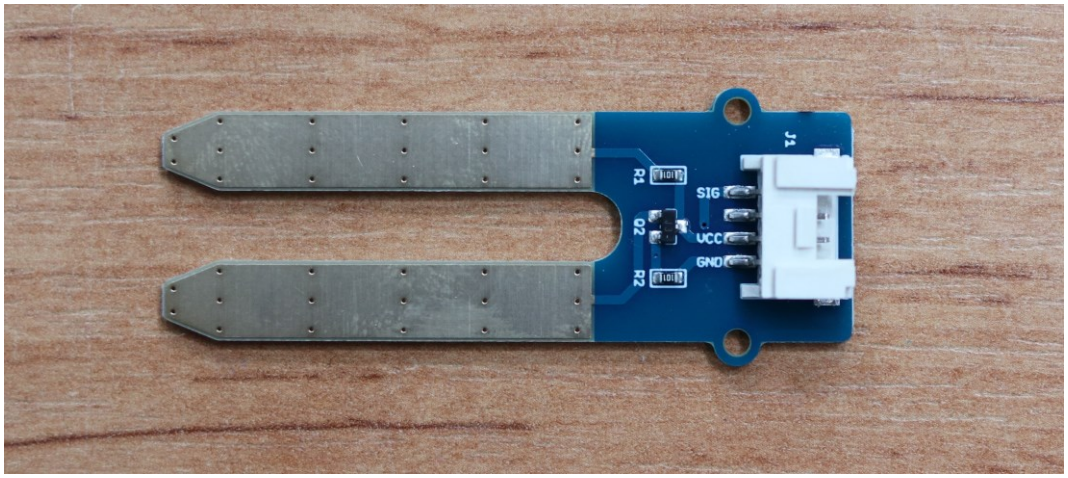


*Figure 22 Resistive soil moisture sensor*

# 5 Stationary measurement system

Following chapter is describing whole stationary measurement system installed on bridge No. 27-117 in Železná Ruda – Alžbětín. First, requirements of ŘSD are introduced, describing sensors, its position in structure and requirements to monitoring. Next paragraph of the chapter are expectations, which have ŘSD and FCE both. Following parts are describing system as designed and its preparation and installation on the site. Last paragraph is dedicated to proposal of measured data evaluation.

## 5.1 ŘSD requirements

Intention of ŘSD was to create monitoring system enabling temperature monitoring of bridge structure for longer period of time. Basic period has been set to one year, however, there is expectation of extension of monitoring. One year is logic step, in setting basic period, while it offers conditions to cover all basic situations which occur during four seasons. Special attention has to be focused on summer and winter, when extreme thermal situations occur. Other two seasons, spring and autumn, offer more moderate thermal conditions, therefore they are not very principal in temperature monitoring.

While one-year period should provide basic data of thermal behaviour in structure, extension for more years cold provide data of several-years extremes. Especially in the times of global warming, when weather extremes become frequent phenomenon. It is hard to distinguish contribution of global warming, but even standard fluctuations of reached temperatures support suitability of monitoring period extension.

For example, in period between years 1989 and 2019, maximal reached temperature was 34,8 °C, however, only during three years temperature of 32,6 °C was exceeded. That is difference of 2 °C. Average maximal reached temperature was 30,7 °C, what makes difference of 4 °C. In case of minimal temperature, minimal temperature reached in period was -22 °C, value exceeded only three times was -18,8 °C. Difference is more than 3 °C. Average minimal reached temperature was -15,4 °C, what makes difference of 6,5 °C. (5)

According to ŘSD requirements, temperature has to be monitored in five spots in entire structure. Two spots are situated in deck, monitoring temperature of filler beam and concrete. Other three spots are in abutment shaft, measurement is taken in concrete.

Spots in bridge deck are chosen according to lane type. One spot is in trough, right under traffic lane, in part loaded by axles. In this place, concrete slab has minimal thickness. Second spot in deck is situated under cornice, in place of pedestrian lane. Different filler beam section and larger thickness of slab is in this place. In longitudinal direction, sensors have to be placed in field, exact position is not specified. Spots are on 5$^{th}$ and 12$^{th}$ beam from SE edge of deck, exact position might be seen in Figure 23.

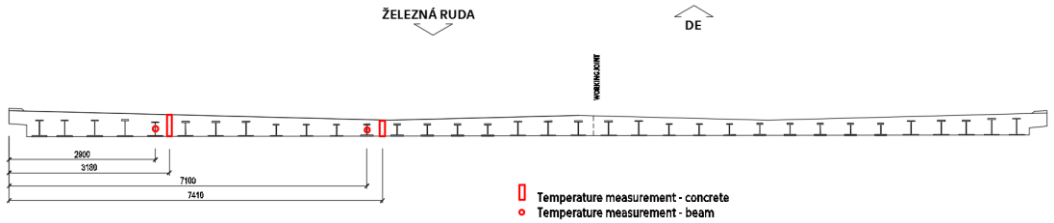


*Figure 23 Position of measured spots in cross-section of bridge deck*

Other three spots are in abutment shaft. Position of these spots is chosen so that temperature differences in longitudinal direction and sunlit effect could be registered. As can be seen in Figure 24, 1st spot is in the distance of 1 m from the edge, 2nd 4 m from edge and 3rd 11 m from edge, approximately on the longitudinal axis of bridge. Vertically are spots located 1,6 m under surface of roadway.

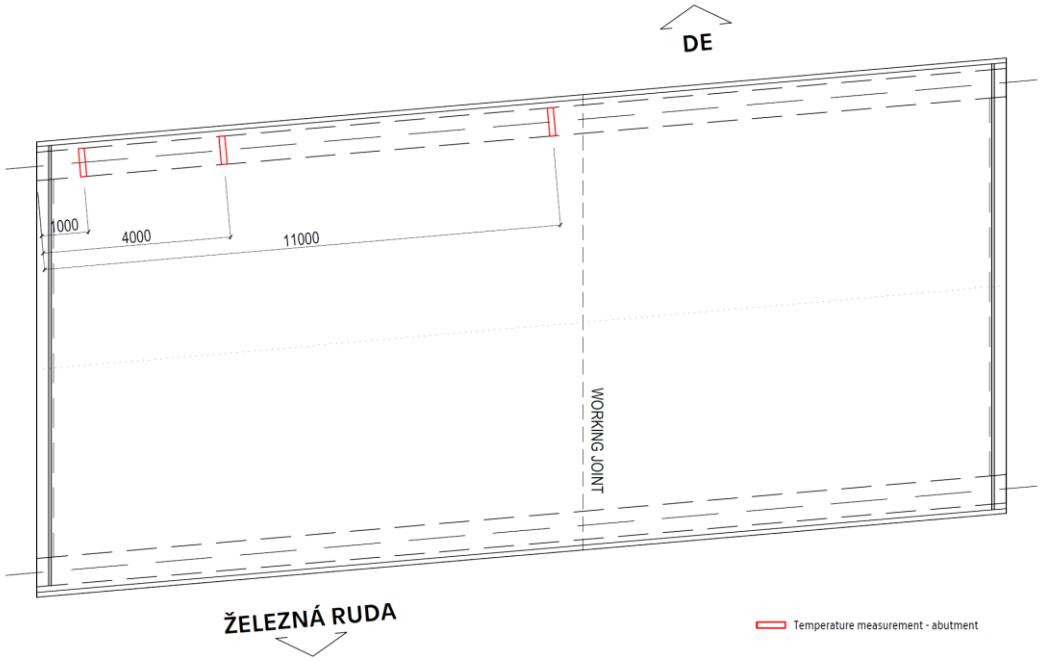


*Figure 24 Horizontal position of measured spots in abutment*

Exact position of sensors in measured spots was also part of ŘSD requirements. In the deck, spot under cornice is given as follows. Whole spot has 13 temperature sensors, 6 measuring temperature of beam, 7 measuring temperature of concrete slab. Division of sensors in the cross-section of beam and in the thickness of slab is marked in Figure 25.

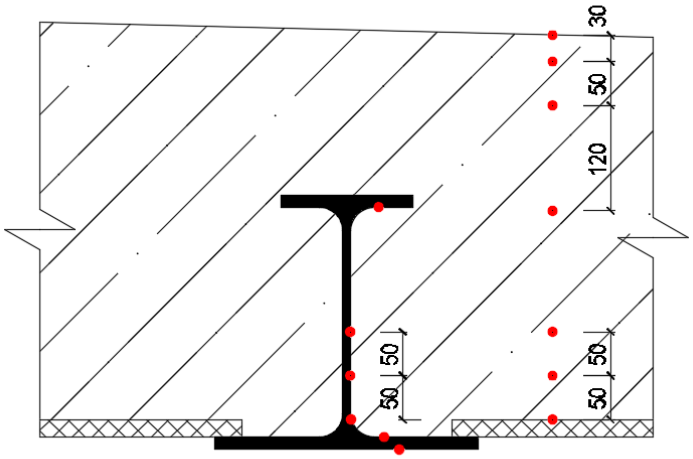


*Figure 25 Division of sensors in deck at spot under cornice, 7 sensors in concrete, 6 sensors on steel*

Spot in deck under traffic lane is similar to spot under cornice, however in this spot, 7 sensors on steel beam and 6 sensors in concrete slab are used. Initially, sensors at top flange of beam had to be from the top. Due to risk of sensors damage during concreting of slab, position of sensor was changed from top to bottom of upper flange. Exact position of sensors is drawn in Figure 26.

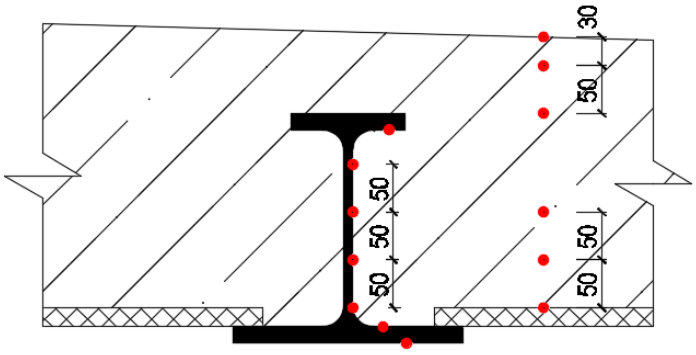


*Figure 26 Division of sensors in deck at spot under traffic lane, 6 sensors in concrete, 7 sensors on steel*

In case of measurement in abutment shaft, all three spots are identically divided along the thickness of concrete shaft. There are two sensors on both surfaces, the remaining sensors are between them in the mass of concrete. Positions of sensors might be seen in Figure 27.

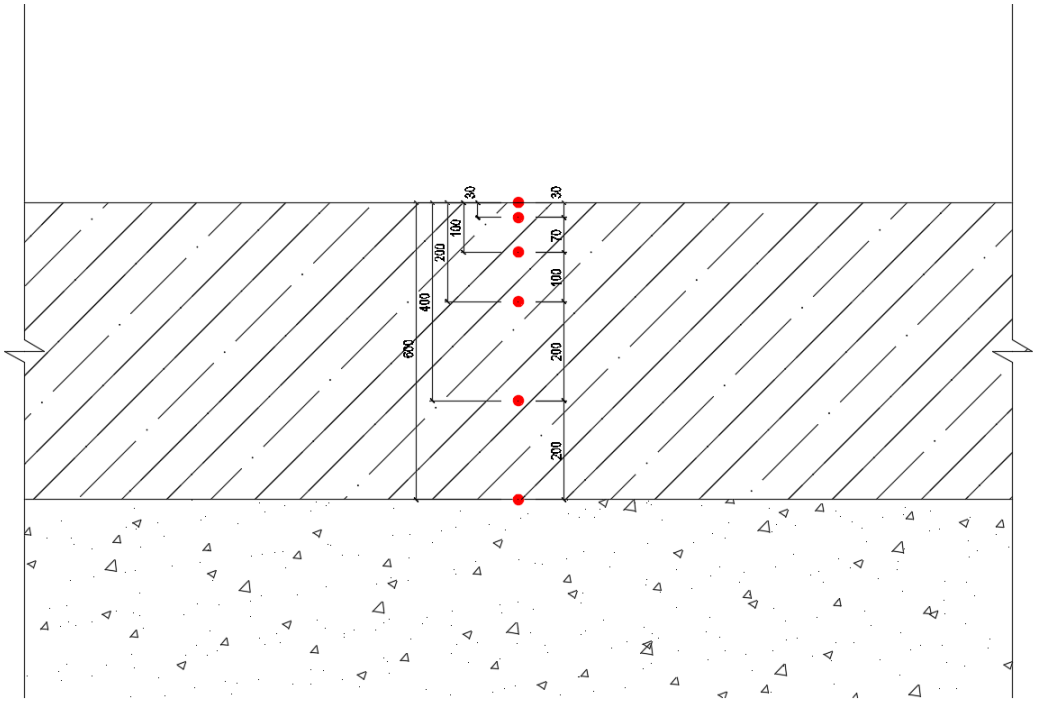


*Figure 27 Horizontal position of sensors in abutment shaft, all three spots are identic. Ambient air is in the top, concrete abutment shaft in mid and soil in the bottom of figure.*

Requirements of ŘSD specify only temperature measurement and its processing. Data have to be read by datalogger unit and sent using GSM module in real time. This reading unit has to be energetically self-sufficient, what should be reached by using battery or solar panel. Connection to electric power grid is in the location available from lamppost near bridge abutments. Sent data have to be processed and available in web interface with possibility of various export. After first year of measurement, complex report has to be processed. When the first year of measurement is finished, monitoring system has to be let in operation for unspecified period of time.

## 5.2 Expectations

Whole system is designed to enable monitoring of temperatures in chosen cross-section of bearing part of structure. Its additional feature is possibility of strain and humidity measurement in bridge deck. All these parameters are expected to be monitored over extended period of time, exceeding originally ordered one-year period.

As the main feature is temperature monitoring, it is based on validation of design standard assumptions. In case of bridge deck, expectation of the measurement is the ability to compare measured and processed data with design load, suggested by standards. Standard should cover all the temperature states of deck and measured values should not exceed maximal or minimal uniform temperature change nor the temperature difference components. In this case, especially non-linear vertical temperature component, which is after uniform temperature change the second most important situation necessary to be considered in design of bridge structure.

Other three spots located in abutment shaft are more interesting due to not very well-known temperature behaviour of this part of structure. Standard requires only linear temperature difference of 5 °C between outer surfaces of concrete pillars. Nothing is exactly specified for abutments, therefore pillar loading is used. As stated above, expected effect to stress in bearing parts of abutment and deck might be not very significant. However, as an extension of standard approach might be suitable.

Sensors installed in abutment shaft in three positions should provide data to evaluate common states appearing in this type of structure part. Three spots are not chosen arbitrarily. Spot in distance of 1 m from abutment edge should cover thermal states induced by outer shade temperature and also sunlit effects. Second spot should be affected by sunlit effects to a lesser extent. In third spot, sunlit is definitely excluded.

According to these assumptions, temperature loading states in abutment should be evaluated and amount of sunlit effect to these states should be rated in order of magnitude. Despite of measurement, these data should be verified by thermal modelling using finite elements method (FEM). All these conclusions might be next used by ŘSD for future designs of structures, as an additional background to standard.

In addition to thermal monitoring, humidity and strain monitoring is deployed in the bridge deck. Strain monitoring is placed under traffic lane approximately in spots loaded directly by vehicle axles. Second spot is under pedestrian lane. Both sensor spots are in lane directions to Czechia. Integral structure of this short and wide bridge is very rigid, redundant states of stress are therefore not expected during common operation of structure. However, strain monitoring could provide information in case of excessive laden trucks transit or about general use of bridge by heavier vehicles. Second possibility of asset is an early signalisation of excessive stress amount in structure caused by serious defects in structure. Hopefully, this state will not occur in the lifetime of bridge or monitoring system.

Humidity sensors are designed to control humidity values in bridge deck, in place of thermal and strain monitoring. Role of these sensors is to provide data about humidity of structure in spots measured by other sensors. While humidity itself does not represent significant negative effect for durability of concrete, corrosion of concrete and reinforcement is commonly linked right with moisture contained in structure. Water might be carrier of chemical substances, which leads to corrosion of concrete or reinforcement, e. g. chlorides, acids, sulphates. In case of water penetration into the mass of concrete, all these undesirable pollutants might be clogged inside and start process of corrosion. (20)

However, with information about rising humidity, proper reaction might be taken to prevent development of material degradation. (20) Higher value might be caused by insulation penetration, development of deep cracks in concrete or by developed transport processes inside of concrete. When higher humidity value is noticed, structure might be visually checked and measures could be taken. Following steps might be diagnostic survey or even reconstruction of whole bridge.

Other feature of double type sensor humidity monitoring is the indication of ion content in concrete material, what directly draws attention to insulation penetration, or other damage of insulation. Rising content of ions represents serious long-term problem with durability of steel parts of structure.

## 5.3 Description of system parts

System consists of 52 sensors systematically deployed in the structure of bridge No. 27-117. Sensors are connected by cables to electric switchboard, which processes measurement and sends data by using GSM module.

### 5.3.1 Sensor deployment

Whole system is based on ŘSD specifications, which require 44 temperature sensors installed in five spots in whole structure. In contrast with original requirements, system was enhanced by sensors of humidity and strain gauges. According to original requirements, thermometers are installed in five spots in structure, two in the bridge deck and three in the abutment shaft.

As listed above, thermometers in deck measure temperature of both concrete slab and filler steel beam. Sensors monitoring temperature of steel are glued to beam surface using proper adhesive and covered by thermal insulation layer to ensure correctness of steel temperature measurement. This technique is shown in Figure 28, thermometers have been fixated to steel beam and then covered by piece of thermal insulation.

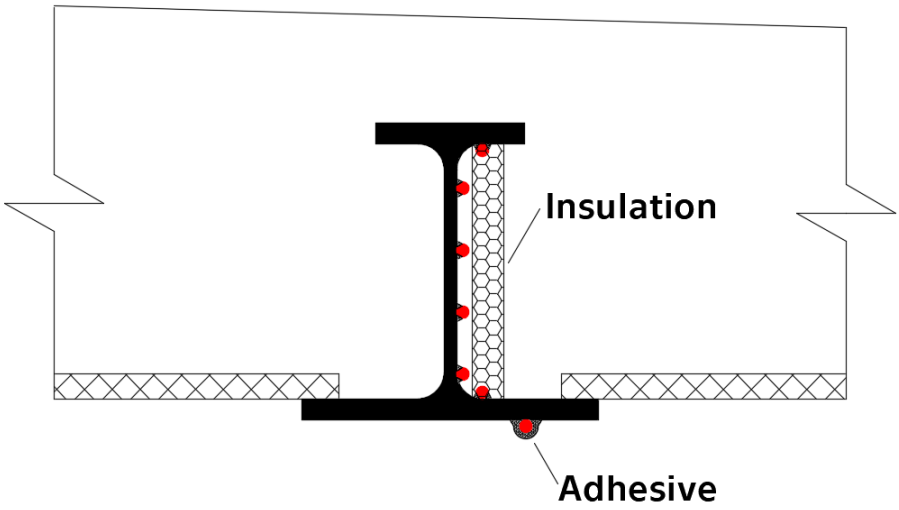


*Figure 28 Technique of sensor fixation and insulation from concrete used in bridge deck*

In case of concrete temperature measurement, concrete casings (little beams) were designed to ensure proper position of sensors, principally easy installation on construction site and protect thermometers from mechanic damage during manipulation and concreting. Before insertion of sensors into concrete casing beams, thermometer probes were cased into miniature HPC (high-performance concrete) tip covers. These casings were made to exclude possible contact between metallic sensor probe and steel parts of concrete casing beams (reinforcement, binding wire) and protect sensor in contact with exterior environment on the exposed edge of casing beams. This technique of deployment is illustrated in Figure 29, dimensions of casing beams are given by slab thickness and eye of reinforcement grid (200x200 mm).

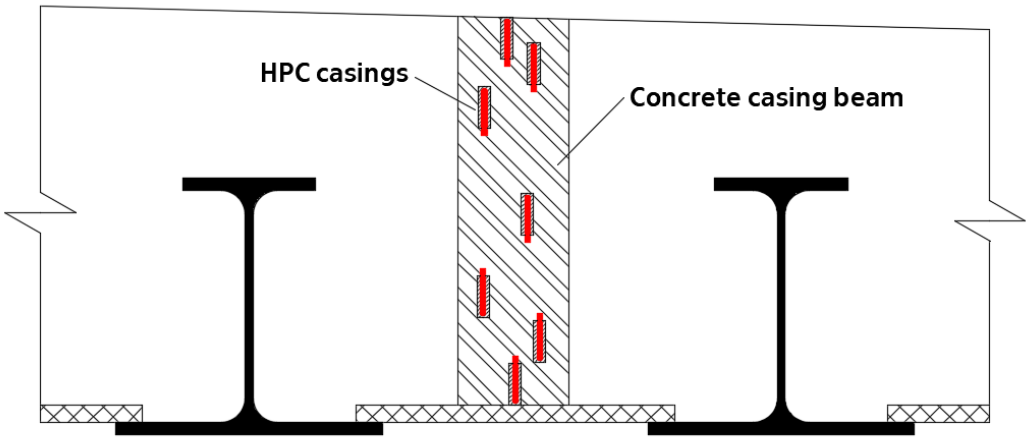


*Figure 29 Technique of thermometers deployment into concrete slab*

Beams are inserted into bridge deck vertically, position is held vertically by CETRIS plate and horizontally by fastening to reinforcement. Beams made for abutment shaft are similar, different are dimensions and position of sensors. Three identic beams are inserted into abutment shaft, their dimensions copy thickness of shaft and eye of reinforcement grid (150x150 mm). Beams are born by horizontal reinforcement rods, fastened to both vertical and horizontal rods.

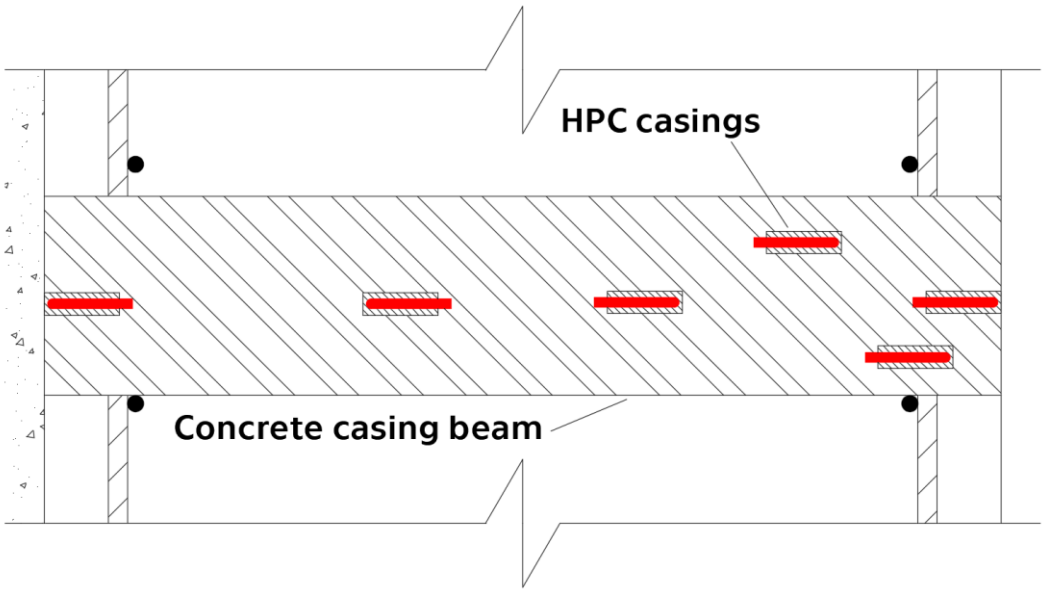


*Figure 30 Mounting of beam with thermometers into abutment shaft. On the left side is contact with the soil, on the right side contact with ambient air.*

Strain gauges and humidity sensors are located next to temperature sensors, creating groups of sensors. All these sensors in deck are grouped due to possibility of connection of measurements, mainly for temperature calibration of humidity and strain sensors. Other reason is clearly pragmatic, if sensors are near to each other, possibility of damage during concreting is lower.

Measurement of strain is located in the middle of span, where maximal positive bending moment acts on deck. As the strain gauges dedicated for steel are used, they are connected to spreading rod, which transfers strain from concrete to sensor. Strain gauges are from the outer side covered by epoxide to protect them from damage. Strain in steel is therefore equal to strain in concrete, stress in concrete can be easily obtained using Hooke's law. Scope of Hooke's law covers elastic behaviour of structure, which is in this case unambiguously expected. For purpose of installation, reinforcement of deck is used. Spreading rods are fastened to grid of reinforcement rods, one on the bottom row of rods, second on the top row. Both sensors are put parallel to the longitudinal axle of filler beams, while strain in this direction is more useful and more suitable for evaluation. This installation is used in two spots in deck, together four strain gauges are used.

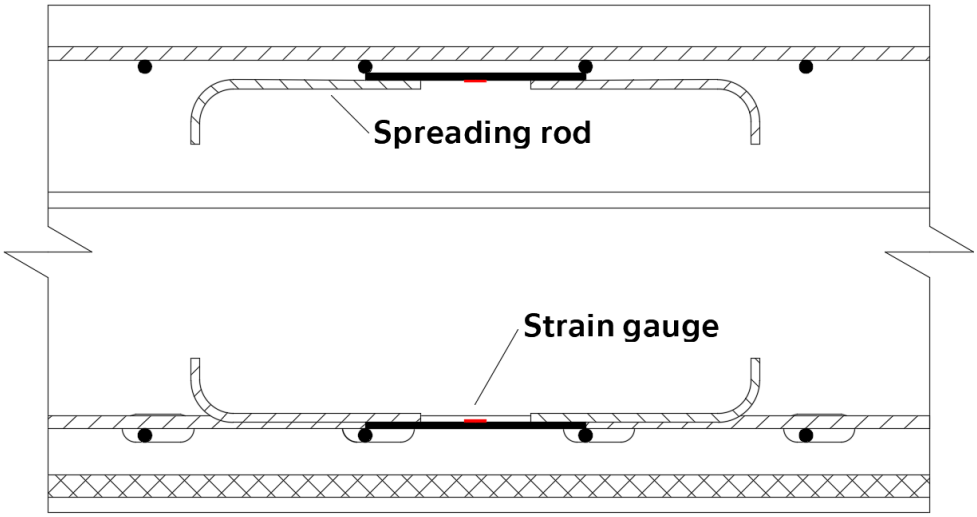


*Figure 31 Technique of strain gauges deployment. Strain gauges are stuck to plate of spreading rod, which is fastened to reinforcement rods.*

Four moisture sensors of two types are installed in structure, resistive and capacitive moisture meter. In one measured spot, one of both type of humidity sensors is used. Both of these sensors are embedded into little branch box, which also converts wires from strain gauges into one cable line heading to main switchboard. Boxes are filled with epoxide to protect its content. Branch box is fastened to filler beam, what ensures right position of both sensors. This way of deployment is illustrated in Figure 31; however, resistive moisture sensor is in the same vertical position as capacitive sensor. Other position in figure is chosen due to suitable illustration of sensor deployment.

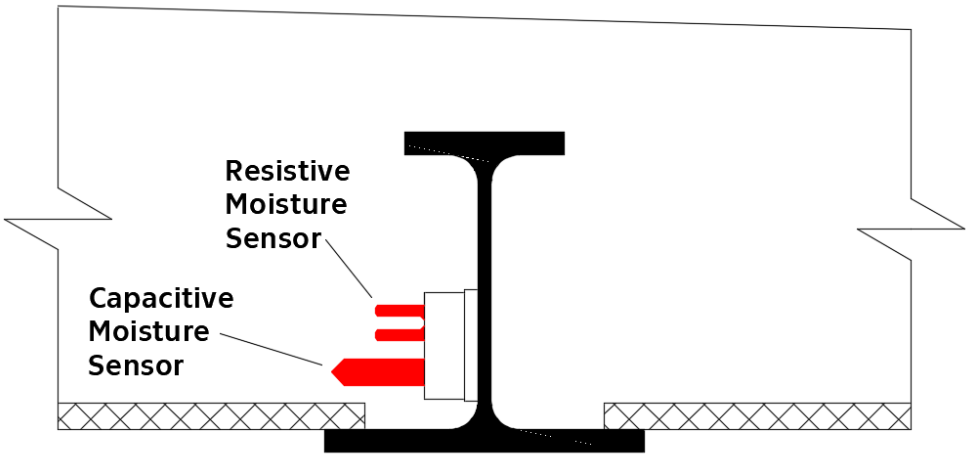


*Figure 32 Humidity sensors deployment technique, branch box is fastened to filler beam*

Overall deployment is shown in following figures, where sensor bunches positions are marked in ground plan of deck and in cross-section of bridge. Sensors are grouped to the bunches according to their position and functionality. Sensor bunches are marked in Figures 33 and 34 by the following labels:

- Ta1 thermometers in abutment, inserted in casing beam
- Ta2 thermometers in abutment, inserted in casing beam
- Ta3 thermometers in abutment, inserted in casing beam
- Td1 thermometers in deck, inserted in casing beam
- Td2 thermometers in deck, inserted in casing beam
- Tb1 thermometers in deck, fastened to filler beam
- Tb2 thermometers in deck, fastened to filler beam
- S1 strain gauges in deck, fastened to reinforcement
- S2 strain gauges in deck, fastened to reinforcement
- H1 moisture meters in deck, attached to branch box
- H2 moisture meters in deck, attached to branch box

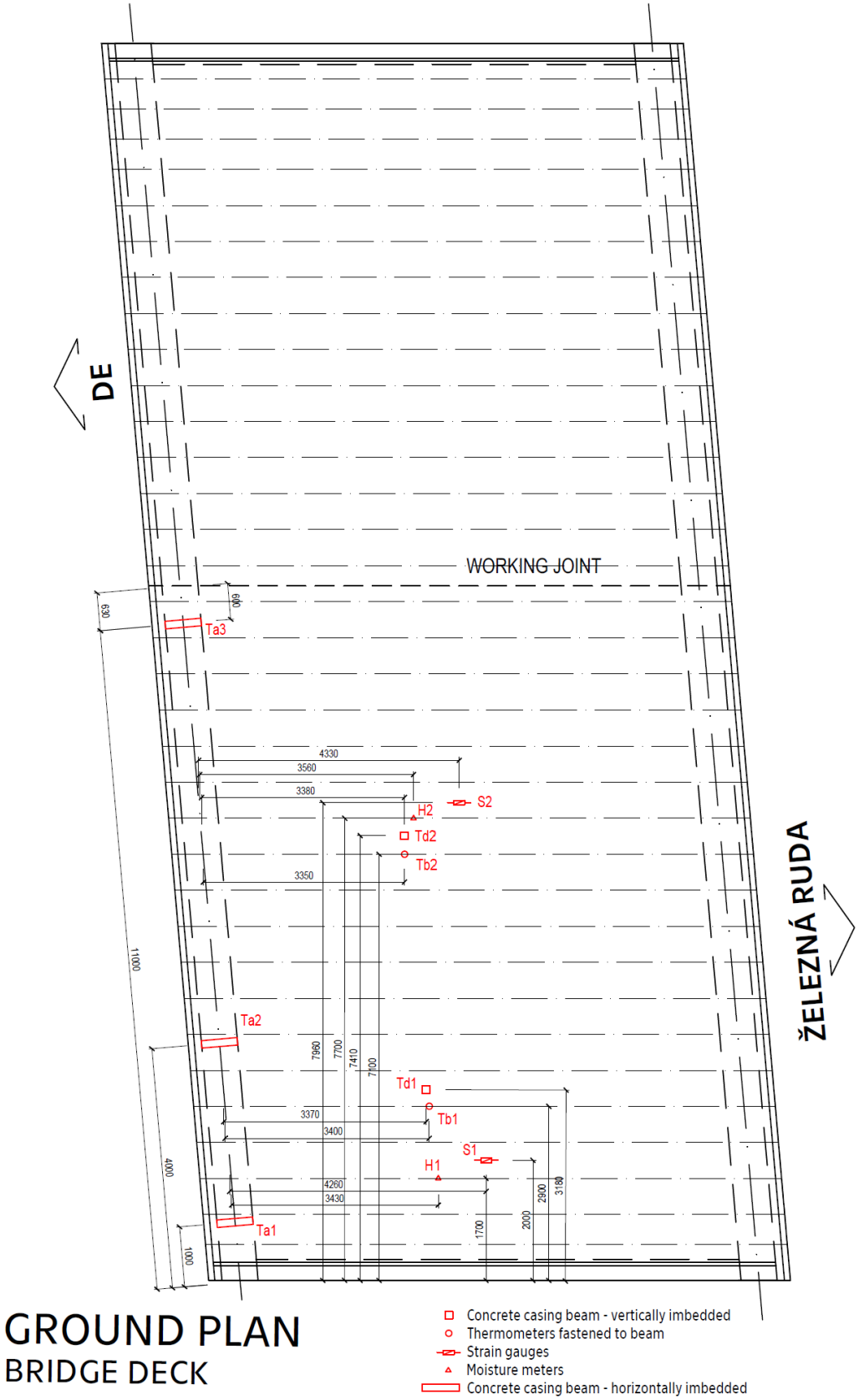


*Figure 33 Deployment of sensors in bridge structure marked in ground plan*

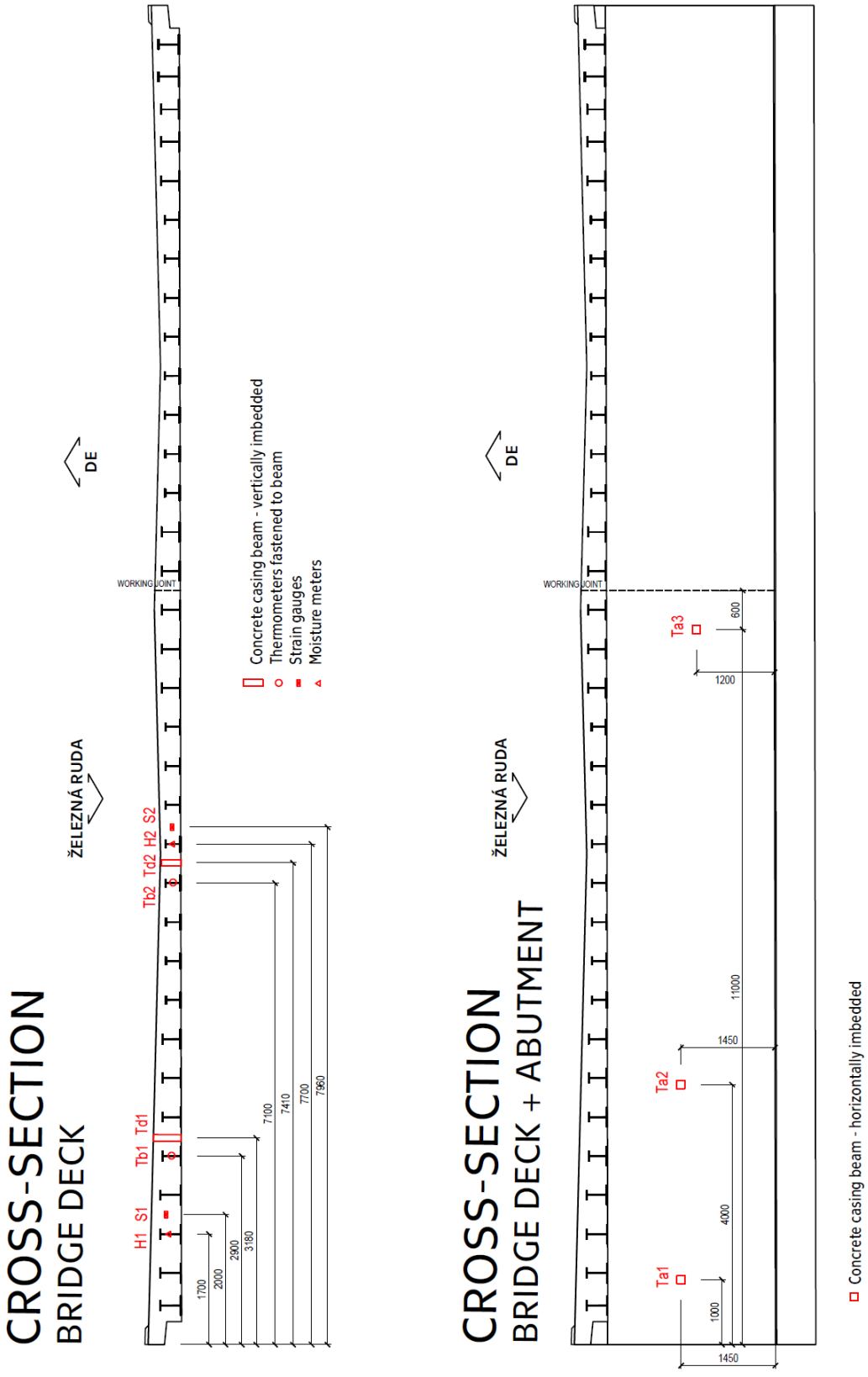


*Figure 34 Deployment of sensors in bridge structure marked in cross-sections*

### 5.3.2 Wiring

All the sensors have to be connected to switchboard by wires, what is ensured by cable lines installed into structure of bridge. Specific ways of their design are described in following paragraph.

Sensors are grouped into bunches, according to their type or deployment in structure. Every sensor (except humidity sensors) has its original wire of certain length. Wires from one bunch of sensors are led into one branch box, where are wires linked to one cable of type J-Y(St)Y. J-Y(St)Y cables are dedicated for transmission of signal from sensors and their cores are arranged to twisted pairs. This multicore cable afterwards transmits information from bunch of sensors directly to switchboard.

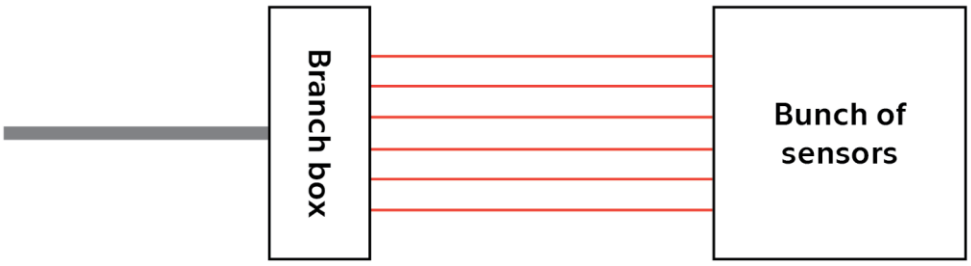


*Figure 35 Solution of sensor connection with collecting cable*

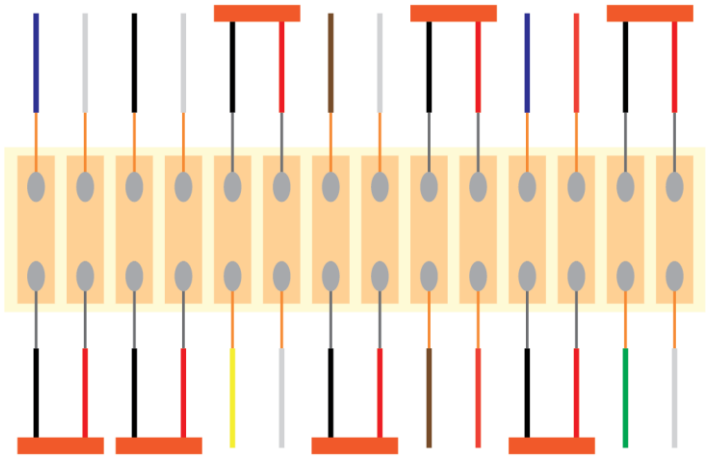

*Figure 36 Example of wire connection between sensors and collecting cable, placed in branch box. Red-black pairs of wires with orange marking are wires from sensors.*

J-Y(St)Y cables of two different number of cores are used, parameters of cores are identic. Diameter of core is 0,8 mm, cross-section of the core is A=0,50 $mm^2$ and resistance of core is R=73,2 Ω/km. Number of cores is 12 and 20. 12-core cable is used for bunches of up to 6 sensors, 20-core cable is used for the bunches with more than 6 sensors. 20-core cable is therefore used for two bunches with 7 sensors. (21)

Thermometers cased in concrete beam have their wires brought to outside from beam through plastic protective ring. Afterwards are wires led into branch box, where are wires reconnected with wires of collecting cable. This solution is used in case of five of these casing beams. During the installation, it is necessary to place cable outlet so that it is protected during concreting as much as possible. This is more important for placement of branch boxes, as this part is more prone to damage than cable outlet from beam.

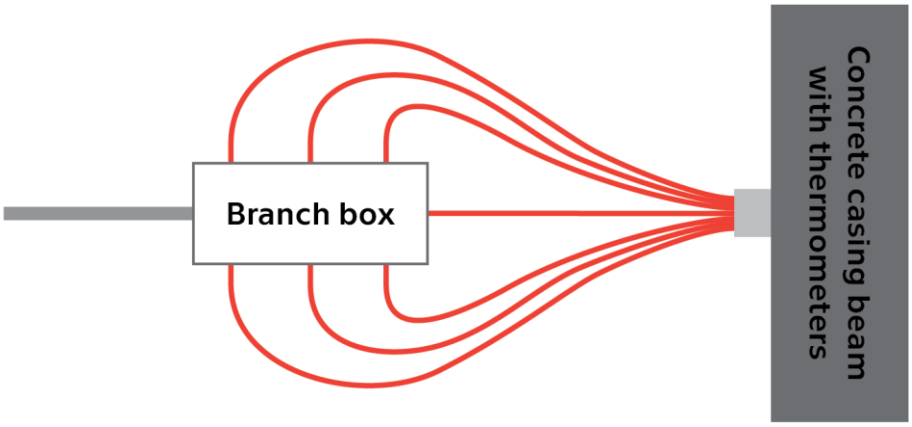


*Figure 37 Solution of thermometers connection to connecting cable in case of concrete casing beams*

Other utilization of PT 1000 thermometers is in thermal monitoring of filler steel beams. Like in case of thermometers in concrete casing, wires are taken into branch box. Bunch of sensors is not especially protected from being damaged, this protection is secured by increased mechanic robustness of sensors and wires.

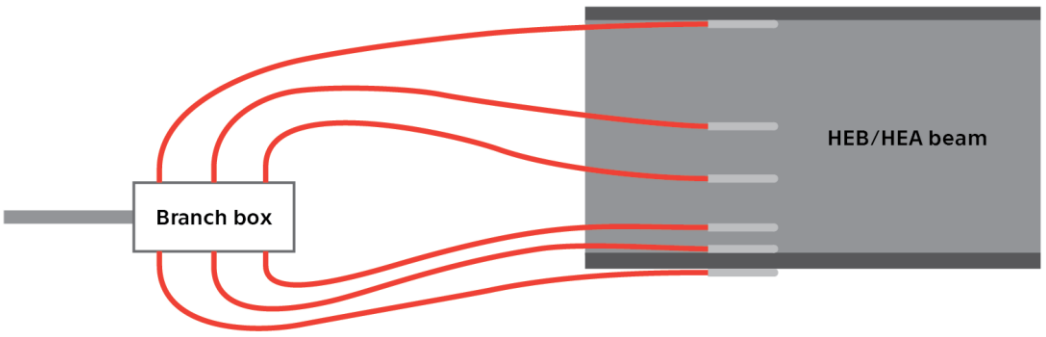


*Figure 38 Connection of thermometers monitoring temperature of beam into branch box*

Last bunch of sensors are strain gauges and moisture meters. Humidity sensors are linked directly into branch box, where are connected with collecting cable. Strain gauges are attached to spreading rod, where are they also connected into connecting cable which leads directly into branch box. There are connecting cables form strain gauges connected with collecting cable.

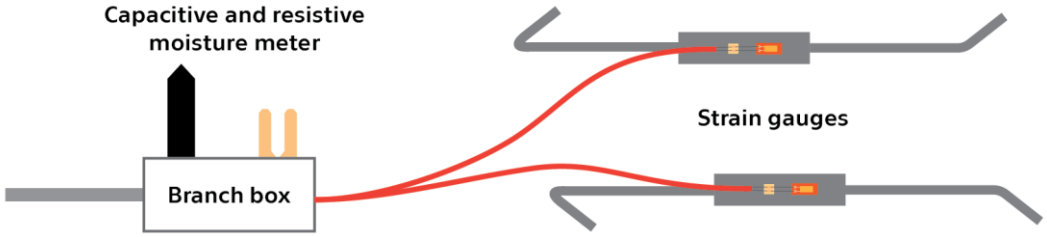


*Figure 39 Connection of moisture meters and strain gauges into branch box*

Collecting cables are laid into structure in flexible PVC tubes, so that maximal protection of cable is provided. Cables are led in direct sections along reinforcement bars, therefore position is fixated and protection is increased. In spots of cable bends are cables fixated to most suitable bar of reinforcement grid.

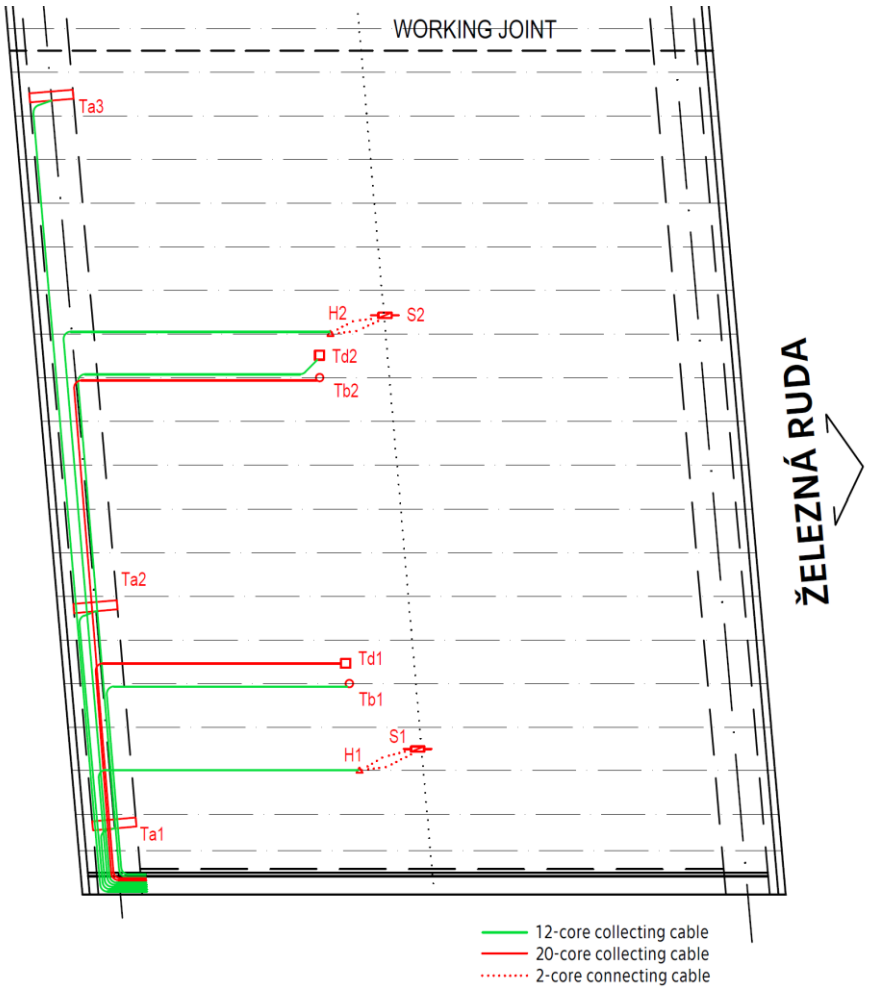


*Figure 40 Schematic plan of cable routes*

Due to utilization of resistive sensors, which operate on principle of changing resistance of sensor, effect of cable resistance has to be taken into order. This effect might not be significant (1000Ω of PT 1000 thermometer vs 73.2 Ω/km of used cable). However, small correction implemented into measurement might help in situations of minimal thermal changes in structure.

Calculation of additional resistance of cable $R_{add}$ is performed very easily. Input values are resistance of one core per meter $R_{core}$ and length of cable in meters l. While current passes from switchboard into sensor and back along the same length, resulting resistance has to be multiplied twice.

$$R_{add} = 2 * R_{core} * l$$

Values of additional resistance of collecting cable are available for every bunch of sensors and is listed in Table 3.

*Table 3 Additional resistance $R_{add}$ for all bunches of sensors*

| Bunch of sensors | Cable type | Length | Resistance per meter | Resistance of cable |
|---|---|---|---|---|
| | Number of cores | l [m] | $R_{core}$ [Ω/m] | $R_{add}$ [Ω] |
| Ta1 | 12 | 2,5 | 0,0732 | 0,366 |
| Ta2 | 12 | 5,5 | 0,0732 | 0,805 |
| Ta3 | 12 | 13 | 0,0732 | 1,903 |
| Td1 | 20 | 8 | 0,0732 | 1,171 |
| Td2 | 12 | 11,5 | 0,0732 | 1,684 |
| Tb1 | 12 | 7 | 0,0732 | 1,025 |
| Tb2 | 20 | 11,5 | 0,0732 | 1,684 |
| S1 | 12 | 7,6 | 0,0732 | 1,113 |
| S2 | 12 | 13,7 | 0,0732 | 2,006 |
| H1 | 12 | 6,6 | 0,0732 | 0,966 |
| H2 | 12 | 12,7 | 0,0732 | 1,859 |

### 5.3.3 Switchboard

Unit responsible for signal transformation, further data processing and sending is switchboard. Switchboard will be installed in special box, prepared on west abutment of bridge structure.

Switchboard consists of variety of subunits, each of specific task. Analog signal from sensors (resistance) is processed by seven Lucid IO modules, which are giving digital output and providing connectivity via USB ports. Thermometers and strain gauges are both resistive, however their initial resistance is different. To spare one Lucid IO module, additional resistance of 880 Ω was added to each strain gauge. By this modification, initial resistance of 1000 Ω for all resistive sensors was reached and strain gauges could be connected together with thermometers. Connection to Raspberry Pi computer is provided via USB hub. Grove sensor provides digital output directly, it is connected to Raspberry Pi via Grove Base Hat and Freedom unit.

Essential core of switchboard is tiny computer Raspberry Pi, which seems as perfect in similar usages. Its dimensions are small, price is more than affordable and usage options are pretty wide. This computer processes measurement and data. Data are sent to servers via internet connection provided by modem unit.

Energy supply of whole switchboard is secured by cable connection to power grid. 230V AC current is transformed in transformer to 12V DC current to reach the same voltage as backup power supply has. Connection to Freedom unit provides possibility of control, which power supply is actually used. 12V DC current is further transformed to 5V DC current to provide supply for Raspberry Pi, modem and USB hub. Backup power supply is secured by usage of 12V batteries.

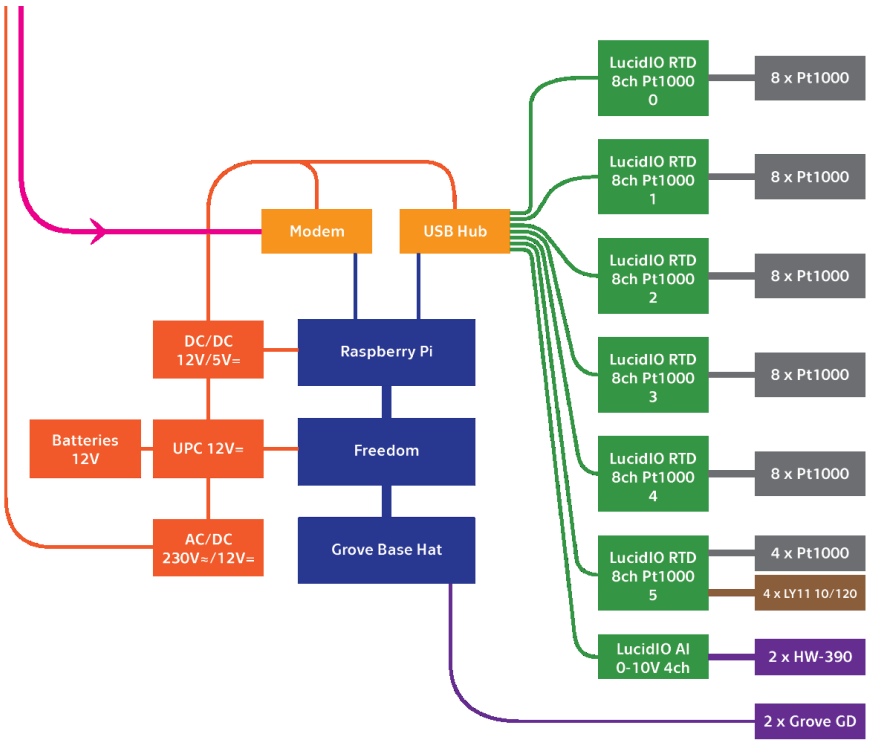


*Figure 41 Scheme of switchboard. Sensors on the right side, grey are thermometers, brown are strain gauges and violet are moisture meters*

## 5.4 Preparation

Instrumentation of bridge structure had to be prepared prior to installation in situ, while limited amount of time was available for installation. Sensors had to be installed during short intermissions between reinforcement of bearing parts and its following concreting. These intermissions were available twice, first after reinforcing and before concreting abutment shaft, second one between these processes on bridge deck.

Several technical solutions had to be realized before installation was possible. In case of thermometers monitoring temperature of concrete, HPC sensor casings were manufactured first. Afterwards sensors were concreted into casing beams. Last step was preparation of junction boxes, collecting cables and their connection with sensors. This step was identic for all the sensors.

### 5.4.1 Thermometer HPC casings

First step before thermometer insertion into concrete beam was their casing into little HPC shells. Purpose of HPC shells on thermometer probes is mainly their insulation from reinforcement steel with material of similar properties than measured concrete mass. Contact with steel might notable influence measured temperature, while steel is very good thermal conductor. Other purpose is mechanical protection of sensors in face of casing beam.

*Figure 42 Sketch of thermometer HPC shell*

Shell is made of HPC concrete, using MSK2 mixture developed by Experimental centre of FCE CTU. This mixture is characteristic with its high compressive strength (~100 MPa), fast solidification and high deformability while processed (SCC). There are three types of MSK mixture, 1, 2 and 3, varying in solidification rate. Second type, MSK2 is most suitable for general usages. (22)

Thermometer casing was processed relatively easily. As a formwork, PVC water pipe was used. This pipe was cut into pieces of suitable length, afterwards pieces were cut longitudinally and plastered around with tape. This step had to ensure simple removing of little formwork. Pipe pieces were then glued to the plate and filled with MSK2 mixture. The only problem consisted of thermometer position securing, while the high deformability of MSK2 while wet worked against it. To fix this issue, special composition was used.

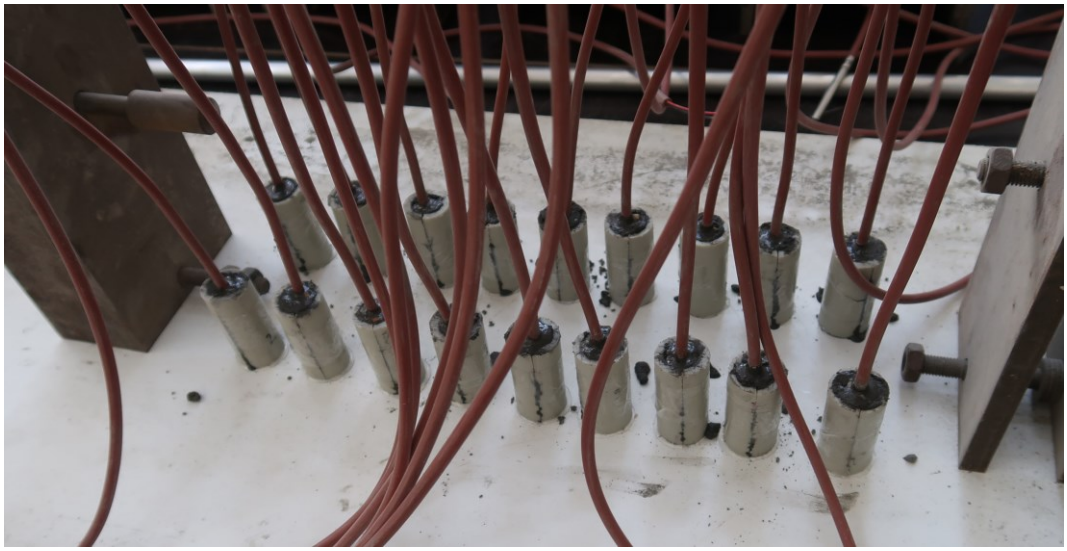

*Figure 43 Preparation of HPC thermometer shells (picture: J. Zatloukal)*

After removing of formwork, quality of shells was inspected. First time, concrete shell fell apart, whole process had to be therefore repeated. This issue was caused by usage of older package of MSK2, which partially hydrated in pack. Package was opened and improperly stored, what caused hydration from air humidity.

*Figure 44 Finished thermometers suitable for insertion into casing beams (picture: J. Zatloukal)*

### 5.4.2 Concrete casing beams

Major part of preparation of measuring system was concrete casing beams manufacturing. These casing beams were designed as a most suitable way of ensuring sensor position in concrete deck and shaft. Other feature of casing beams in protection of sensors during handling, installation and concreting. Casing beams also provides considerable advantage during installation in situ, while installation of sensors itself than consist only of beam insertion to formwork.

Various possible mechanical loads might act on the beam, while it is transported, inserted and loaded by wet concrete on the site. Beam should bear these loads without deformation or damage. Therefore, reinforcement was designed to ensure integrity of casing beams. Other advantage of reinforcement is to enable precise sensor placement in the casing beams. Without this reinforcement, it would be challenging to ensure correct position of sensors even with small shifts.

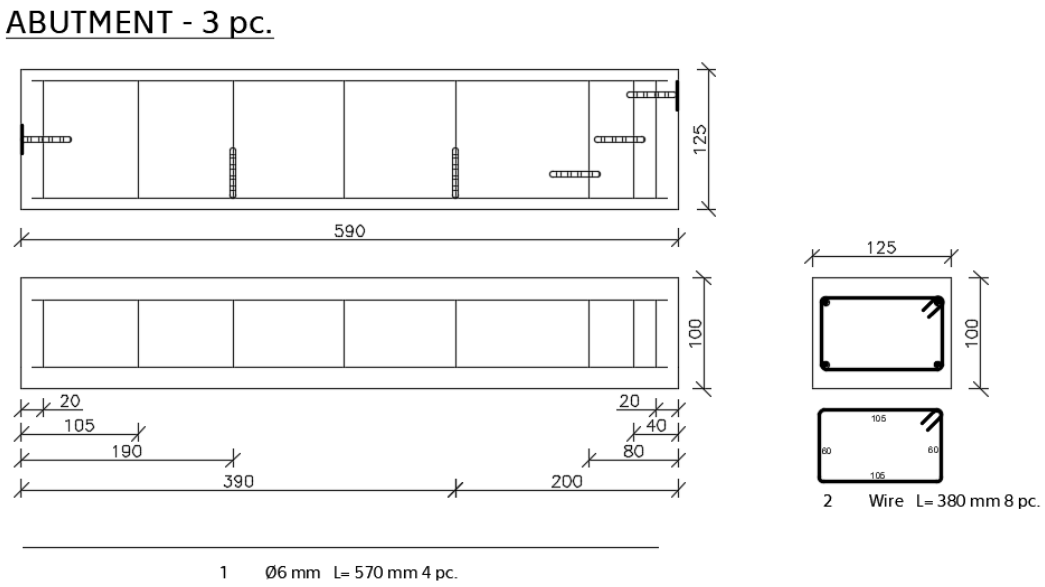


*Figure 45 Example of designed reinforcement of casing beam*

Sizing of beams was given by dimensions structure parts (deck, abutment shaft). Beams were concreted in standard forms with dimensions of test specimens. Reaching of specific dimensions was solved by insertion of special pads made of XPS. These pads were cut out from XPS plates using wire EDM.

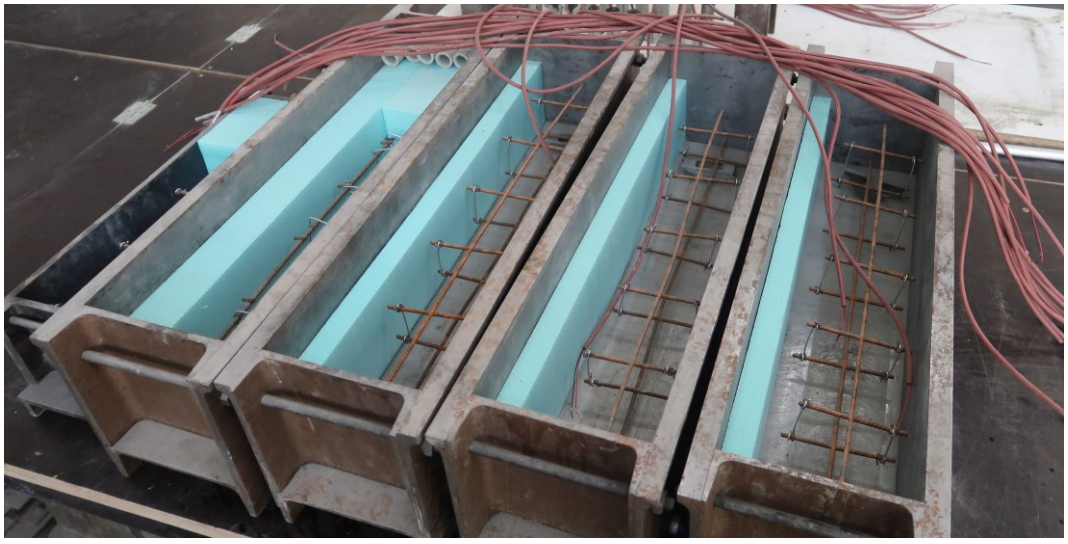

*Figure 46 Padded forms with prepared reinforcement (picture: J. Zatloukal)*

Thermometers were fastened to reinforcement rods in exact positions using ordinary binding wire. Positions were given by ŘSD requirements, according to spots, where temperature have to be measured. After binding, positions were not stable, they have had to be checked multiple times before concreting.

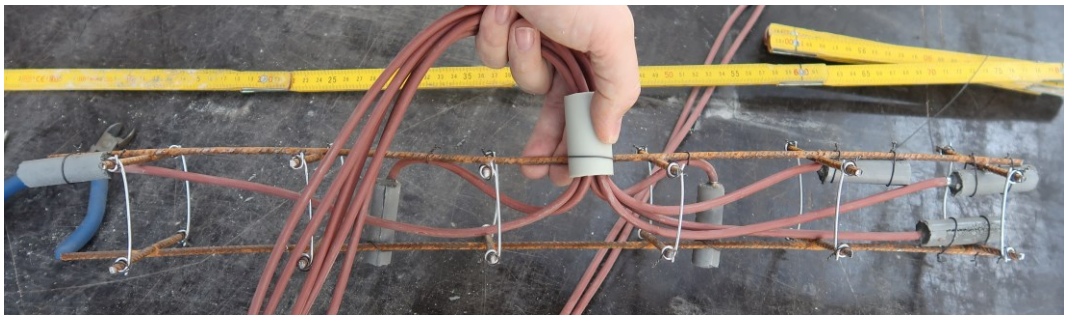

*Figure 47 Reinforcement with bound sensors (picture: J. Zatloukal)*

Wires from sensors were fastened to reinforcement and led out from casing beams through plastic protective ring. This ring is made of PVC water pipe, same as the one used for HPC shells as formwork. Task of this ring is to protect wires in place of exhaustion from casing beam and to secure position and integrity of wire bunch.

*Figure 48 Casing beam ready for concreting, plastic ring protects wires and secures exhaustion position (picture: J. Zatloukal)*

Concreting was performed in two phases. First one took place on 29th of July 2020, when three beams dedicated into abutment shafts were concreted. As a suitable concrete substance for casing beam might be considered MSK2, however, used amount of substance would be excessive when price and availability is considered. Therefore, following mixture devised by doc. Kolář was used

- MSK2 substance 25 kg
- Aggregates 0/4 6 kg
- Aggregates 4/8 5 kg
- Aggregates 8/16 8 kg
- Water 3 l

Second phase was performed on 18th of August 2020, when remaining two beams dedicated into bridge deck were concreted. Beams from first phase had a problem with insufficient concreting of edges, therefore, caverns were filled and edges shaped by MSK2 substance. Due to these problems, concrete mixture was adjusted and its composition was

- MSK2 substance 26 kg
- Aggregates 0/4 6 kg
- Aggregates 4/8 12 kg
- Water 3 l

After concrete setting, forms were removed, beams were checked and got ready for further preparation before installing.

*Figure 49 Finished concrete beams after concreting and cavern filling (might be seen on central beam, as darker stain on edge in back) (picture: J. Zatloukal)*

### 5.4.3 Strain gauges preparation

Strain gauges available on the department were not primarily suitable for application in concrete, nevertheless for steel. Therefore, spreading rod to spread strain from concrete to steel was designed. It consists of steel plate, with two bended reinforcement bars welded to its edges. Four of these spreading rods were made to place four strain gauges into structure.

Strain gauges HBM LY11-10/120 were used. Sensors were attached to spreading rod by X60 glue, special glue dedicated for usage in experimental mechanics. Whereas used type of strain gauges is very subtle, sensors were covered by protective cap made of epoxide.

To enable connection to branch box, 2-wire connecting cable was used. This wire is connected into branch box and at the other end it is connected to strain gauge through conductive plate, like connections in branch box. Spreading rods with attached sensors and connecting wire in this state were suitable to connect with collecting cable and to install into structure.

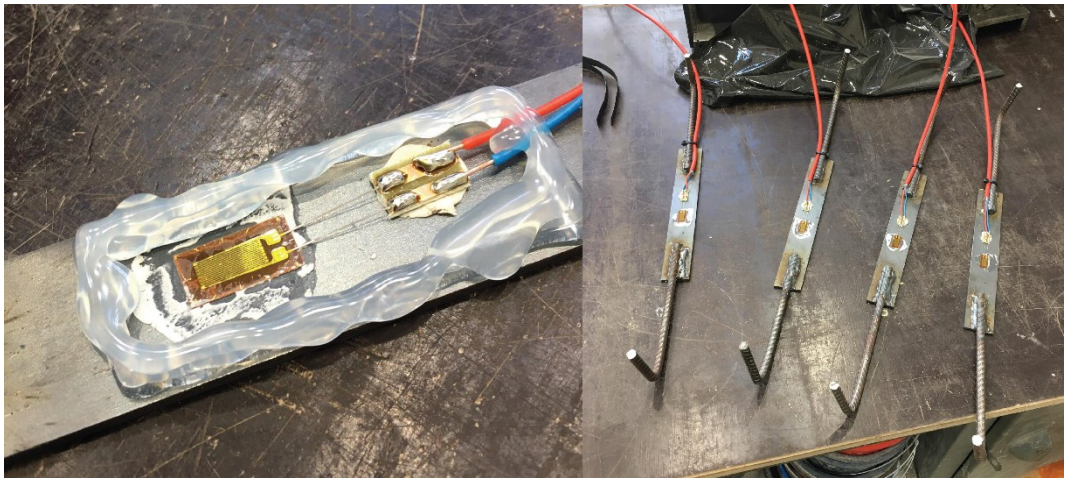

*Figure 50 Strain gauges on spreading rods. Making of protective cap on the left, hot glue framing works as formwork for epoxide. (picture: J. Zatloukal)*

### 5.4.4 Further preparation of sensors

As a next step and last step of preparation, branch boxes and wiring were prepared. Branch boxes are providing connection of collecting cable with sensor wires from thermometers, strain gauges and moisture meters. Sensor wires are connected with wires of collecting cable through conductive plates, wires are connected by tin solder. After the connection of wires was made, conductive plate with connected wires was inserted into branch box and wires were properly pulled out. Then was box filled with epoxide to avoid corrosion or other improper processes, which could occur in empty branch box.

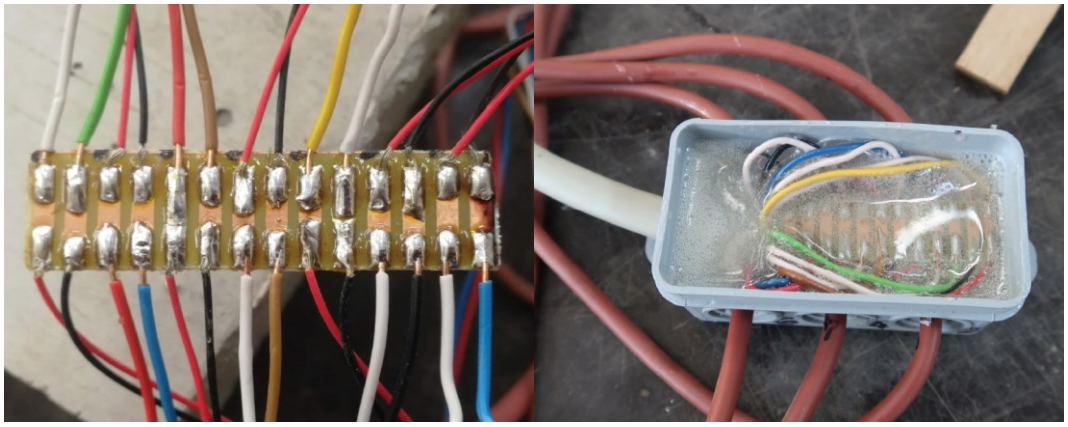

*Figure 51 Example of connection between sensor wires and collecting cable through conductive plate. Branch box filled with epoxide on the right side.*

Moisture meters, in contrast with other sensors, are sending digital signal instead of analog, therefore their connection to collecting cable is different. They are placed directly into the branch box, only probes are led out from box to enable measurement in concrete.

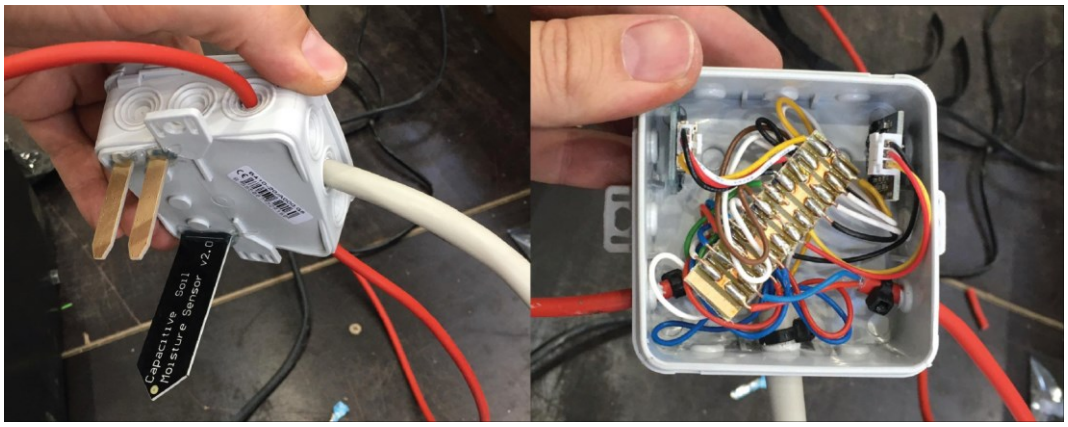


*Figure 52 Connection of moisture meters into branch box (picture: J. Zatloukal)*

Collecting cables were cut in pieces of proper length, to enable placement in structure and ensure sufficient overlap for manipulation with switchboard. These cables were connected into branch boxes prior to installation in structure.

*Figure 53 Beams ready for installation into structure (picture: J. Zatloukal)*

## 5.5 Installation

All the prepared sensors had to be installed into bridge structure in specific time, according to construction phase on the site. Until today, installation took place three times, during intermissions in constructing and after completion of bridge.

First installation took place on 10th of August 2020. During this installation, three casing beams were installed into abutment shaft. Intermission on site came after completion of reinforcement in abutment shaft. Casing beams were inserted in requested position into reinforcement grid and fastened to rods. Branch boxes were fastened to the bottom edge of casing beams. This position should be ideal for protection of branch boxes and wires.

*Figure 54 Installed casing beam with thermometers in abutment shaft. Branch box is placed on the bottom side of beam. Cables are led along reinforcement rods. (picture: P. Švecová)*

Prior to installation of collecting cables into structure were cables inserted into flexible plastic protective pipes. Flexible protective pipes should avoid damage of cable shaft or cores. Cables were led along horizontal reinforcement rods and fastened to them in proper distances. Fastening to rods was done by usage of plastic cable ties, mostly because of simplicity of work with them. All the bends were done with the emphasis on maximal radius of cable. Cables were brought to edge of formwork along reinforcement rods in concrete hinges. Cables outlet had to be placed so that cables could be led to final outlet from structure in following phases of construction.

Second phase of installation took place on 25th of August 2020, when the remaining sensors were installed into unfinished bridge deck. Sensors which have been installed during this phase were thermometers in two casing beams, thermometers dedicated for steel, strain gauges and moisture meters. Bridge deck was in phase before concreting, while filler beams and reinforcement were prepared in place.

Similar to casing beams in abutment shaft, casing beams in bridge deck were placed in the eyes of reinforcement grid and fastened to it. Branch boxes were in this case put under the flange of filler beam, where were fastened to web by cable ties.

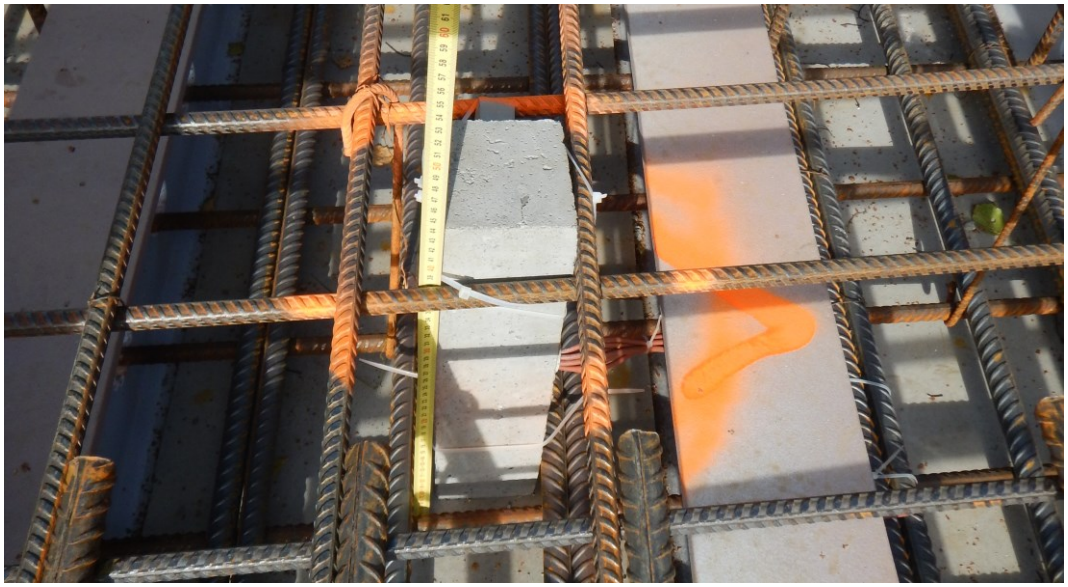

*Figure 55 Casing beam inserted into bridge deck (picture: J. Zatloukalová)*

Thermometers, which are dedicated for monitoring of steel beam were prepared as bunch of wires with probes connected to branch box. Sensors were freely laid to enable manipulation during installation. Sensors were attached to beam in required position, according to ŘSD order. As a fastening bond, hot glue was used. Sensor probe was pressed against the steel to ensure contact with beam and then stuck around with hot glue. To ensure proper measurement of steel temperature, thermometers were covered by XPS thermal insulation from side which is in contact with concrete. Branch box is attached to beam web like in the case of thermometers in concrete.

*Figure 56 Bunch of thermometers on filler beam, covered by XPS insulation. Casing beam is behind the filler beam. (picture: J. Zatloukalová)*

Strain gauges were also prepared in laboratory prior to installation, with usage of spreading rods could be installation much faster. Spreading rods were inserted into reinforcement grid and attached to rods. In one spot, two strain gauges were installed, one to the bottom layer of reinforcement, second one to the top layer of reinforcement. Sensors were placed in the mid of the span, in the place of maximal bending moment. Connecting cables from strain gauges are led along reinforcement to branch box, where are connected to collecting cable.

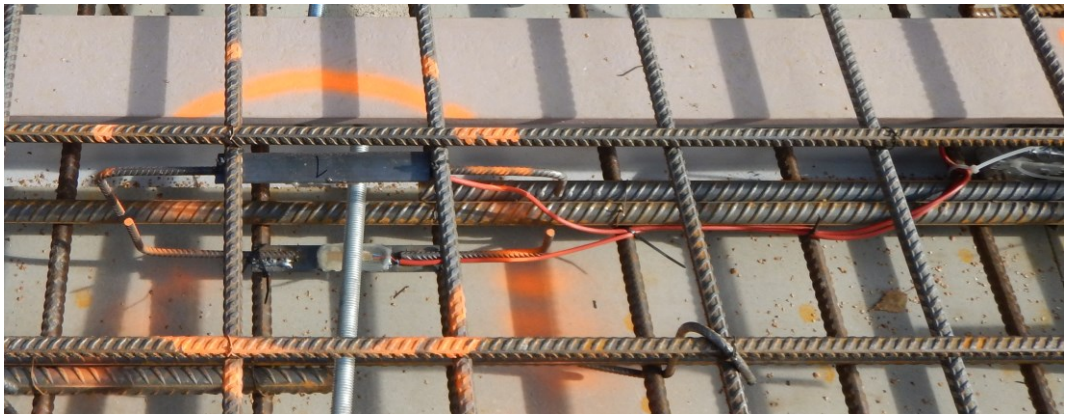

*Figure 57 Strain gauges on installed spreading rods (picture: J. Zatloukalová)*

Moisture meters are installed directly into branch box, which collects signal also from strain gauges. Probes of sensors are led out from box to be accommodated in the concrete environment. The box was fastened to web of filler beam using cable ties. All the branch boxes are tied to web as can be seen in Figure 58, using holes in web, which are designed as transitions for reinforcement bars.

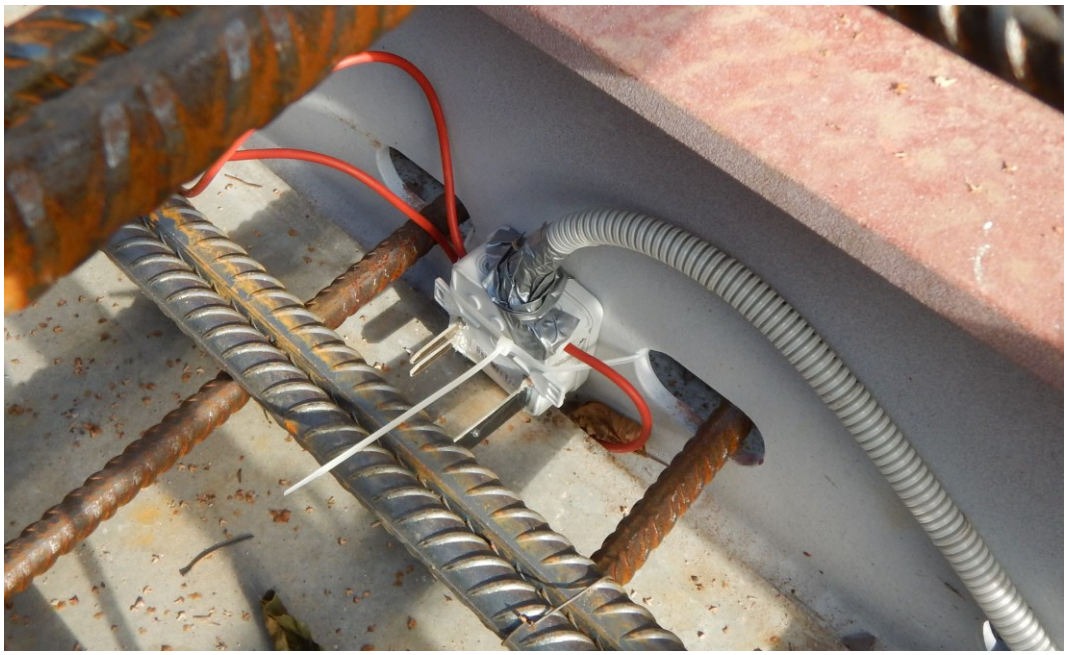

*Figure 58 Branch box attachment to filler beam. Probes of moisture meters are led out from branch box. (picture: J. Zatloukalová)*

Exactly as in case of abutment shaft, collecting cables leading from all sensor bunches are protected by flexible plastic pipe. Cables were led along reinforcement bars to concrete hinges, where were bent and led perpendicular to axle of the bridge. Collecting cables from all bunches of sensors were concentrated in one bunch, which is led out from formwork in outlet designed solely for the measurement system.

After completion of bridge, box for switchboard was mounted to the abutment shaft. This phase took place on 2nd of December 2020. Cables leading from outlet were cut in proper distance from outlet, marked and led into switchboard box. The switchboard box is ready for installation of switchboard.

*Figure 59 Bridge No. 27-117 with installed switchboard box on the left abutment (picture: J. Zatloukal)*

## 5.6 Data evaluation

First processing of measured data will be realized in switchboard unit. These processed data will be sent via internet connection to server, where they will be stored and evaluated. Frequency of values reading will be initially set to each 30 minutes, what is based on smooth thermal change in measured profiles. However, it might be changed in moment according to actual needs.

### 5.6.1 Uniform temperature

First evaluated characteristic will be uniform temperature in measured spots. Neither spot has sensor placed in the mid of height of measured profile. Therefore, this value will be taken as value corresponding with mid of profile height in measured temperature profile.

Uniform temperature will vary in the time, most important will be extreme reached values in summer and winter. Maximal and minimal reached temperature will be evaluated after one year of measurement and may be replaced by values measured in further monitoring.

According to thermal models, which were processed as other part of this thesis, there is not real expectation of standard values excessing. However, real situations might bring different values, while the measurement will run. Due to this reason, evaluation of uniform temperature is necessary.

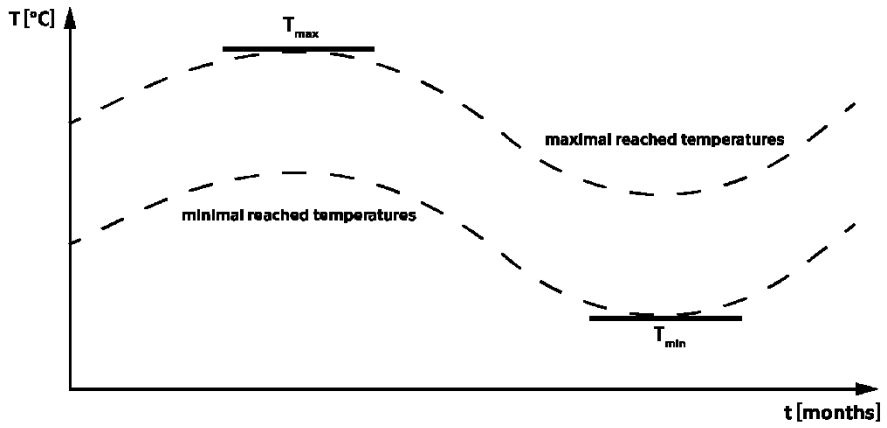


*Figure 60 Illustration of uniform temperature evaluation*

### 5.6.2 Non-linear vertical temperature difference

Vertical temperature differences will be most important and interesting part of measurement. As it was modelled in further part of the thesis, vertical thermal differences reached in real might be significantly higher than standard considers.

Thanks to design of numerous thermometers in measured profiles, non-linear vertical temperature differences might be evaluated after measurement processes. Vertical temperature differences will be watched over whole time period of measurement. Extreme profiles will be evaluated and compared with values provided in standard. It will be necessary to consider proper temperature profile in further design of bridges within the scope of ŘSD.

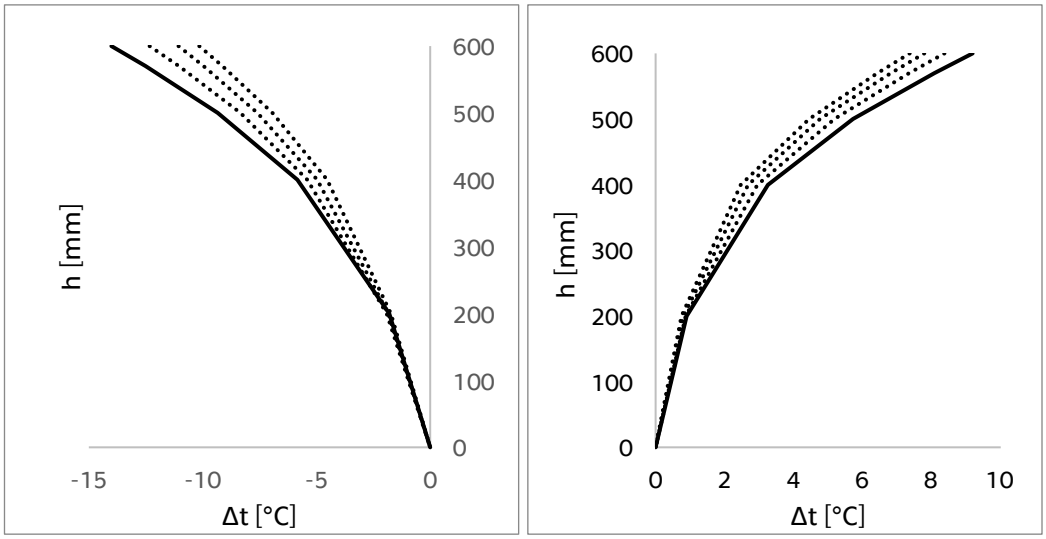


*Figure 61 Possible extreme temperature profiles*

### 5.6.3 Linear vertical temperature difference

Bound with non-linear vertical differences are linear differences which ease everyday praxis of structural design. They might be useful for purpose of usage in computation programmes like SCIA Engineer, DIubal RFEM, ANSYS and others, where linear temperature difference on minor structure parts is commonly used.

Linear vertical temperature differences will be evaluated from the same temperature profiles as non-linear differences. These will be obtained as maximal difference between temperatures reached on the opposite surfaces of measured profile in the same moment.

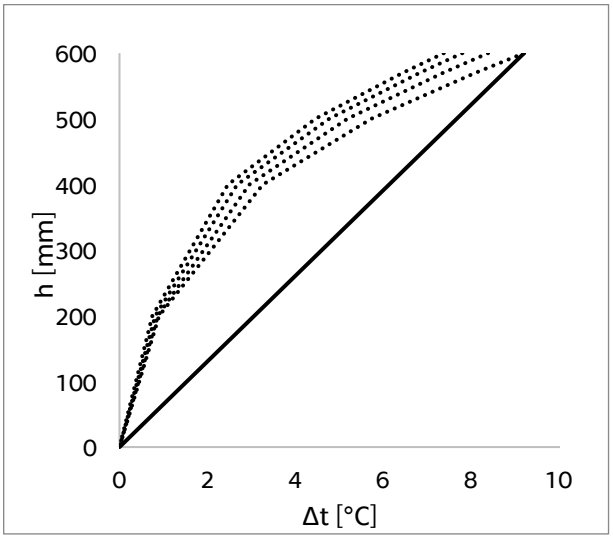


*Figure 62 Example of maximal linear vertical temperature difference*

### 5.6.4 Strain

Strains and stresses are the least important monitored quantity in this system. Their purpose is long-term indication of possible structure defects, which could occur in some specific situations. However, due to low importance and small dimensions of bridge together with its stiffness it is really improbable, that this situation could occur in real life.

Despite of expectations, strain gauges could provide information about extremely loaded vehicles passing the bridge, if the frequency of values reading is set high enough to notice these situations. It might be tested for specific period of time. During the whole time period, strains will be monitored in the same frequency as the other sensors.

### 5.6.5 Humidity

Humidity monitoring shall be possibility for indication of structure degradation. While the humidity of concrete rises, it might be signal of defects in structure. Also, the difference between two types of sensors (resistive and capacitive) might signalize problems. Resistive moisture meter measures resistance of environment, which falls with higher humidity and ion content. For example, most common ion appearing in degraded structures might be $Cl^-$. This chloride ion comes from chemical defrost agents (e. g. NaCl, $CaCl_2$) used in winter period. Water contaminated with these ions might get to bearing structure through defects in insulation and process of material degradation might begin.

Rising values of humidity from resistive moisture meter might therefore indicate rising content of ions in structure. Rising content of ions represents significant problem, which should be considered and being solved.

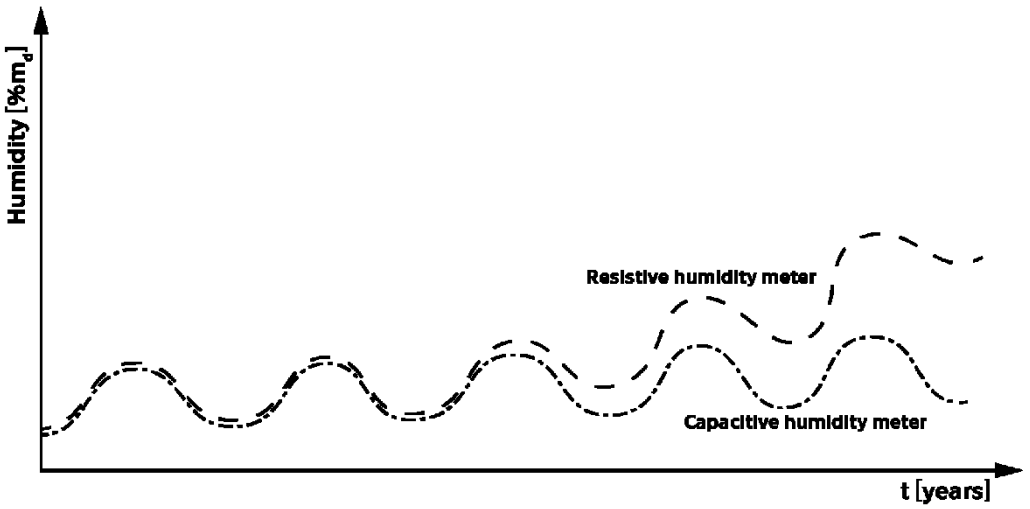


*Figure 63 Example of humidity measurement development. Rising humidity value from resistive humidity meter might indicate rising content of ions.*

# 6 Thermal FEM models

Computer modelling provides solid base for problem solution in structural engineering, where quick and inexpensive analysis is preferred. In case of this thesis, project of stationary measurement system was delayed due to unpleasant realities in year 2020. Therefore, last part of measurement system is still not on-line and data are not available. Based on these facts, heat transfer models seemed as a suitable replacement of first data evaluation.

2D heat transfer models of measured spots in structure should provide first data of temperature division along the thickness of abutment shaft or bridge deck during season extremes. However, their main purpose is verification of measured data in following months, when measurement system will start its operation.

For purpose of modelling, OOFEM software have been used. This free software was developed by collective of authors led by prof. Bořek Patzák at Department of Mechanics, FCE, CTU. OOFEM provides FEM solver, inputs are created in text editor as a set of commands defined in OOFEM and geometry of model is drawn in Salome software. Solved problem results might be browsed in ParaView browser, where very good modes of graphic representation of results are available. (23) (24) (25)

All the three models are simplified in way which excludes huge systematic errors, but might affect results only marginally. In case of abutment shaft, simplification comes by exclusion of reinforcement and usage of one concrete type. In real situation, two concrete types are used. Our mixture is used in casing beam, surrounding concrete is C 30/37 or C 35/45. Deck models are simplified more, inclination of surface, reinforcement, two concrete types and radiuses of filler beam between web and flange are neglected.

Thermal loading is based on data from CHMI and work of doc. Vít Šmilauer with collective. Models are loaded with simplified time-temperature profile and sunlit profile in case of maximal temperature models. Loading functions are taken from models of doc. Vít Šmilauer, temperature values are substituted from long-term data of CHMI. (5)(26)

## 6.1 Concrete parameters measurements

During the preparation of casing beams, samples of used concrete were made. These samples were further used for determination of their thermal parameters. In the first step, basic parameters like dimensions and weight were measured as background for later evaluation.

Thermal parameters of samples were measured by doc. Eva Vejmelková and Ing. Vojtěch Pommer from the Department of Material Engineering and Chemistry at FCE CTU. For purpose of heat transfer modelling, average values for each material were used. While the samples from the construction site were not available for longer time, only one type of concrete in each model is considered. Used parameters match with the concrete used for casing beams. Measured and average values are available in Table 4:

*Table 4 Measured and used average parameters of concrete used in casing beams*

| Sample marking | | | m [g] | a [mm] | b [mm] | c [mm] | ρ [kg/m$^3$] | λ [Wm$^{-1}$K$^{-1}$] | c [J.kg$^{-1}$K$^{-1}$] |
|---|---|---|---|---|---|---|---|---|---|
| 227-017 | I | 1 | 2380 | 100.7 | 100.4 | 100.3 | 2347 | 2.835 | 836 |
| 227-017 | I | 2 | 2372 | 100.6 | 100.7 | 101.8 | 2300 | 2.420 | 813 |
| 227-017 | I | 3 | 2335 | 100.2 | 100.3 | 99.6 | 2333 | 2.659 | 769 |
| Abutment shaft average | | | | | | | 2327 | 2.638 | 806 |
| 227-017 | II | 1 | 2257 | 100.3 | 100.3 | 99.5 | 2255 | 2.364 | 793 |
| 227-017 | II | 2 | 2298 | 100.3 | 100.5 | 101.3 | 2250 | 2.266 | 800 |
| 227-017 | II | 3 | 2280 | 100.0 | 100.3 | 100.8 | 2255 | 2.085 | 716 |
| Bridge deck average | | | | | | | 2253 | 2.238 | 770 |

## 6.2 Abutment shaft model

### 6.2.1 Model description

First created model was model of abutment shaft, due to its simplicity, which is best for possible debug process. Model consists of three layer, 2 concrete layers and one layer of soil. These layers replace real materials in cross-section of the shaft. Two layers of concrete are used to enable finer element mesh in the contact of concrete with air.

Dimension of model are following. Width of model is 3 m, height is 1,8 m. Layer of concrete takes 0,6 m, rest height of 1,2 m represents soil. Concrete is split into two layers, first layer with height of 0,1 m, second of 0,5 m. Quadrangle mesh was used, always 10 elements per edge of face, resulting in 100 elements per one face. Size of mesh is chosen so that positions of sensors in real structure are in mesh nodes.

Initial and boundary conditions are for this model very simple. Initial temperature is set for all nodes to equal initial value. Boundary condition is set for both edges. Dirichlet's condition is used on bottom edge (immutable set temperature). Top edge has two boundary conditions, Newton's (contact with ambient air) and Stefan-Boltzmann's (heat radiation). Load is performed by temperature profile typical for extreme situations.

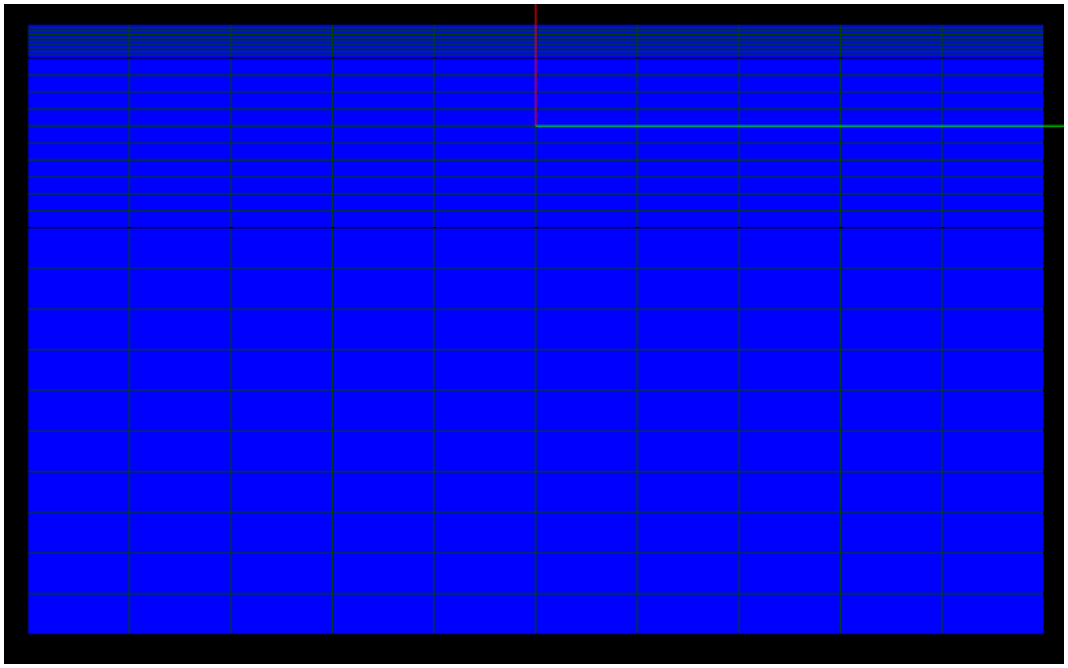

*Figure 64 Model of abutment shaft with quadrangle mesh, contact with ambient air on the top, contact with soil at the bottom of figure. Finest and mid-fine mesh represents layer of concrete and coarse mesh represents soil layer.*

Material properties are set as follows (27)

Concrete
- c=800 $Jkg^{-1}K^{-1}$
- λ=2,6 $Wm^{-1}K^{-1}$
- γ=2330 $kgm^{-3}$
- ε=0,85

Soil
- c=950 $Jkg^{-1}K^{-1}$
- λ=2,0 $Wm^{-1}K^{-1}$
- γ=2350 $kgm^{-3}$

### 6.2.2 Minimal temperature

First computed task was model of abutment shaft loaded by temperature profile typical for coldest days in winter. According to data from CHMI, lowest reached air temperature was -22 °C, what was considered into design of thermal loading function. Time period for computation was set to 200 hours (8 days and 8 hours) and model was loaded with following temperature function:

$$t(t) = 6\sin\left[\left(\frac{2\pi}{86400}\right) * (t - 9 * 3600)\right] - 16$$

This function represents cold winter day with clear sky, when minimal temperature of -22 °C is reached before sunrise and highest day temperature rises to -10 °C. Initial temperature was set to 0 °C for all nodes.

Results of computation are following. In the next figures, two specific repeating situations are shown. First situation in Figure 65 shows maximal vertical temperature difference and second situation in Figure 66 shows cooling of external edge, when ambient air temperature falls down in night.

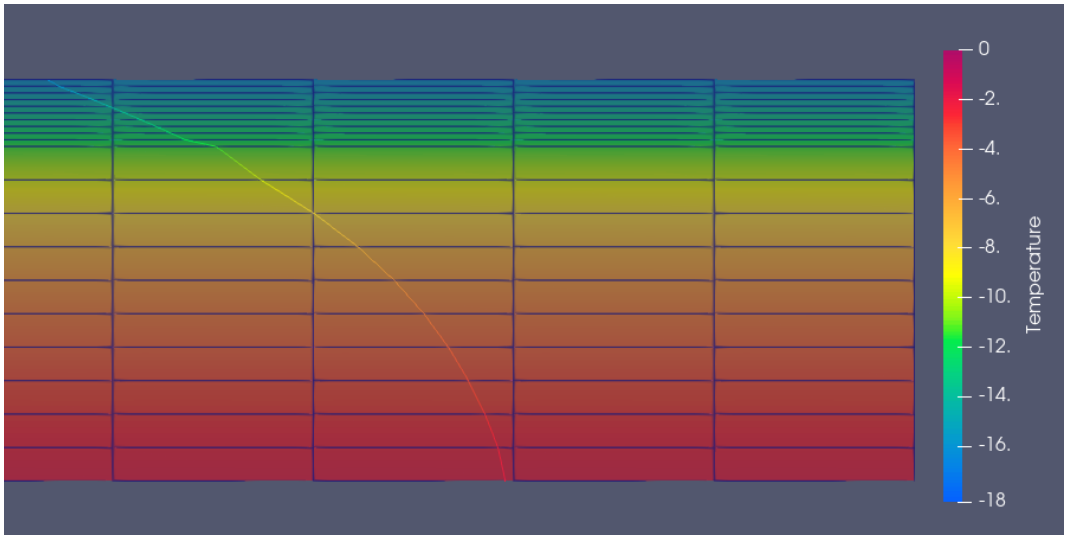


*Figure 65 Maximal vertical temperature difference reached at t=28 h*

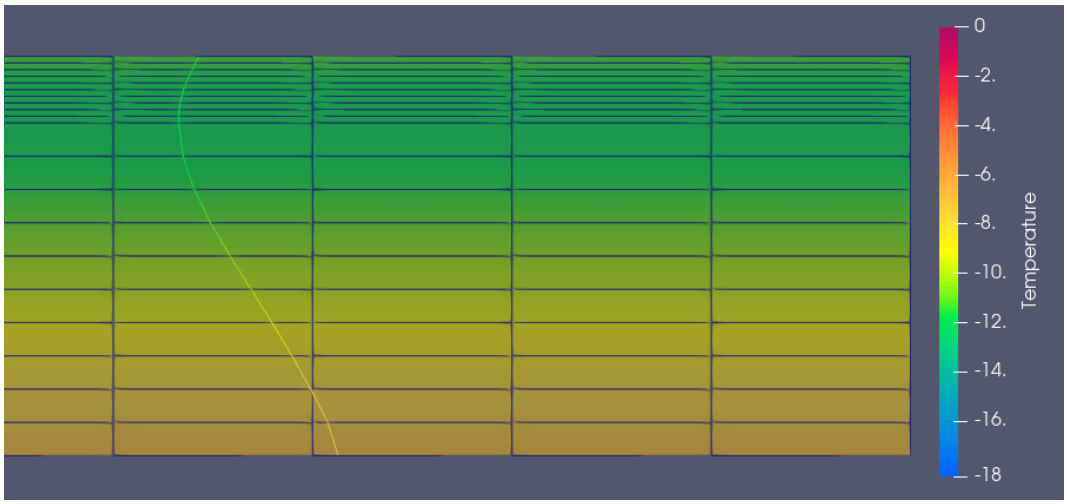


*Figure 66 Cooling of external edge, when ambient air temperature falls down in night, t=87h*

Computed data were loaded into table editor, where was temperature development evaluated. As first, temperature development in sensor spots was evaluated in chart, what can be seen in Figure 67. This should represent temperatures, which would be measured, if the modelled situation would occur in reality. From this chart, convergence to settled temperature development is nicely visible. In this state, surface temperature of concrete varies between -12 °C to -18 °C and temperature of contact between concrete and soil reaches approximately -10 °C. Time shift between individual lines is caused by time delay, which arises from time needed for heat transfer processes.

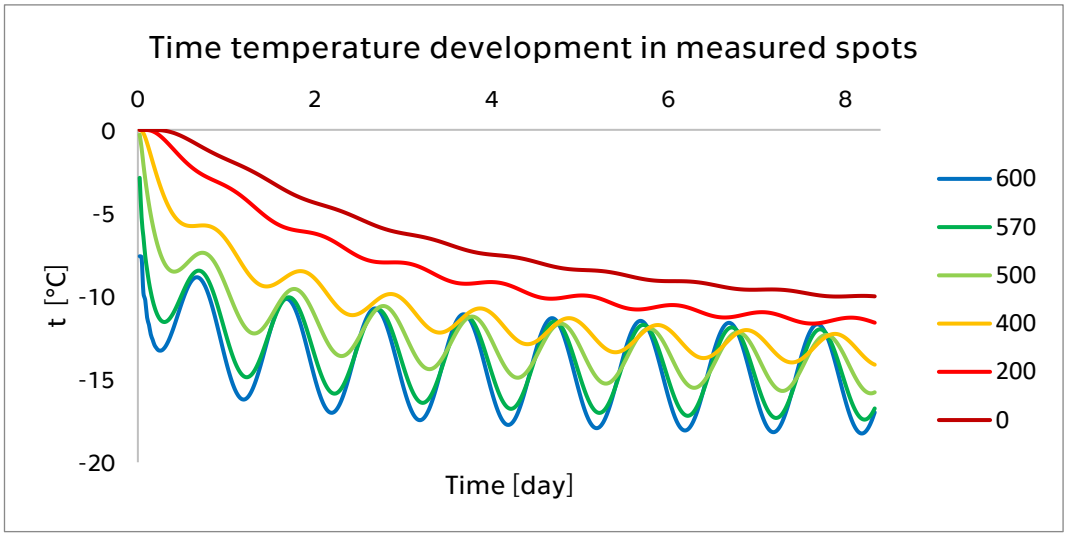


*Figure 67 Temperature development in sensor spots, surface is represented by blue line (600 > 600 mm from contact soil-concrete), contact with soil by dark red line*

However, most important and interesting are vertical temperature differences along the thickness of shaft. These were evaluated for five most extreme situations reached during considered time period of 200 hours. These profiles are shown in chart in Figure 68 and will be used for comparative computation of inner forces on simplified bridge model.

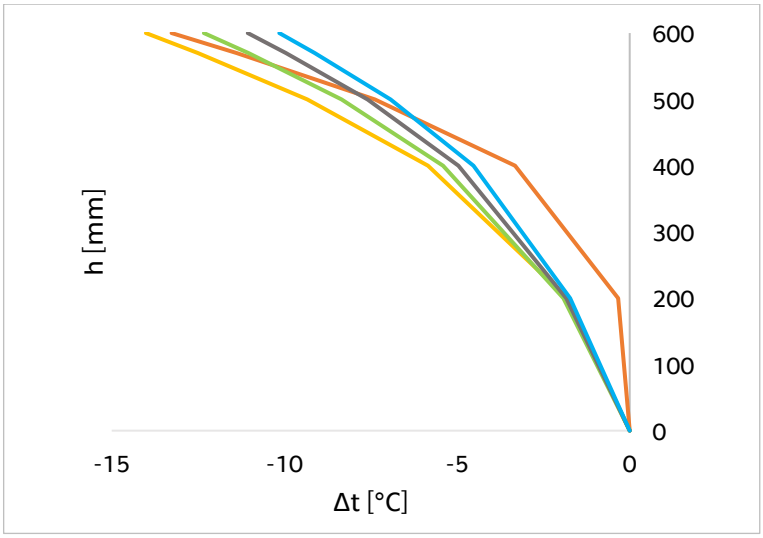


*Figure 68 Five maximal temperature vertical differences during loading period*

### 6.2.3 Maximal temperature

In the second step, model of abutment was loaded by maximal temperature profile. Profile expects warm summer day with maximal temperature of 35 °C (maximal reached temperature was 34,8 °C) and minimal temperature of 21 °C in the night. Period of time was 200 hours and initial temperature 20 °C.

$$t(t) = 7 \sin\left[\left(\frac{2\pi}{86400}\right) * (t - 9 * 3600)\right] + 28$$

Extremes of vertical temperature difference occurs in period of heating in the morning, what is shown in Figure 69. Average temperature of concrete rises in time, however significant fluctuation run in the surface parts. Other figure shows surface cooling in the night.

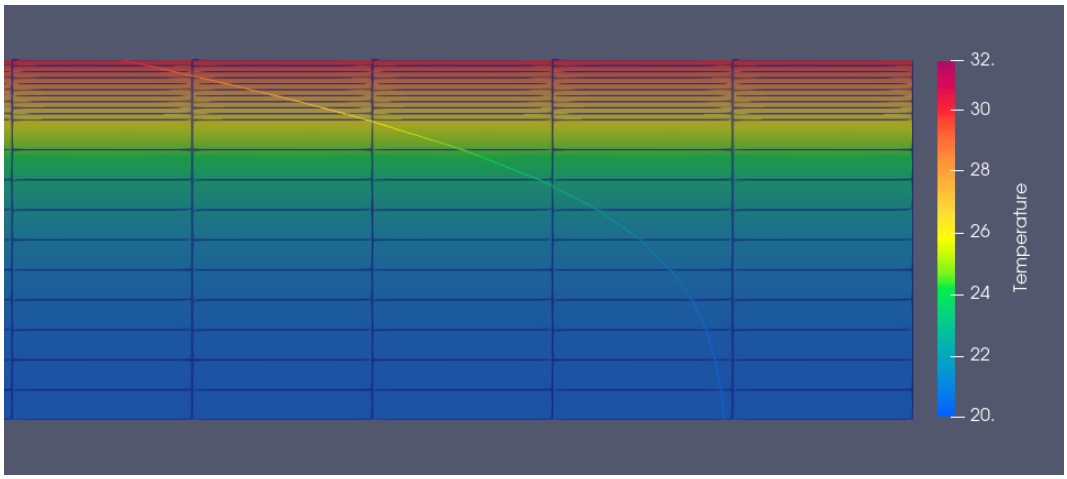


*Figure 69 Maximal vertical temperature difference occurs in t=16,5h*

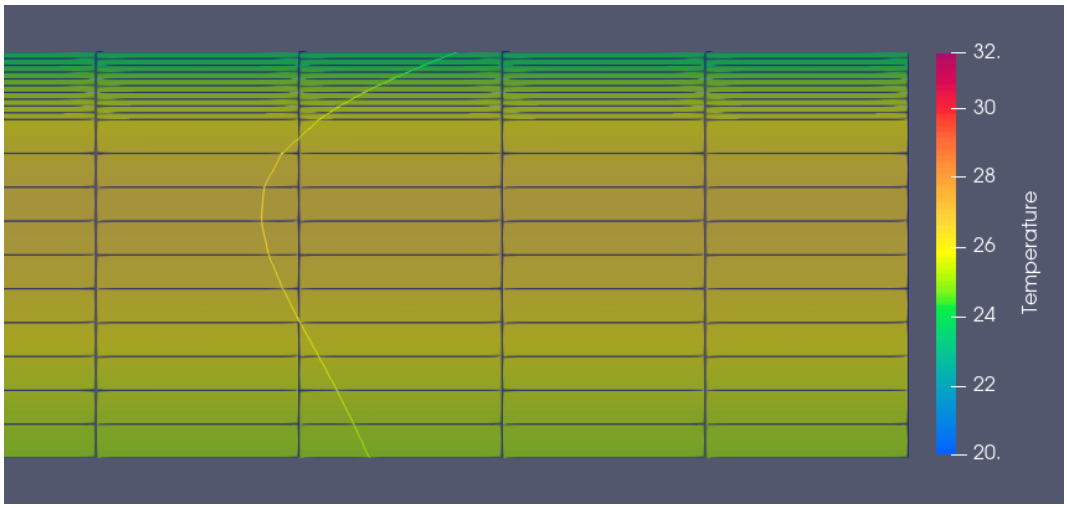


*Figure 70 Cooling of concrete surface in the night in t=171,5h*

Temperature values reached in spots, where sensors are designed are shown in Figure 71. Spots are marked according to their distance from contact soil-concrete in millimetres. Settled temperature fluctuation occurs on surface approximately after three days, on the soil-concrete contact is not finally settled even after eight days.

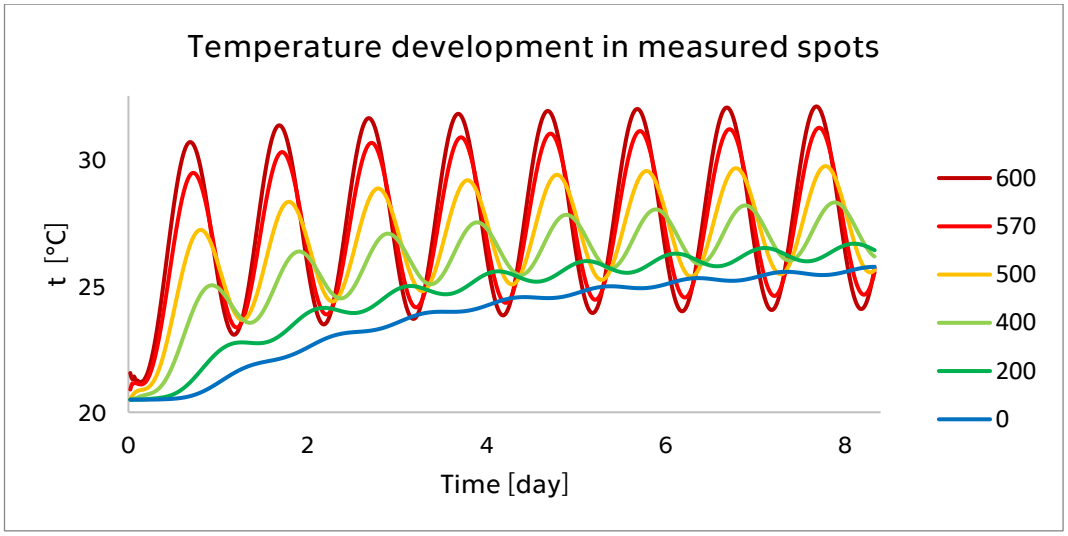


*Figure 71 Temperature development in sensor spots, surface is represented by dark red line (600 > 600 mm from contact soil-concrete), contact with soil by blue line*

Maximal vertical temperature differences are shown in chart in Figure 72. Differences are gradually declining, while the settled time-temperature development is being reached. If the values from modelling are compared to values demanded by standard, values from model are 2-3 times larger than standard values (5 °C vertical temperature difference).

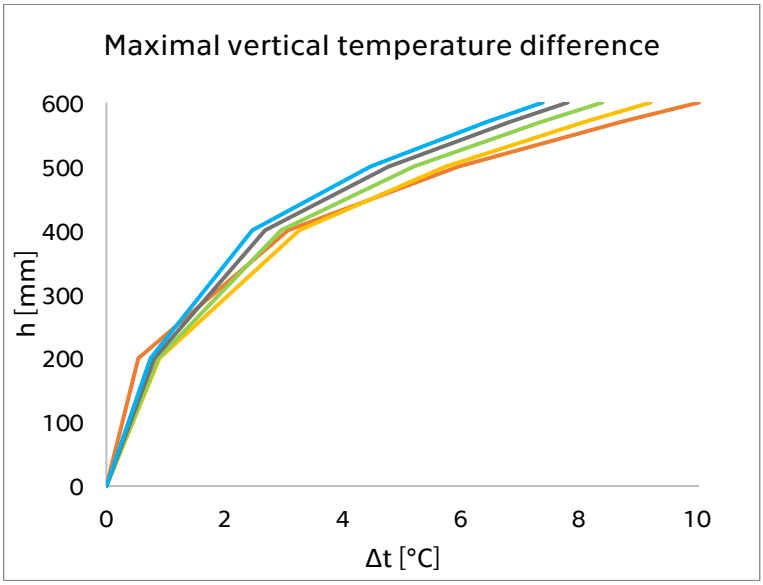


*Figure 72 Five maximal temperature vertical differences during loading period*

### 6.2.4 Maximal temperature fluctuation

Third model situation being evaluated on abutment was day with maximal temperature fluctuation. It might be considered as a day with high afternoon temperatures, which falls deep in the night before dawn. This period occurs in the early autumn months and is called Indian summer.

$$t(t) = 13 \sin\left[\left(\frac{2\pi}{86400}\right) * (t - 9 * 3600)\right] + 13$$

Representative day with extreme temperature fluctuation was modelled. Maximal temperature is 26 °C and minimal during the night falls to 0 °C (ground frosts). Initial temperature was set to 10 °C and period of time to 200 hours.

Extremes are reached in the morning heating, similar to the model with maximal temperature. Some situations are shown in figures. Maximal vertical temperature difference occurs in early time of 16,5 hours. However, it is affected by initial condition and would be more suitable to consider situations after specific period of time.

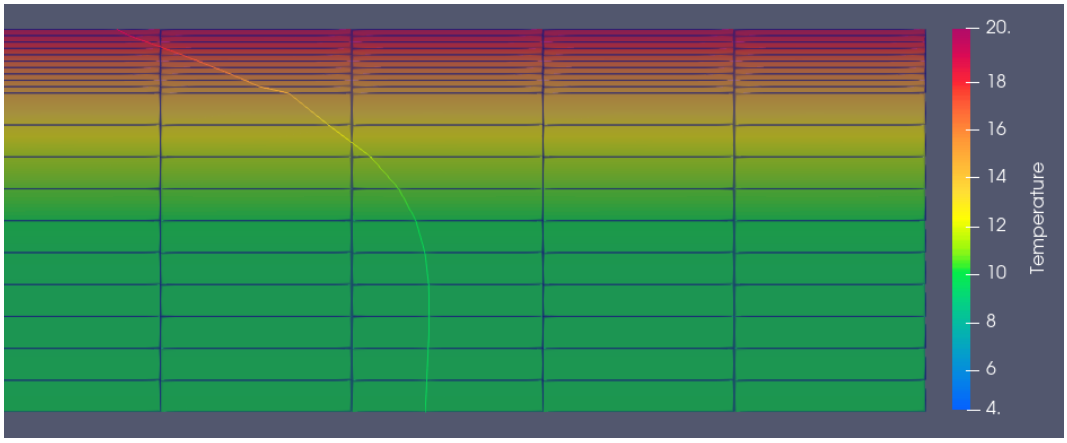


*Figure 73 Maximal vertical temperature difference occurs in t=16,5h*

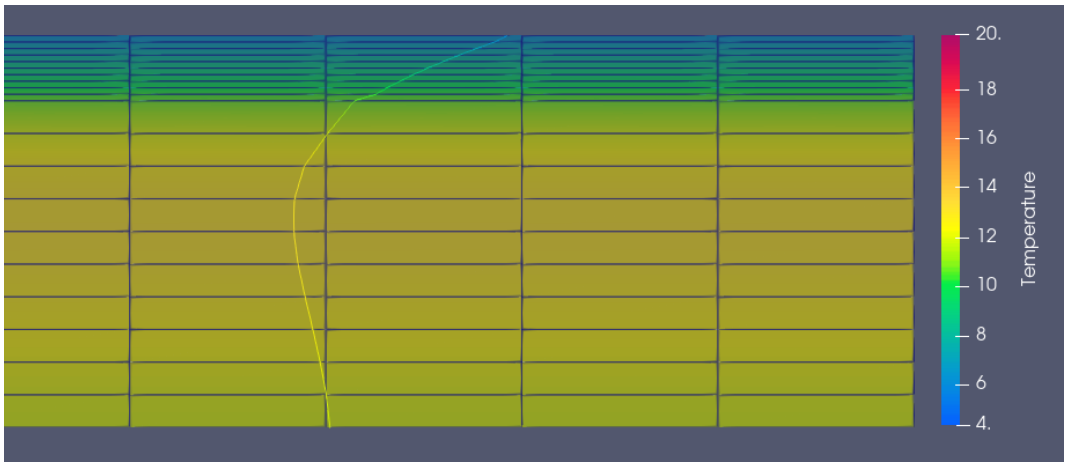


*Figure 74 Surface cooling in t=171h*

Temperature development in the measured spots shows that initial condition was chosen more suitable in this case. Settled temperature development on the surface occurs after only a day. On the contact soil-concrete, development might be considered as settled after approximately 5 days.

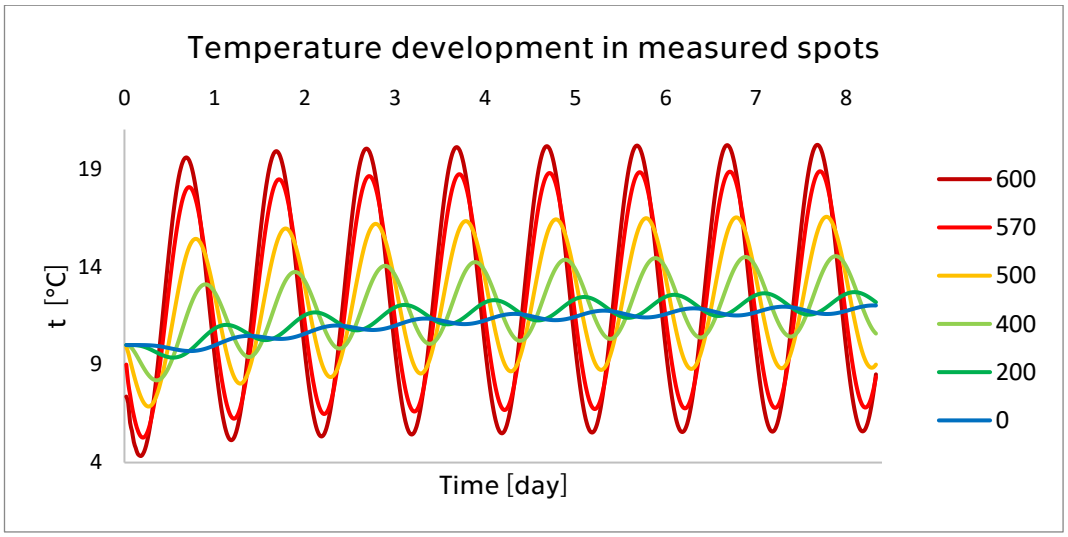


*Figure 75 Temperature development in sensor spots, surface is represented by dark red line (600 > 600 mm from contact soil-concrete), contact with soil by blue line*

Better selection of initial condition will manifest in the following figure, showing vertical temperature differences. Maximal differences reach similar values over whole evaluated period of time. As in the last two models, values considerably exceed values given by standard.

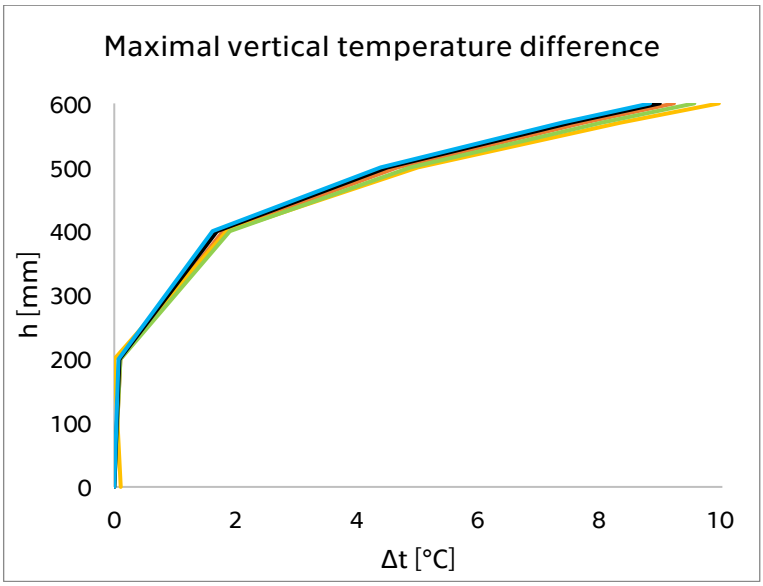


*Figure 76 Five maximal temperature vertical differences during loading period*

## 6.3 Bridge deck model – under traffic lane

### 6.3.1 Model description

Second model is dedicated to spot under traffic lane in bridge deck. Model consist of cut out from cross-section of bridge deck. Model contains all materials of bearing structure, insulation and layers of roadway. Bearing structure is a composition of steel filler beams, CETRIS plates and concrete, which fills whole remaining area. On the top of concrete, insulation made of asphalt strips (NAIP) is made. Three layers of different asphalt concretes are laid on the insulation. These three layers are modelled as one layer, while the thermal parameters are similar and would have be necessary to obtain them experimentally.

Filler beams are of HEB240 profile with narrowed top flange. On the bottom flanges, CETRIS plate of 20 mm thickness is put as lost formwork. Concrete layer of 280 mm thickness is concreted. Insulation layer (NAIP) is 10 mm thick. Three layers of asphalt concrete are embedded into one, 135 mm thick. Whole model is 1200 mm wide.

Triangular mesh with minimal element size of 5 mm edge is used. Maximal element size with 100 mm is set. Initial condition represents initial temperature of all nodes varying to situation being solved. Three boundary conditions are used on the top edge of model, Newton's (contact with ambient air), Stefan-Boltzmann's (heat radiation) and Neumann's (sun glare). On the bottom edge is Neumann's boundary condition omitted. Temperature and glare functions are set according to available information.

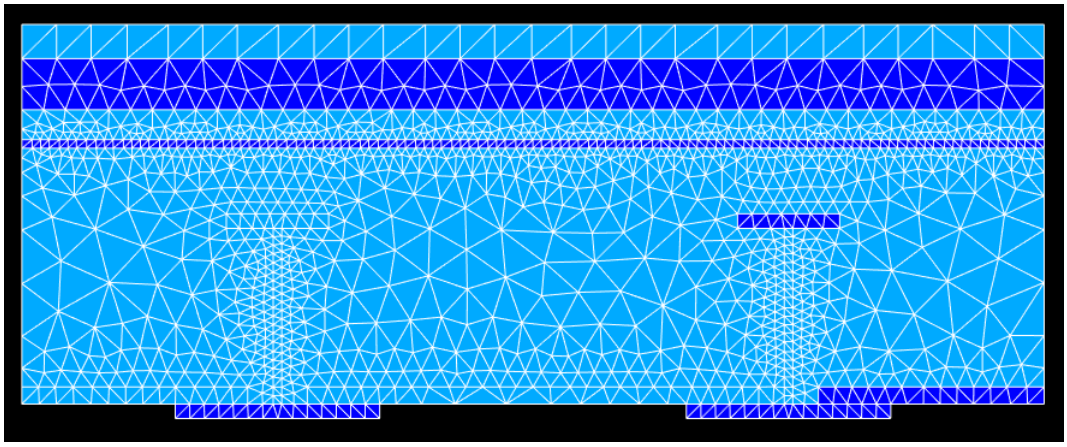

*Figure 77 Model of spot in bridge deck under traffic lane with created mesh*

Material properties are set as follows (27)

Concrete

- $c=770\ Jkg^{-1}K^{-1}$
- $\lambda=2{,}2\ Wm^{-1}K^{-1}$
- $\gamma=2250\ kgm^{-3}$
- $\varepsilon=0{,}85$

Steel

- $c=490\ Jkg^{-1}K^{-1}$
- $\lambda=54\ Wm^{-1}K^{-1}$
- $\gamma=7850\ kgm^{-3}$
- $\varepsilon=0{,}79$

CETRIS plate
- c=1270 $Jkg^{-1}K^{-1}$
- λ=0,251 $Wm^{-1}K^{-1}$
- γ=1350 $kgm^{-3}$
- ε=0,85

NAIP insulation
- c=1600 $Jkg^{-1}K^{-1}$
- λ=0,75 $Wm^{-1}K^{-1}$
- γ=1041 $kgm^{-3}$

Asphalt concrete
- c=920 $Jkg^{-1}K^{-1}$
- λ=1,6 $Wm^{-1}K^{-1}$
- γ=2400 $kgm^{-3}$
- ε=0,93

### 6.3.2 Minimal temperature

Model of bridge deck under traffic lane was in the first step loaded by minimal temperature profile, which is most simple. Same model day as in the abutment model was used, temperature development is given by following function:

$$t(t) = 6\sin\left[\left(\frac{2\pi}{86400}\right) * (t - 9 * 3600)\right] - 16$$

Initial temperature was set to 0°C and period of time to 200 hours. Following figures are showing temperature profiles in specific situations.

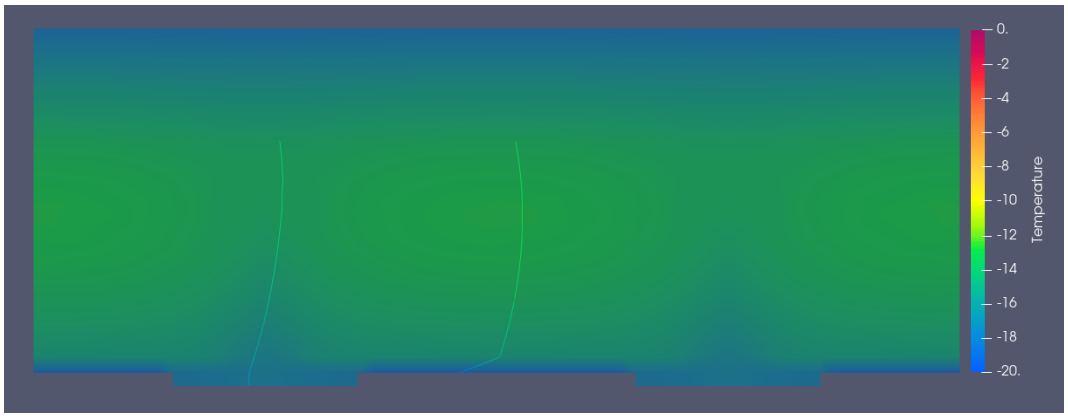


*Figure 78 Maximal vertical temperature difference occurs in t=28h*

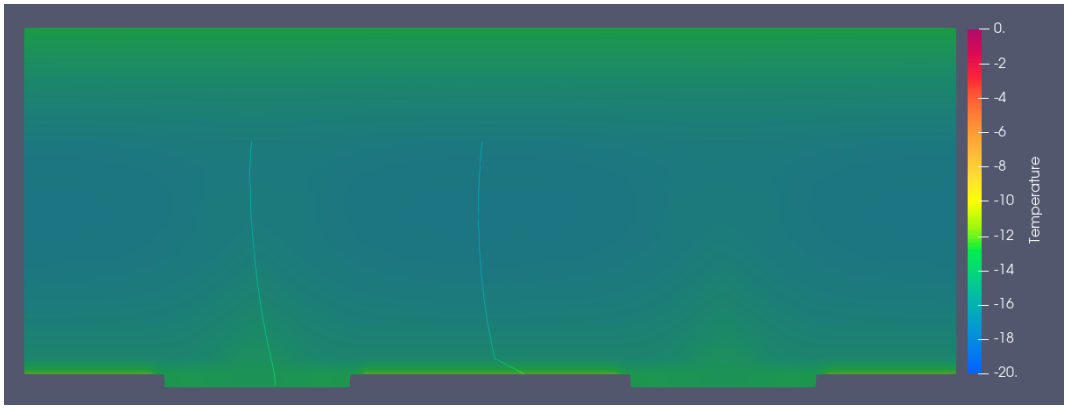


*Figure 79 Heating of both surfaces in t=183 h*

Time-temperature development and vertical temperature differences are evaluated on this model twice. First evaluation covers measured spots in concrete, second covers other spots on steel. In the following figure, temperature development in concrete is shown. Due to subtility of structure and conductivity of materials, cooling of cross-section is quick, therefore thermal fluctuations are lower. Waveforms in chart represent measured spots by their distance from contact CETRIS-concrete (bottom of concrete layer).

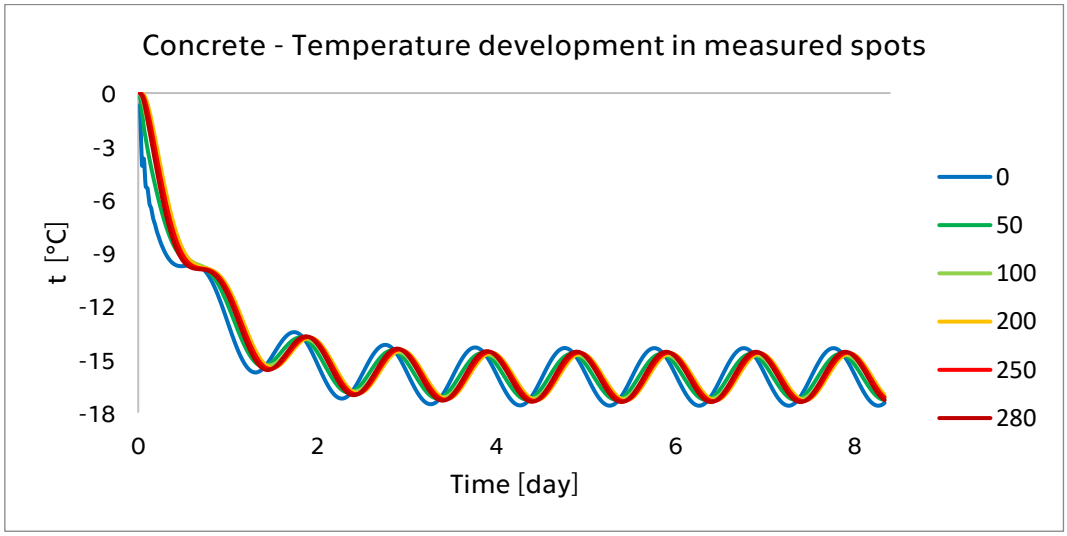


*Figure 80 Temperature development in sensor spots, bottom is represented by blue line (0 > 0 mm from contact CETRIS-concrete), contact with asphalt insulation by red line*

Vertical temperature differences are evaluated after settling to values without inadequate fluctuations. Reached values are considerably low, what is given by subtility of cross-section. Peak in the height of 200 mm is caused by cooling from both surfaces. Effect of cooling from the top surface influences temperature of concrete from the top.

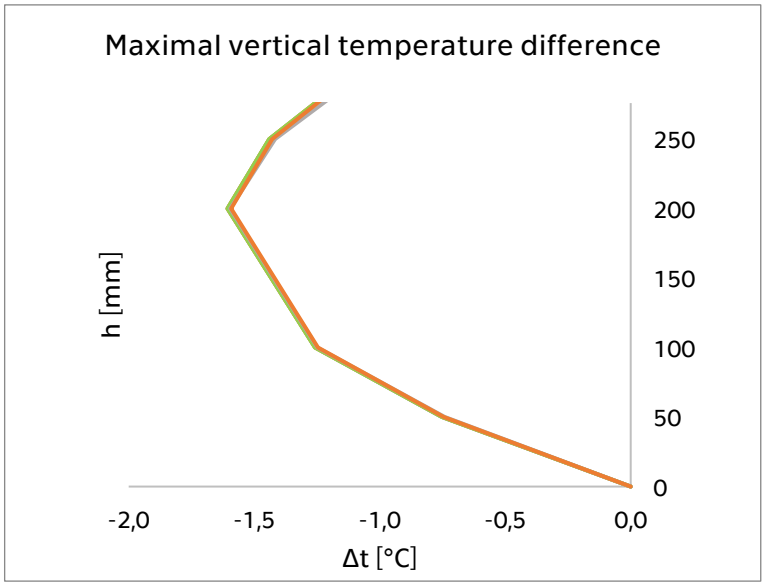


*Figure 81 Concrete - five maximal temperature vertical differences during loading period*

Fluctuations reached on steel beam are slightly higher in comparation to those in concrete. It is given by heat conductivity of steel, which is multiple times higher than the one valid for concrete and its lower specific heat capacity.

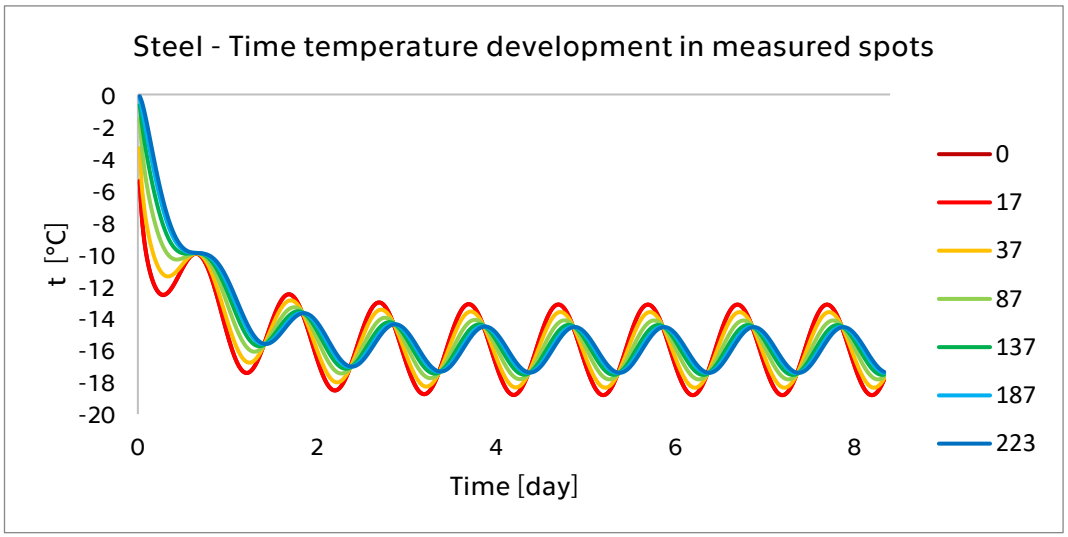


*Figure 82 Temperature development in sensor spots, bottom is represented by dark red line (0 > 0 mm from bottom surface of steel), bottom surface of top flange by dark blue line*

Similar to vertical differences in concrete are vertical temperature difference along the height of steel beam. However, in this case peak is not present, what might be caused by the conductivity of steel.

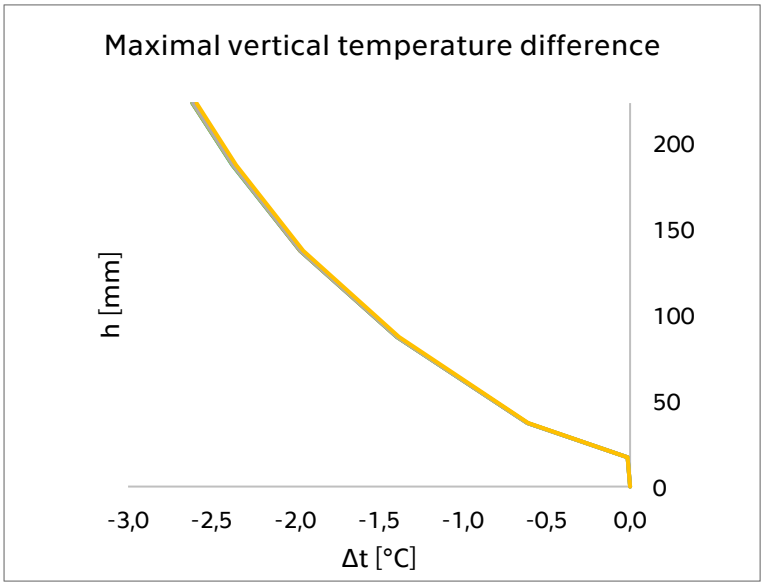


*Figure 83 Steel - five maximal temperature vertical differences during loading period*

### 6.3.3 Maximal temperature

Significant difference to previous situations comes in the model situation of deck loaded by maximal temperature. Except of classic time-temperature development function is model loaded also by glare. Glare is represented by time-dependent function of heat flow. This function might be seen below, marked as *Q(t)*. To ensure exclusion of negative part of sine wave, Heaviside step function was used.

$$t(t) = 7\sin\left[\left(\frac{2\pi}{86400}\right) * (t - 9 * 3600)\right] + 28$$

$$Q(t) = 200 * \sin\left[0.85\left(\frac{2\pi}{86400}\right) * (int(t - 6 * 3600) mod 86400)\right]$$
$$* H\left\{\sin\left[0.85\left(\frac{2\pi}{86400}\right) * (int(t - 6 * 3600) mod 86400)\right]\right\}$$

Temperatures during the model day and therefore whole function of ambient air temperature is the same as the one in chapter 6.2.4. For the purpose of heat flow function, amplitude of 200 W was used. This value was chosen after proper consideration of available sources. Initial temperature of structure was set to 20 °C and period of time for evaluation was set to 200 hours. (26)

Examples of results might be seen in following figures. Glare has very significant impact to heating of asphalt layers and therefore also heating of top of concrete slab.

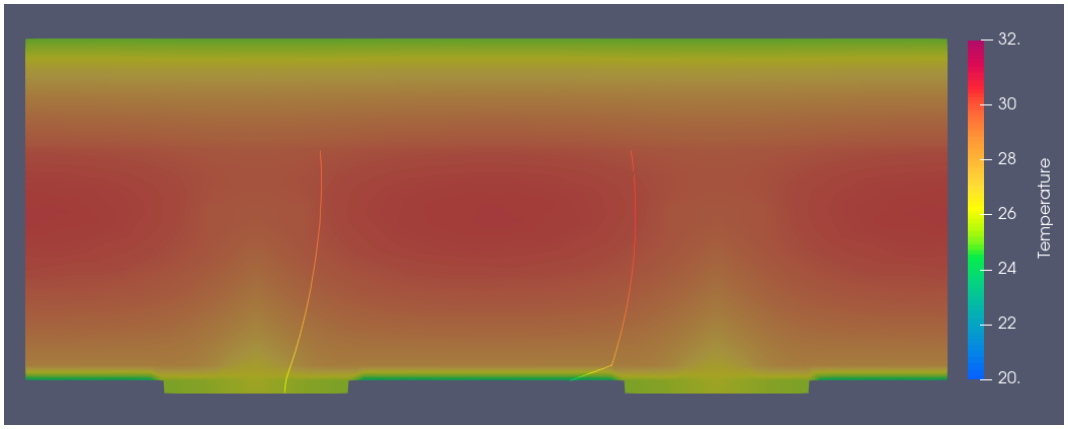


*Figure 84 Cooling of both surfaces during the night in t=146,5 h*

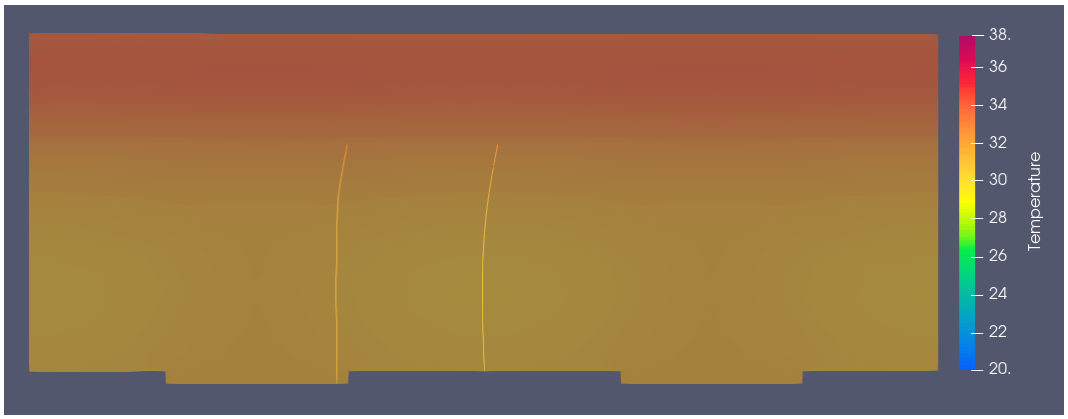


*Figure 85 Relatively balanced temperature both in steel and concrete in t=67,5 h*

Thanks to the heat flow from glare, bridge deck is heated to settled average temperature much sooner than it was in the previous examples. In case of minimal temperature on bridge deck, settled temperature development occurred approximately after 3-4 days. In this case, settled temperature development in concrete occurred after about 1,5-2 days.

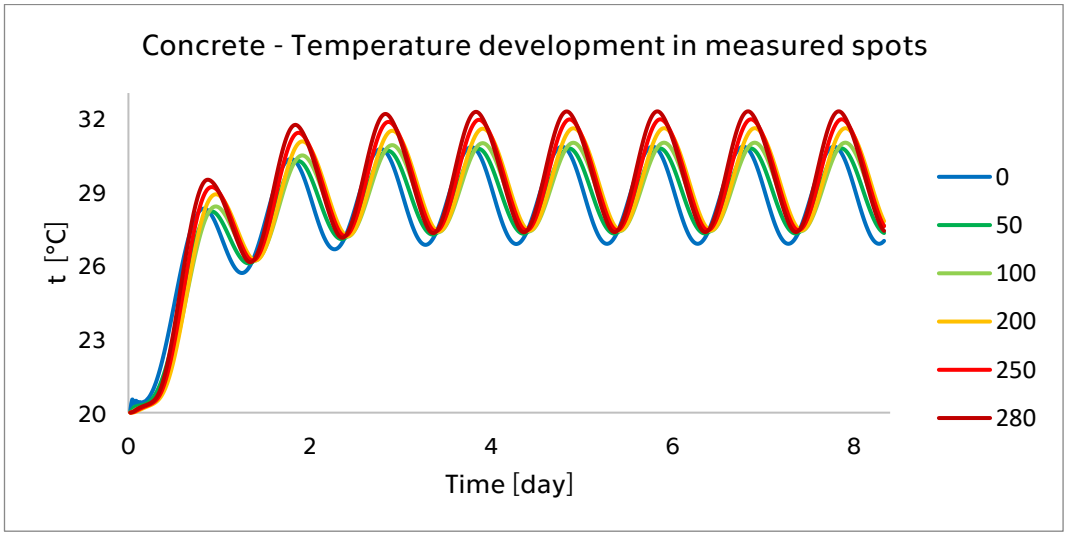


*Figure 86 Temperature development in sensor spots, bottom is represented by blue line (0 > 0 mm from contact CETRIS-concrete), contact with asphalt insulation by red line*

Settling rate of temperature fluctuation in concrete manifested also in vertical temperature differences, which are after 2 days practically identic over all of the rest of time period. Again, cooling or heating from top surface of roadway makes an impact to vertical temperature difference.

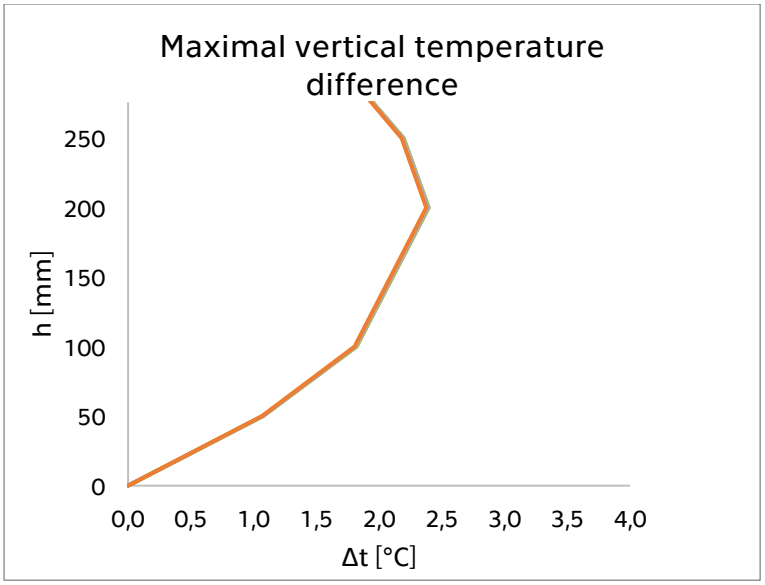


*Figure 87 Concrete - five maximal temperature vertical differences during loading period*

In case of steel filler beam is situation similar except of amplitudes of temperature fluctuations. Higher amplitudes are caused by significantly higher heat conductivity and lower specific heat capacity of steel in comparison with concrete. As might be seen from following figure, temperatures in the top and bottom of the bottom flange are nearly identic. However, amplitudes of temperature fluctuation in the spots in web are lower. This should be caused by cooling effect of surrounding concrete.

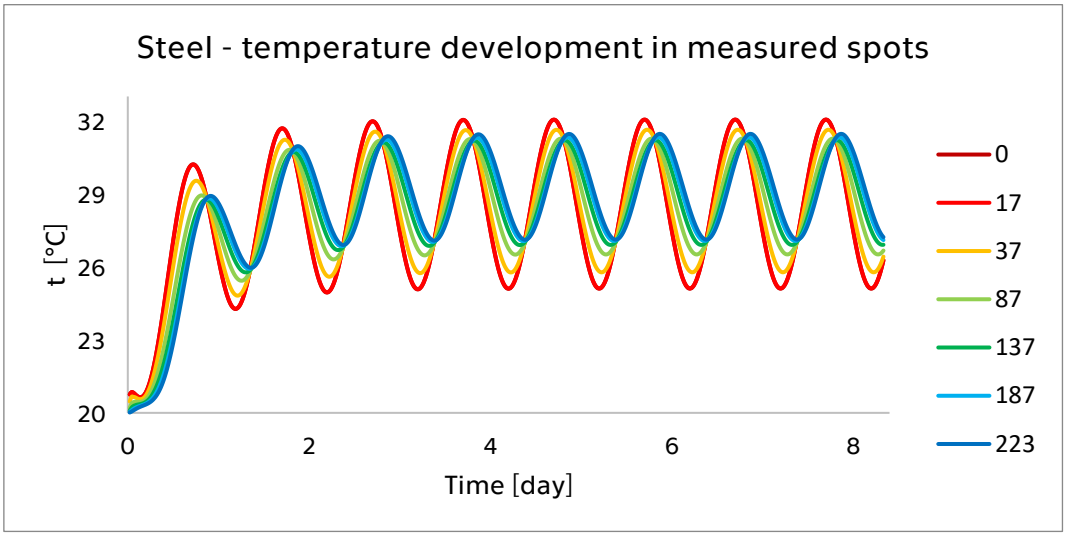


*Figure 88 Temperature development in sensor spots, bottom is represented by dark red line (0 > 0 mm from bottom surface of steel), bottom surface of top flange by dark blue line*

Situation described in last paragraph might be also seen in Figure 89, temperature differences in bottom flange are almost zero.

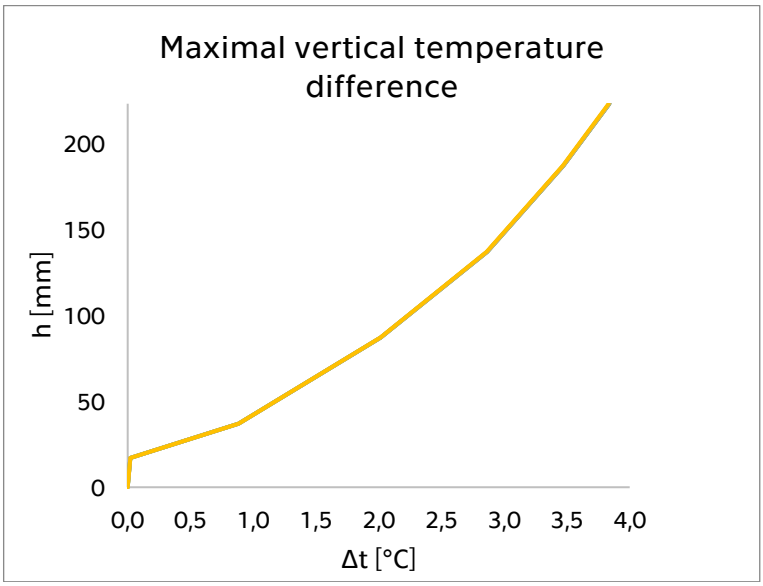


*Figure 89 Steel - five maximal temperature vertical differences during loading period*

### 6.3.4 Maximal temperature fluctuation

Loading of last model of bridge deck under traffic lane is very similar to previous models. Temperature development of ambient air is taken from abutment model and heat flow from previous model situation. Period of time is 200 hours again and initial temperature was set to 10 °C.

$$t(t) = 13\sin\left[\left(\frac{2\pi}{86400}\right) * (t - 9 * 3600)\right] + 13$$

$$Q(t) = 200 * \sin\left[0.85\left(\frac{2\pi}{86400}\right) * (int(t - 6 * 3600) mod 86400)\right]$$
$$* H\left\{\sin\left[0.85\left(\frac{2\pi}{86400}\right) * (int(t - 6 * 3600) mod 86400)\right]\right\}$$

Significant effect of glare heating might be seen again. However, extreme vertical temperature difference occurs during night cooling.

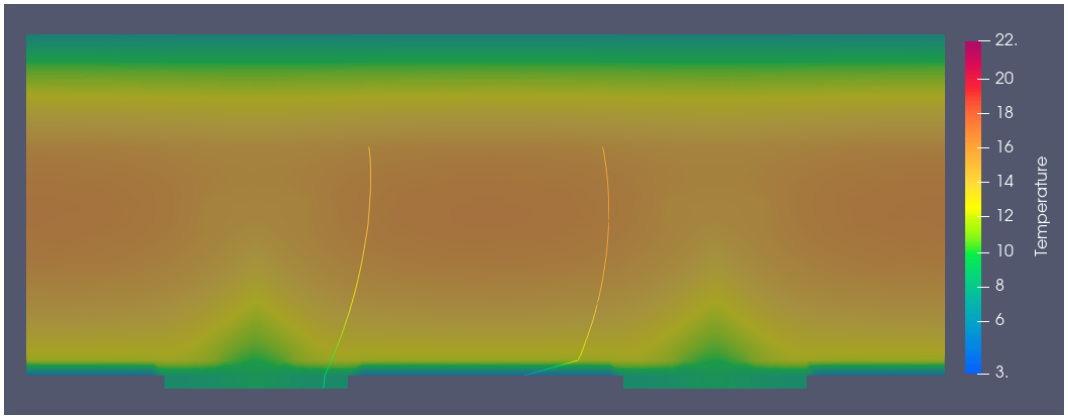


*Figure 90 Cooling of both surfaces during the night in t=170,5 h*

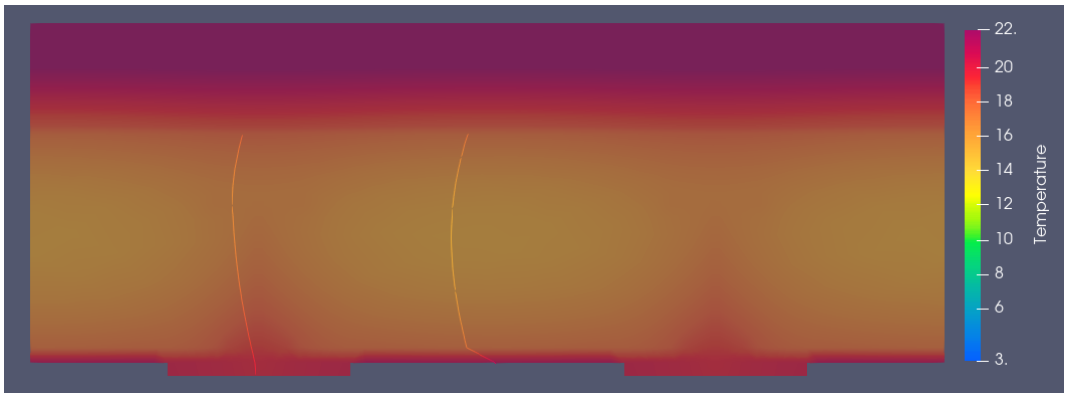


*Figure 91 Heating of both surfaces with significant effect of glare in t=65,5 h*

Proper initial condition ensured quick settlement of temperature fluctuation in concrete and steel. Fluctuation settles after about 1,5-2 days.

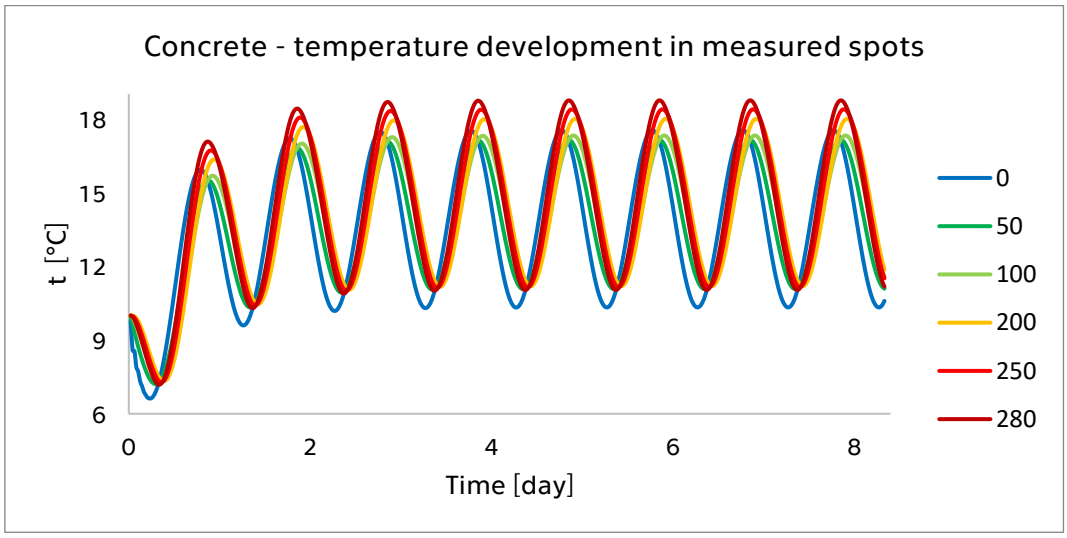


*Figure 92 Temperature development in sensor spots, bottom is represented by blue line (0 > 0 mm from contact CETRIS-concrete), contact with asphalt insulation by red line*

Again, quick settlement causes almost identic vertical temperature differences during whole time period. Unlike last two model situations, vertical temperature difference values are reaching higher values, close to difference of 4 °C.

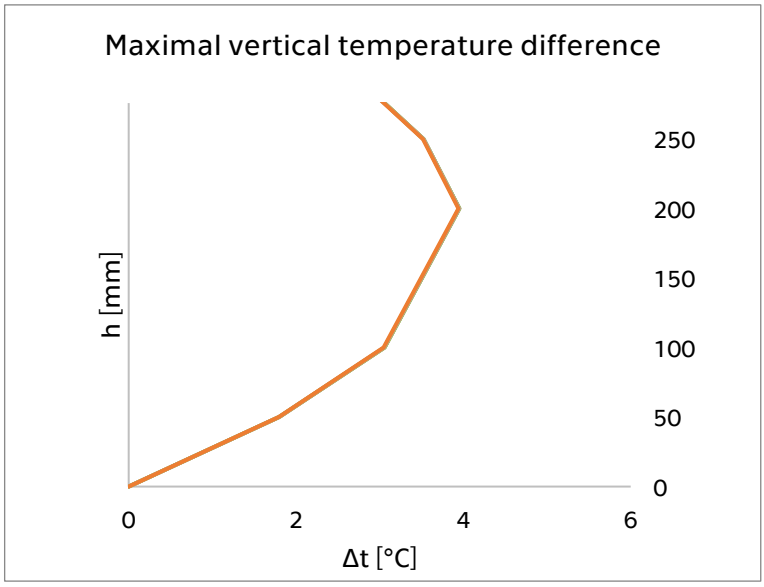


*Figure 93 Concrete - five maximal temperature vertical differences during loading period*

Temperature fluctuation reached in steel settles in similar time to those in concrete. It is caused by significant impact of concrete to steel temperature. Without concrete, temperature fluctuation in steel would be settled sooner. Higher amplitudes are caused by high heat conductivity and lower specific heat capacity of steel.

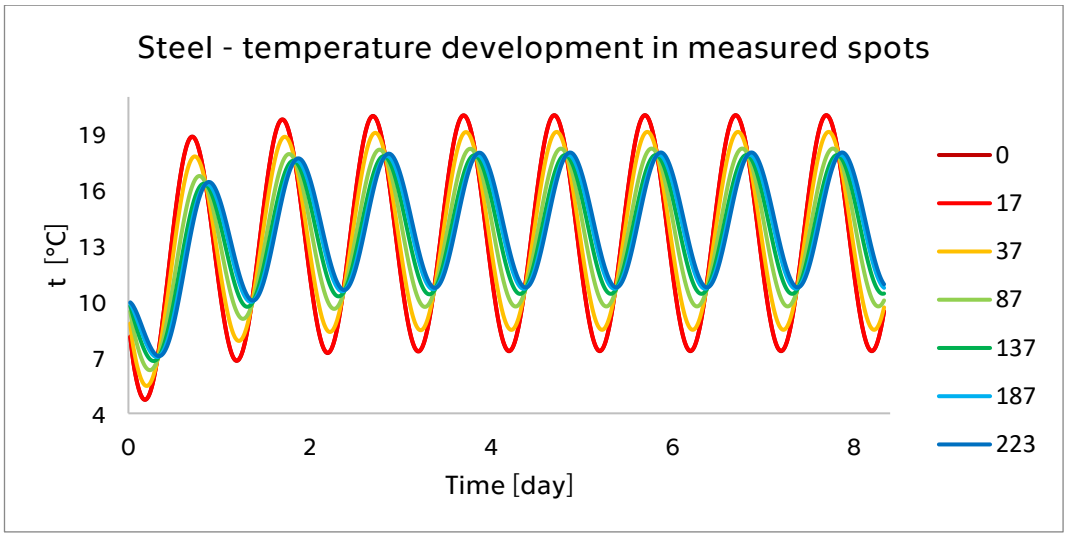


*Figure 94 Temperature development in sensor spots, bottom is represented by dark red line (0 > 0 mm from bottom surface of steel), bottom surface of top flange by dark blue line*

Maximal vertical temperature differences in this case reach relatively higher values, about 6,5 °C.

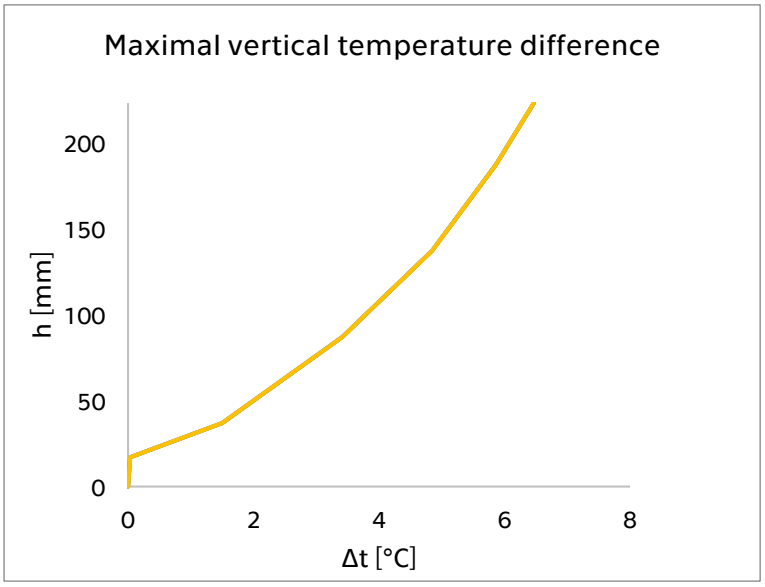


*Figure 95 Steel - five maximal temperature vertical differences during loading period*

## 6.4 Bridge deck model – under pavement

### 6.4.1 Model description

Third and last model is situated on the edge of cross-section under pavement. Model consist of cut out from cross-section of bridge deck. Model contains all materials of bearing structure and layers of pavement. Bearing structure is a composition of steel filler beams, CETRIS plates and concrete, which fills whole remaining area. Pavement consist of two layers, bed layer of concrete and granite pavement.

Filler beams are of HEA300 profile with narrowed top flange. On the bottom flanges, CETRIS plate of 20 mm thickness is put as lost formwork. Concrete layer of 440 mm thickness is concreted. Concrete bed layer of pavement is 100 mm thick with 200 mm thick layer of granite pavement on it. Whole model is 1200 mm wide.

Triangular mesh with minimal element size of 5 mm edge is used. Maximal element size with 100 mm is set. Initial condition represents initial temperature of all nodes varying to situation being solved. Three boundary conditions are used on the top edge of model, Newton's (contact with ambient air), Stefan-Boltzmann's (heat radiation) and Neumann's (sun glare). On the bottom edge is Neumann's boundary condition omitted. Temperature and glare functions are set according to available information.

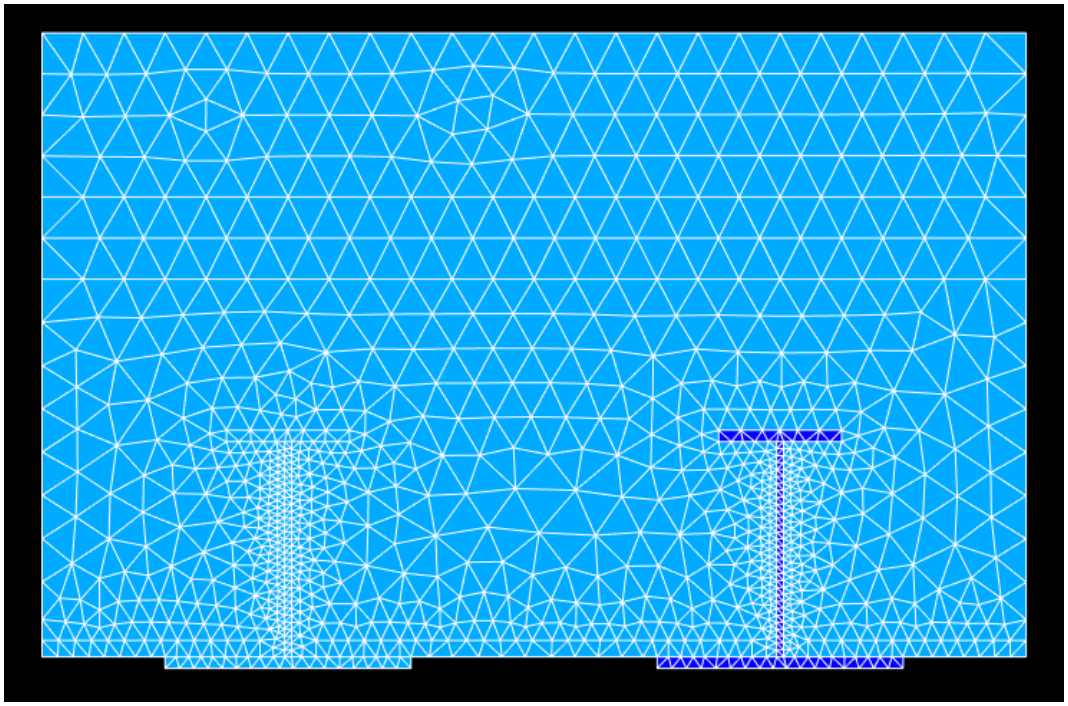

*Figure 96 Model of spot in bridge deck under pavement with created mesh*

Material properties are set as follows (27)

Concrete
- c=770 $Jkg^{-1}K^{-1}$
- λ=2,2 $Wm^{-1}K^{-1}$
- γ=2250 $kgm^{-3}$
- ε=0,85

Steel
- c=490 $Jkg^{-1}K^{-1}$
- λ=54 $Wm^{-1}K^{-1}$
- γ=7850 $kgm^{-3}$
- ε=0,79

CETRIS plate
- c=1270 $Jkg^{-1}K^{-1}$
- λ=0,251 $Wm^{-1}K^{-1}$
- γ=1350 $kgm^{-3}$
- ε=0,85

Concrete bed layer
- c=950 $Jkg^{-1}K^{-1}$
- λ=2,0 $Wm^{-1}K^{-1}$
- γ=2200 $kgm^{-3}$

Granite pavement
- c=790 $Jkg^{-1}K^{-1}$
- λ=2,5 $Wm^{-1}K^{-1}$
- γ=2500 $kgm^{-3}$
- ε=0,40

### 6.4.2 Minimal temperature

Third model of structure segment was in first evaluated situation loaded by minimal temperature profile representing winter day. Time-temperature function is the same as used in first two models. Initial condition was set to 0 °C again and period of time to 200 hours.

$$t(t) = 6 \sin\left[\left(\frac{2\pi}{86400}\right) * (t - 9 * 3600)\right] - 16$$

Evaluated results are displayed in following figures, where temperature differences might be visible with accent to profiles, where measurement proceed in reality.

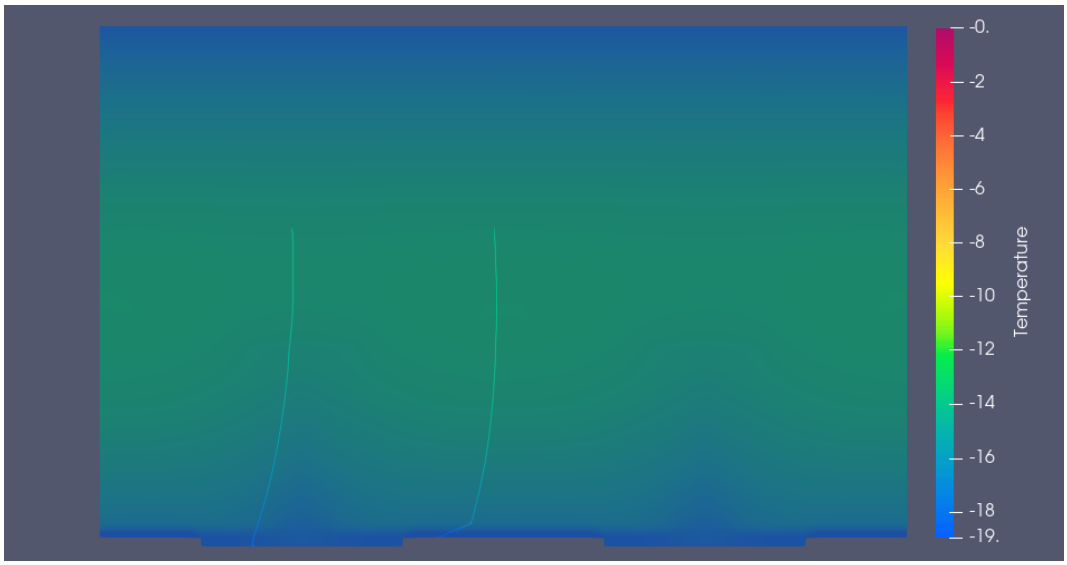


*Figure 97 Cooling of both surfaces during the night in t=75,5 h*

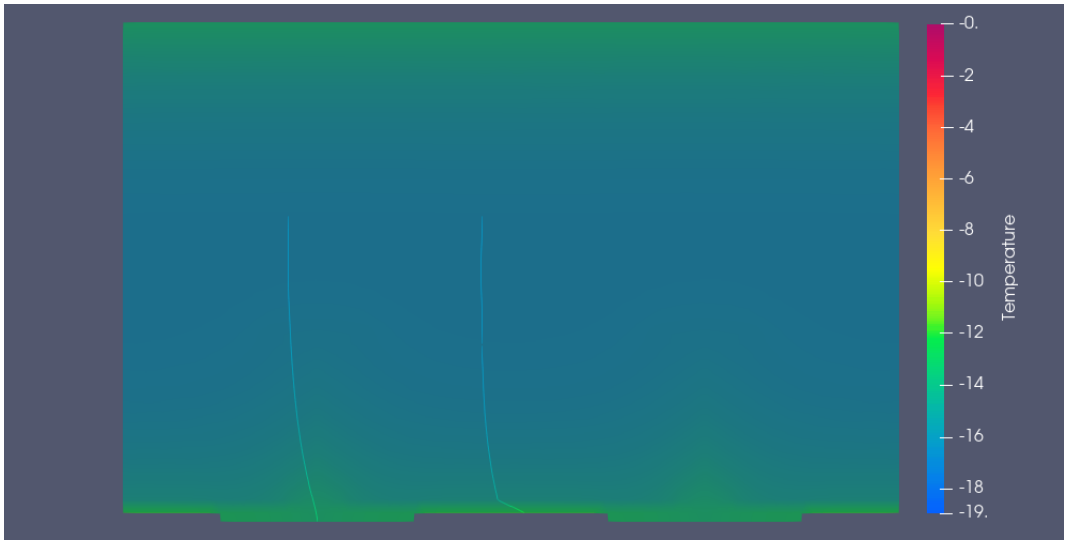


*Figure 98 Heating of both surfaces during the day in t=134,5 h*

This model is in comparation with previous one more massive, what makes differences in amount of time necessary for settlement of temperature fluctuation. Settlement occurs after about 5 days, previous model needed about 3 days for settlement.

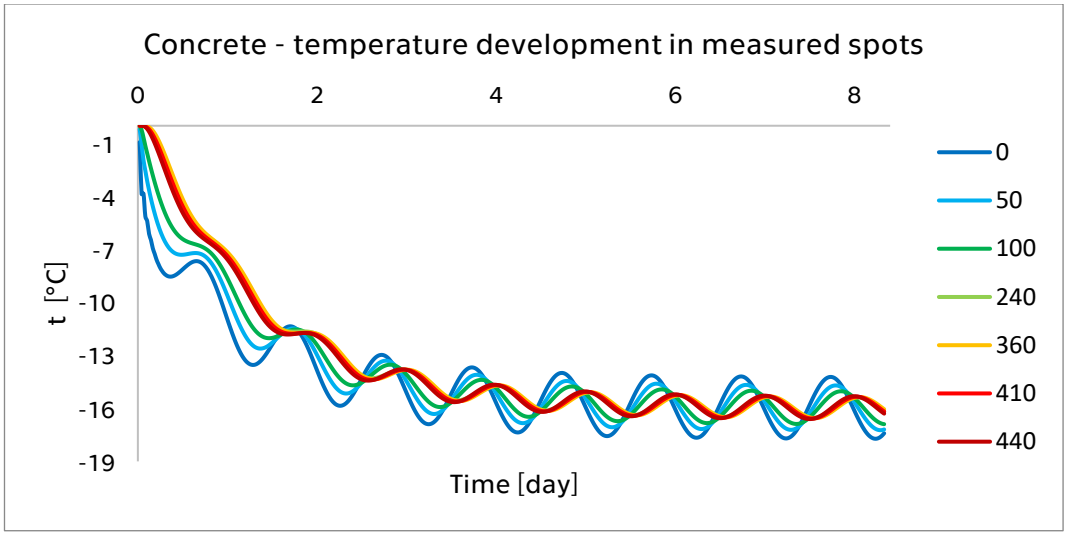


*Figure 99 Temperature development in sensor spots, bottom is represented by blue line (0 > 0 mm from contact CETRIS-concrete), contact with pavement layers by red line*

Slower temperature fluctuation settlement manifests in chart of maximal vertical temperature differences. Individual profiles differ from each other up to 0,5 °C. Heating and cooling effect from the top is also present in this model.

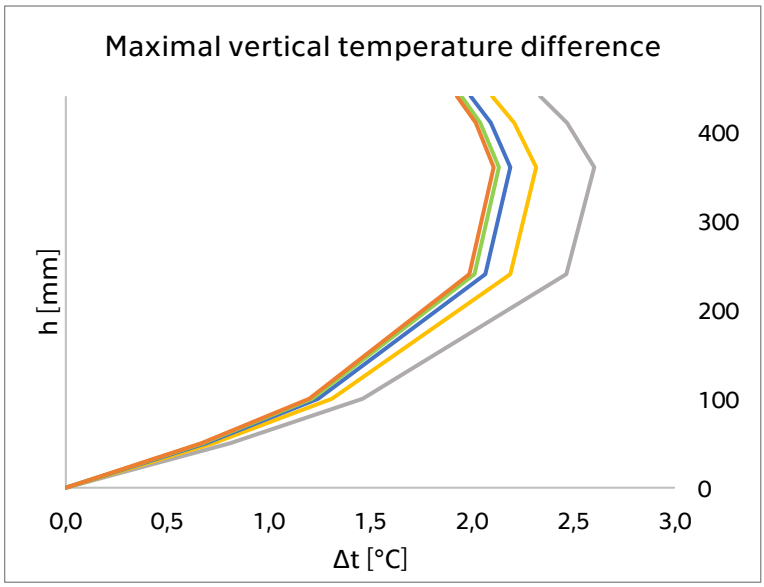


*Figure 100 Concrete - five maximal temperature vertical differences during loading period*

Situation in case of steel filler beam is very similar to situation in concrete and can be seen in following figures.

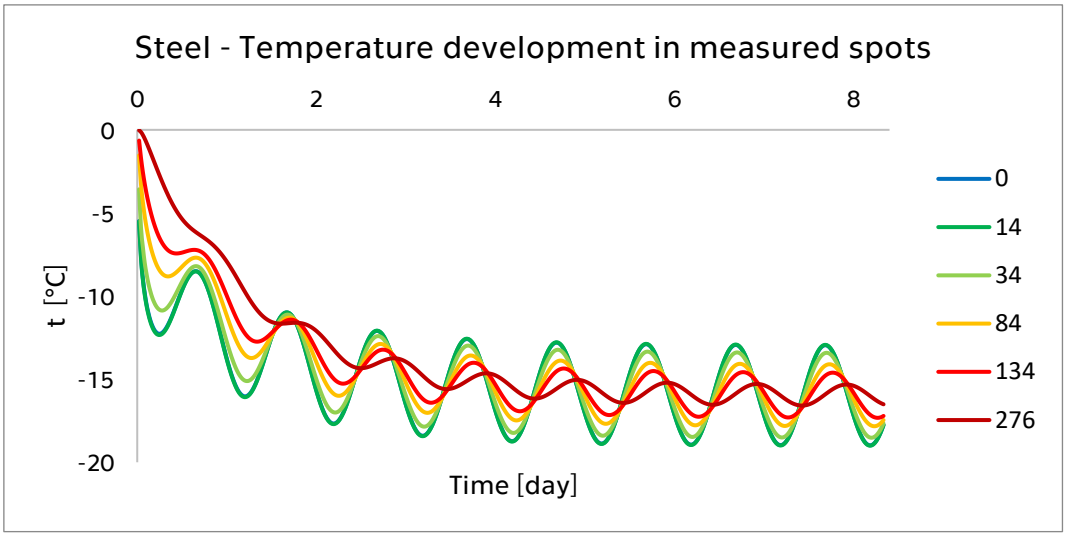


*Figure 101 Temperature development in sensor spots, bottom is represented by dark red line (0 > 0 mm from bottom surface of steel), bottom surface of top flange by dark blue line*

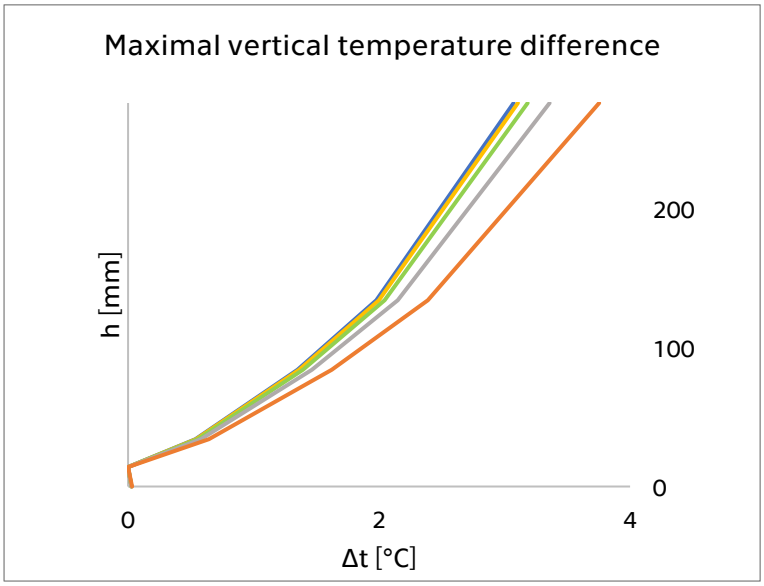


*Figure 102 Steel - five maximal temperature vertical differences during loading period*

### 6.4.3 Maximal temperature

Second evaluated situation of this model was simulation of warmest summer days. Loading functions have been taken over from previous model situations. Initial temperature was set to 20 °C and time period to 200 hours.

$$t(t) = 7\sin\left[\left(\frac{2\pi}{86400}\right) * (t - 9 * 3600)\right] + 28$$

$$Q(t) = 200 * \sin\left[0.85\left(\frac{2\pi}{86400}\right) * (int(t - 6 * 3600) mod 86400)\right]$$
$$* H\left\{\sin\left[0.85\left(\frac{2\pi}{86400}\right) * (int(t - 6 * 3600) mod 86400)\right]\right\}$$

Some typical situations occurring during time period are shown in following figures. Extreme vertical temperature difference occurs during cooling of both surfaces. Significant impact of glare can be seen in Figure 99, where top surface is heated much more.

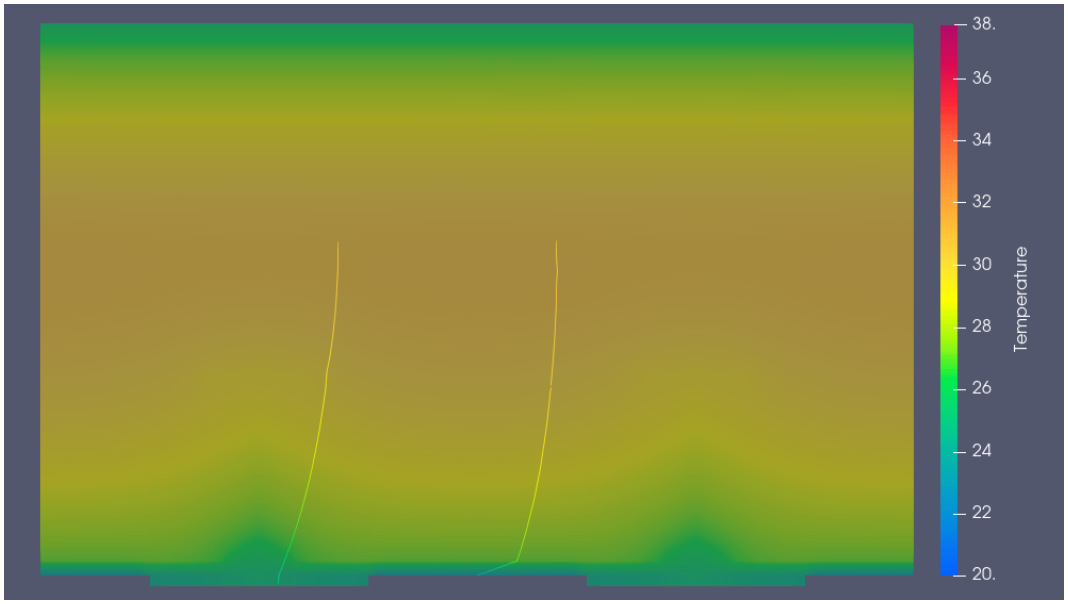


*Figure 103 Cooling of both surfaces during the night in t=171,5 h*

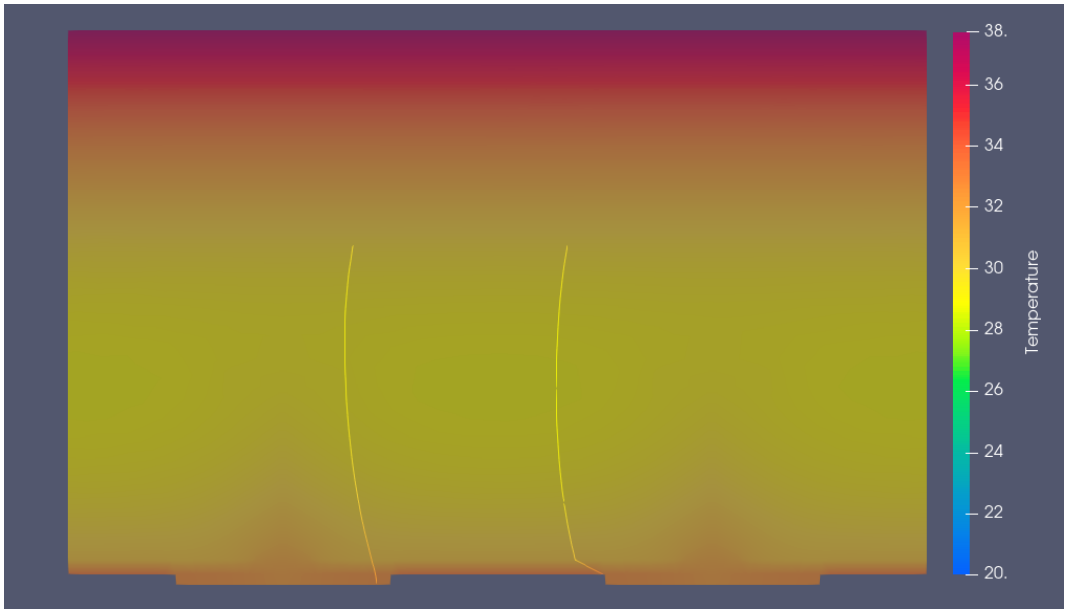


*Figure 104 Heating of both surfaces during the day in t=136 h*

Massiveness of the model results in the time, when settlement of temperature development is reached. It occurs after about four days. In contrast with previous situation, settlement occurs about one day sooner, what should be given by quicker overheating caused by glare. Vertical temperature differences are all similar, varying only in small range.

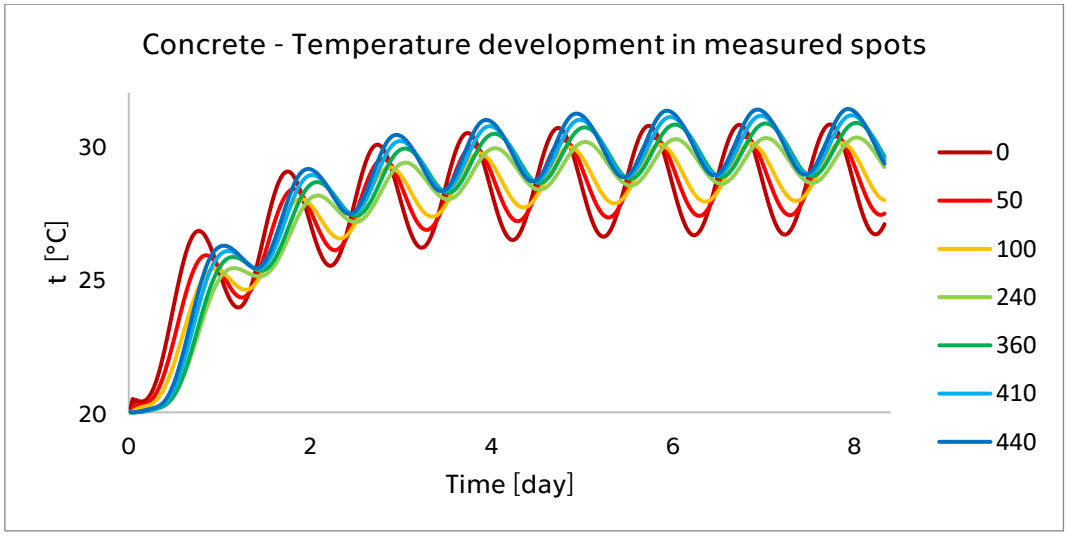


*Figure 105 Temperature development in sensor spots, bottom is represented by dark red line (0 > 0 mm from contact CETRIS-concrete), contact with pavement layers by dark blue line*

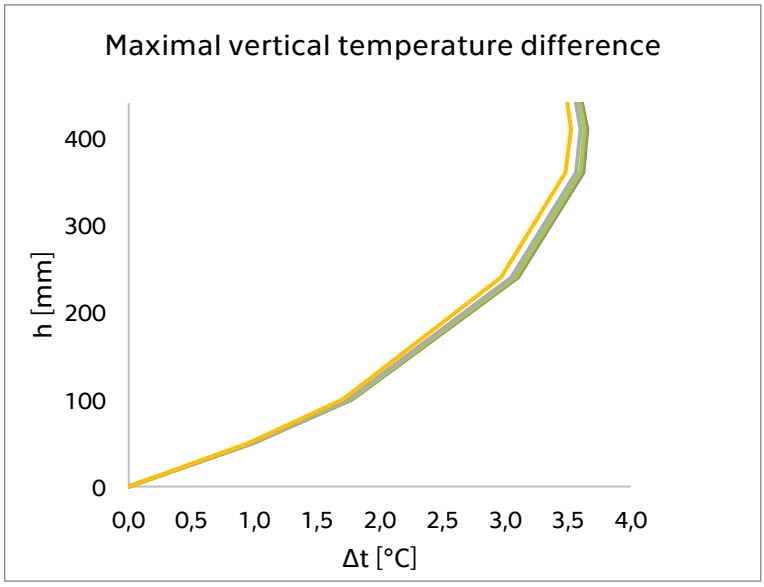


*Figure 106 Concrete - five maximal temperature vertical differences during loading period*

Temperature fluctuation in case of steel is typically higher, settlement occurs approximately in the same time as in concrete. Vertical temperature differences are also similar, they vary in small range. Effect of quick heating or cooling of bottom flange is nicely visible.

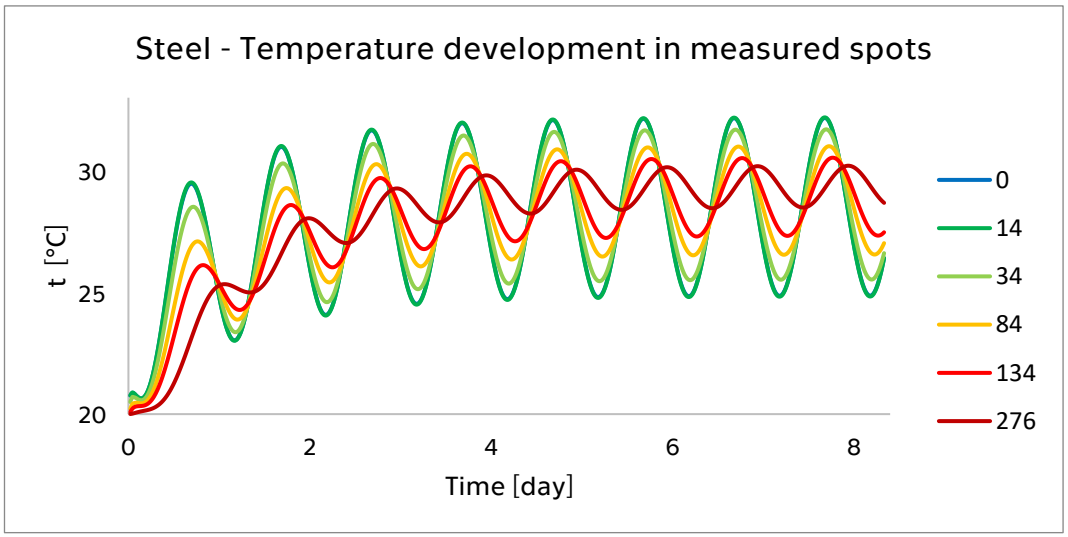


*Figure 107 Temperature development in sensor spots, bottom is represented by dark blue line (0 > 0 mm from bottom surface of steel), bottom surface of top flange by dark red line*

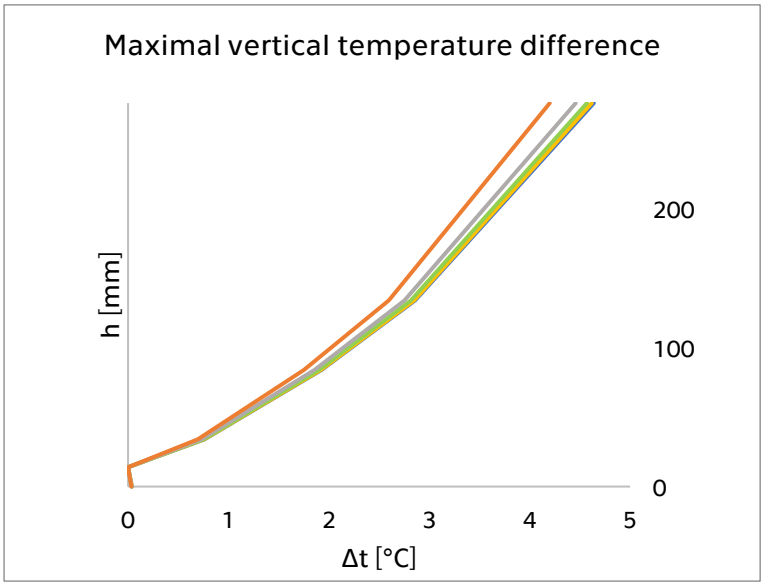


*Figure 108 Steel - five maximal temperature vertical differences during loading period*

### 6.4.4 Maximal temperature fluctuation

Finally, last evaluated model is representing spot under pavement in the weather situation replaced by model temperature development and glare. Both functions used for loading are taken over from previous models. Typical surface heating and cooling situations are shown in following figures.

$$t(t) = 13 \sin\left[\left(\frac{2\pi}{86400}\right) * (t - 9 * 3600)\right] + 13$$

$$Q(t) = 200 * \sin\left[0.85\left(\frac{2\pi}{86400}\right) * (int(t - 6 * 3600) mod 86400)\right]$$
$$* H\left\{\sin\left[0.85\left(\frac{2\pi}{86400}\right) * (int(t - 6 * 3600) mod 86400)\right]\right\}$$

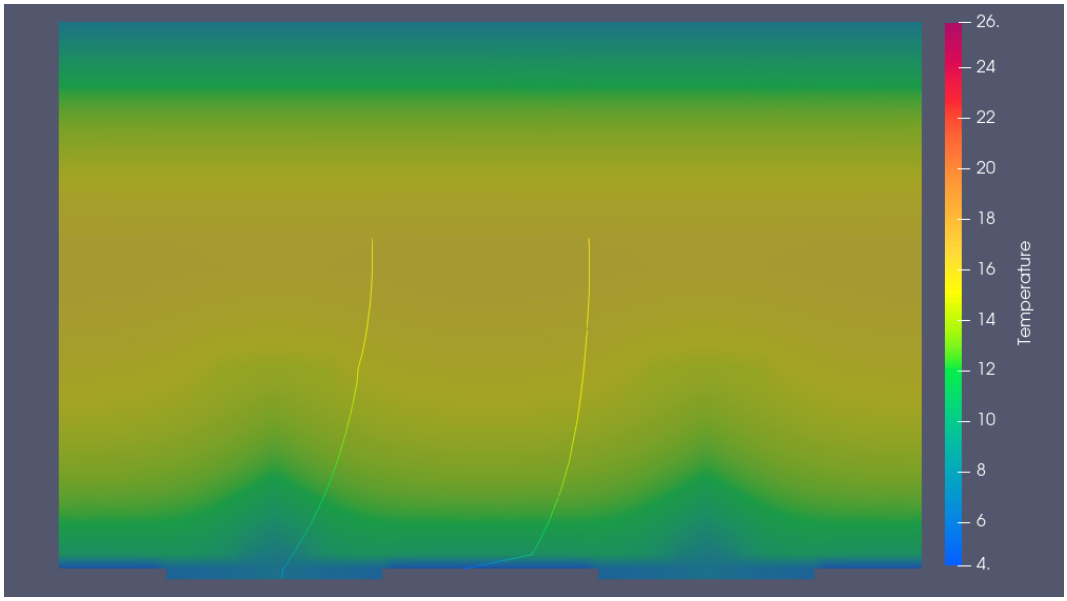


*Figure 109 Cooling of both surfaces during the night in t=75 h*

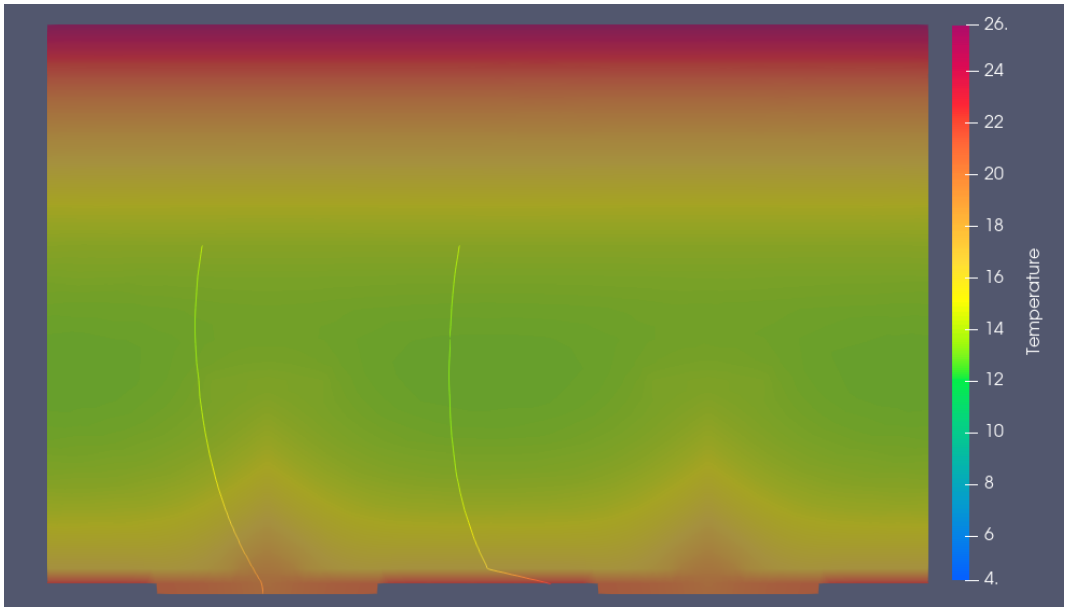


*Figure 110 Heating of both surfaces during the day in t=111 h*

Settlement of temperature fluctuation occurs after approximately 3,5-4 days, slightly sooner than in previous situation. This might be caused by more suitable initial condition. Vertical temperature differences are practically identic all over the second half of time period.

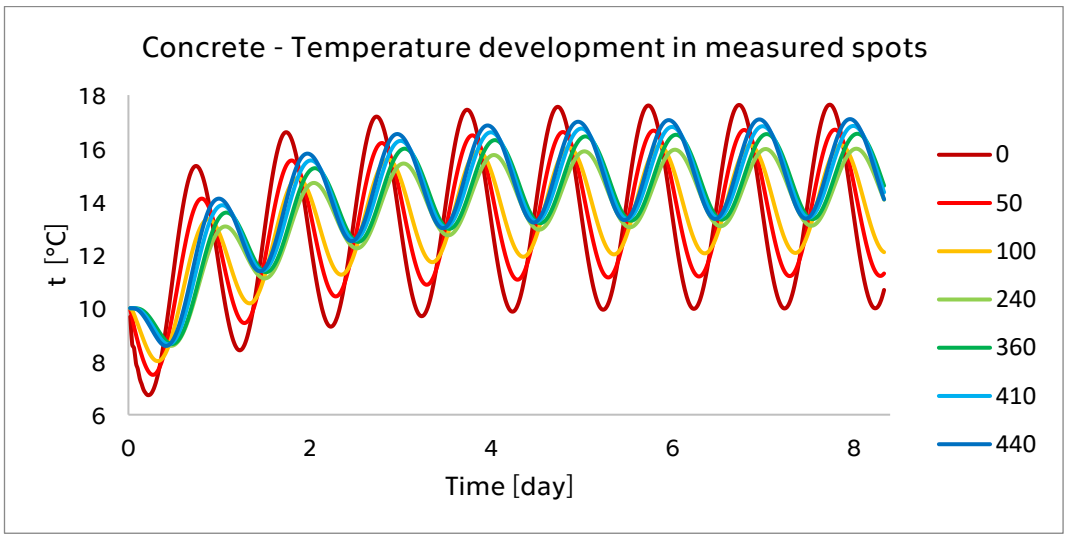


*Figure 111 Temperature development in sensor spots, bottom is represented by dark red line (0 > 0 mm from contact CETRIS-concrete), contact with pavement layers by dark blue line*

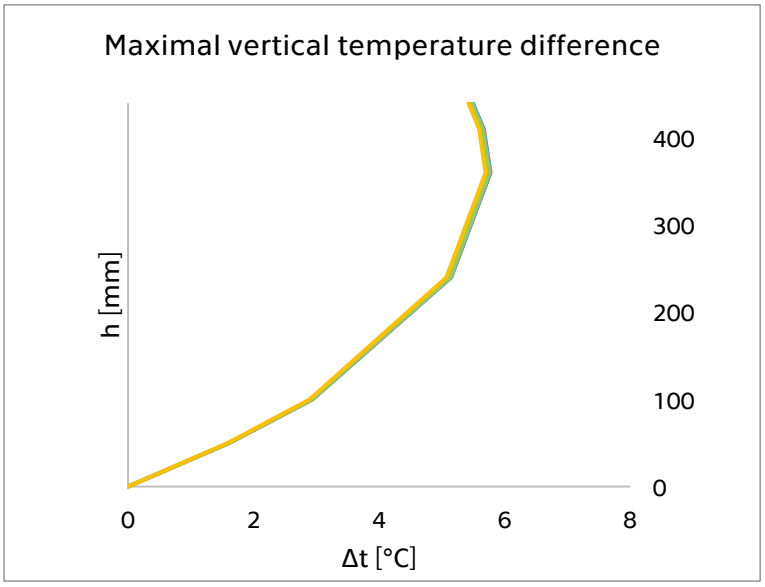


*Figure 112 Concrete - five maximal temperature vertical differences during loading period*

Situation in steel filler beam gets stable after about 3,5-4 days. Temperature fluctuation is specially in bottom spots dramatically higher, than in concrete. This is caused by higher heat conductivity and lower specific heat capacity of steel and absence of CETRIS plate, which is present in the bottom of concrete slab. Vertical temperature differences are very similar to each other and reach values up to 8 °C. This is an extreme situation for this model.

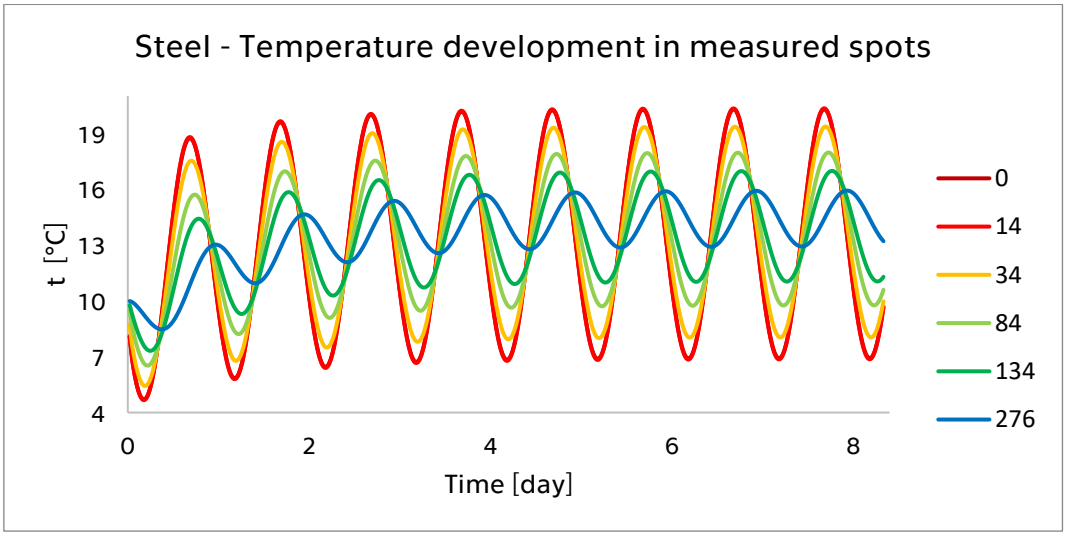


*Figure 113 Temperature development in sensor spots, bottom is represented by dark blue line (0 > 0 mm from bottom surface of steel), bottom surface of top flange by dark red line*

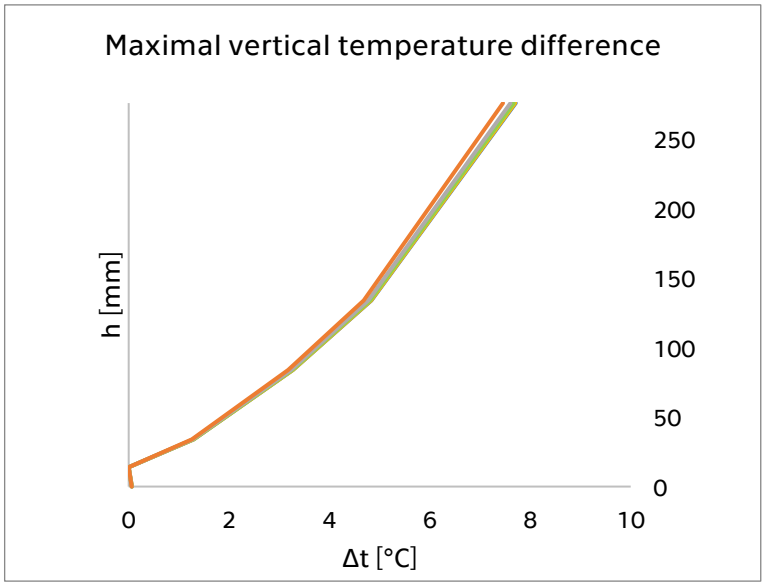


*Figure 114 Steel - five maximal temperature vertical differences during loading period*

## 6.5 Comparison of thermal effects on structure model

For purpose of illustration of standard shortcomings, simplified model of structure was created in SCIA Engineer (28). This model has been loaded by linear vertical components of temperature distribution. Comparison of effects caused by vertical components based on standard and on our thermal FEM models is shown.

Loading was based on previous data from heat transfer modelling. While the uniform temperature is not exceeding values given by standard, it was not used in the structural model. Only used values are linear vertical differences, which are easy to use and nicely shows differences between loading according to standard and heat transfer models.

Two modes of loading were used in each of two situations. First mode corresponds with standard and shows inner forces caused by thermal changes given in standard. Second mode is combination of results of thermal models and standard. In case of deck, values from standard are used, because they exceed values from thermal models. However, in case of abutment, values from thermal models are used, because they significantly exceed values from standard. Models loaded like this were computed and results were compared.

### 6.5.1 Model

While the purpose of model is neither structural design of the bridge in question, it was possible to significantly simplify geometry of bridge. Model consist of filler beam deck with variable height and filler beams and abutment shafts.

Bridge deck was modelled as ribbed slab, designed filler beams were used as ribs. Variable height and varying filler beams were modelled as several different slabs. Each slab used one profile of filler beam and had uniform height, representing average height in modelled part. Materials corresponded with project documentation. C35/45 was used for concrete part and S355 J2 for filler beams.

Abutment shaft was divided into two individual slabs. Both were of 600 mm thickness. Upper one of 200 mm height was rigidly allied with bridge deck. Second one of 2800 mm height was connected to the upper one through linear joint modelling concrete hinge. C30/37 class was used. Bottom line was rigidly supported (all 6 reactions). Outer sides of abutments were supported by elastic subsoil (Winkler-Pasternak's model). Stiffness was set to 10 $MNm^{-1}$.

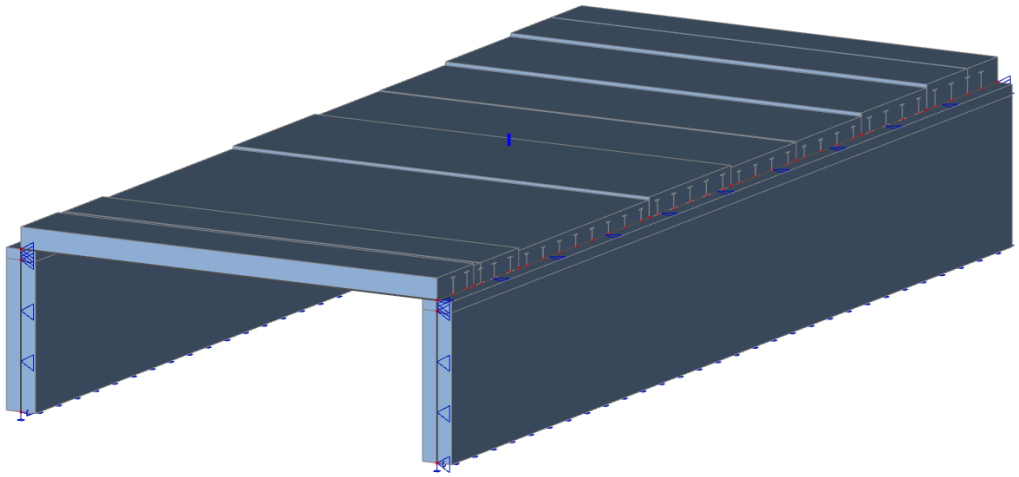

*Figure 115 Spatial view of model*

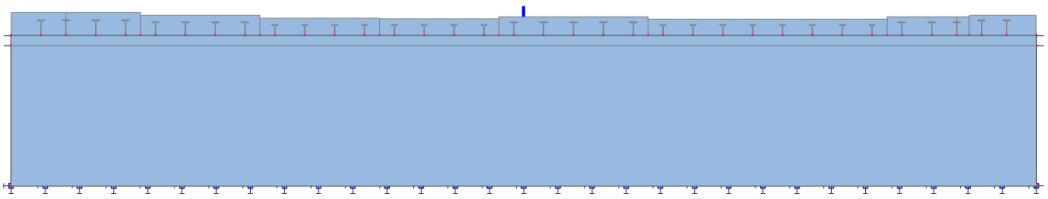

*Figure 116 Side view of model showing individual slabs with filler beams*

### 6.5.2 Heating

First evaluated situation was heating, two modes of loading were used. First mode is based on standard and uses values from first two charts in Figure 117. Second mode takes vertical difference for deck from standard and for abutment from FEM model.

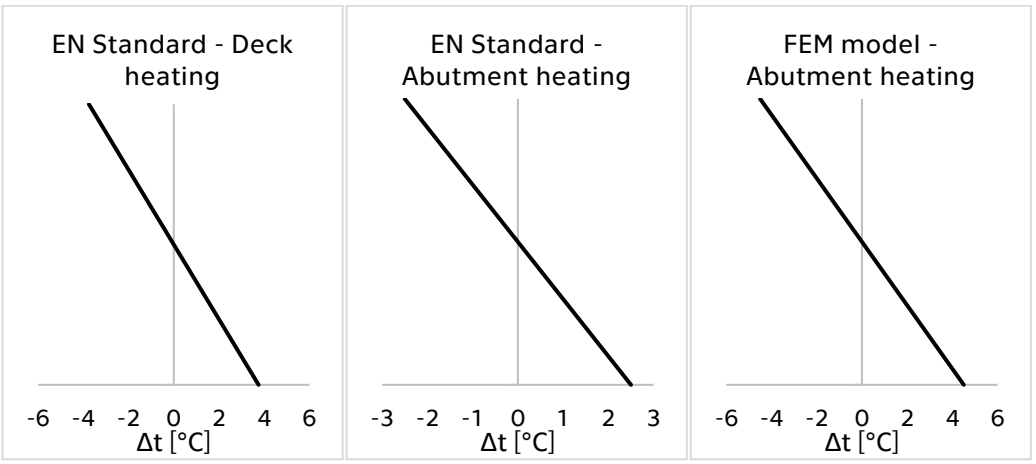


*Figure 117 Temperature profile used for loading*

Results from computation are shown in following figures, where significant differences might be seen. Bending moment on abutment shafts is shown, internal forces on filler beams are not shown, because internal forces in them are not reaching fundamental differences. As might be seen, if temperature difference from thermal models is used on abutments, bending moment in shafts is approximately 2,5 times higher, what represents fundamental difference. However, if all other loads are applied in combination, difference would be less important. Based on these facts, it is at least suitable to think about proper consideration of linear vertical temperature differences in design.

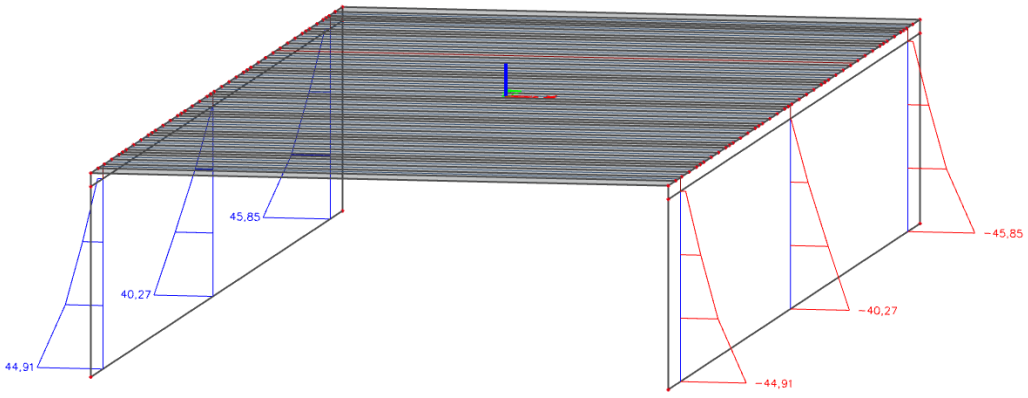


*Figure 118 Bending moments based on loading according to standard*

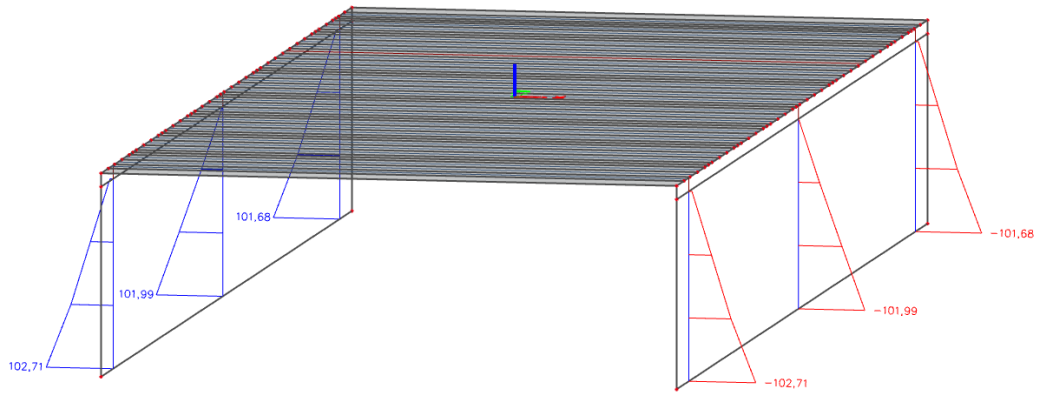


*Figure 119 Bending moments after loading by combination of standard and computed values. Significant difference might be seen.*

### 6.5.3 Cooling

Second evaluated situation was cooling, again, two modes of loading were used. First mode uses standard values from first two charts in Figure 120. Second mode takes vertical difference for deck from standard and for abutment from FEM models.

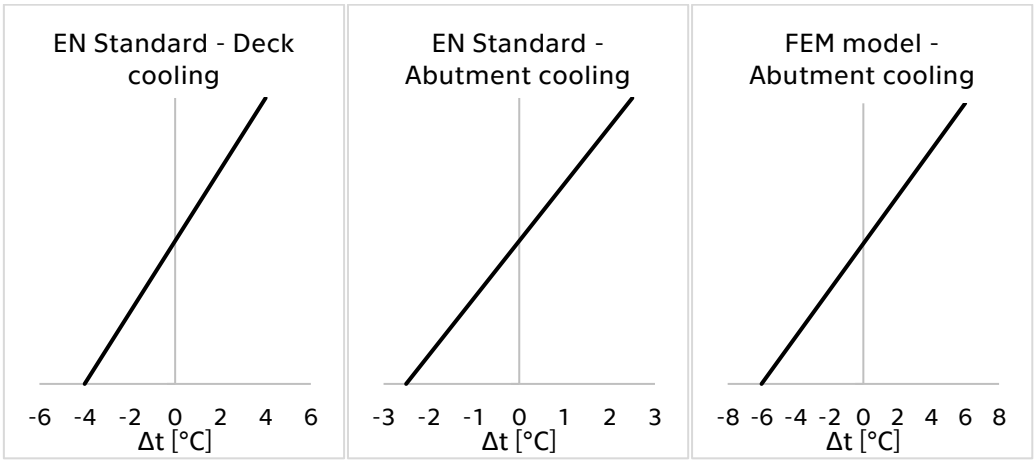


*Figure 120 Temperature profile used for loading*

Situation in this case is similar to previous, however reached differences between bending moments from two modes of loading are even higher. While the values in previous were approximately 2,5 times higher, in this case they are approximately 3,25 times higher. Again, influence of other loads in combinations has to be considered. However, this example confirms statement about suitability of proper model thermal loading from previous sub-chapter. Differences between bending moments are shown in following figures.

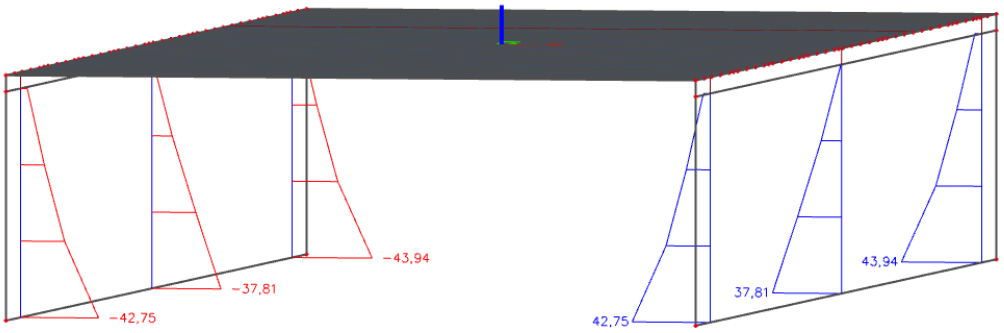


*Figure 121 Bending moments based on loading according to standard*

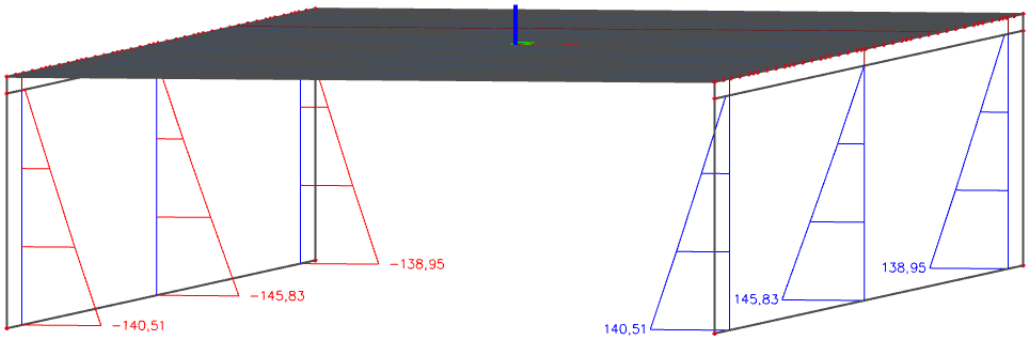


*Figure 122 Bending moments after loading by combination of standard and computed values. Significant difference between this and previous figure might be seen.*

# 7 Conclusion

During the last six months, stationary measurement system was designed, prepared and installed on the construction site of bridge No. 27-117 in Železná Ruda – Alžbětín. Commissioning of system will follow in the beginning of the year 2021.

Due to delay of start of system operation, heat transfer models of measured profiles were created and not yet validated. These models shew, what situations might be expected during measurement in real time. Other benefit of models was provision of data for assessment of thermal actions on abutments, which were used in simplified model of structure. This model served for illustration of differences in internal forces reached in abutment shafts.

Further work will be focused on commissioning of system and proper functionality of system. Measured data will be stored and evaluated. First evaluations might come after winter 2020/2021, when minimal temperatures will occur. For the maximal temperature, evaluation can come after summer of year 2021. In the case of maximal vertical temperature differences of measured profiles, this situation might occur during whole year according to possibly weather extremes. After one-year period of operation, which is ordered, measurement system will proceed for longer period of time.

Other continuation should be done in thermal FEM models, where would be suitable to split concrete into two parts according to used material for casing beams and concrete used in bridge structure. Changes would be suitable also in loading, where real reached temperature profiles should be modelled and implemented. Models adjusted in this way should be suitable for real verification of measured values in the examined profiles in bridge structure.

However, it is already possible to say today, that standard provides significantly insufficient values of thermal actions on piers and abutments. This statement is based on data obtained from thermal models. As was shown on the structure model, differences in inner forces of models loaded by standard and model values might be significant.

Proper binding of measurements in structures and computer models seems as ideal opportunity for verification or adjustment of expected thermal loads on bridge structures. It is not expected and even not necessary to change the European or national standard, however results of the monitoring could provide solid additional information for thermal loading of bridge structures and their further design.

# Literature

1. EN 1991-1-5. *Eurocode 1: Actions on Structures–Part 1-5: General Actions–Thermal Actions.* 2003.

2. ČSN EN 1991-1-5. *Eurokód 1: Zatížení konstrukcí - Část 1-5: Obecná zatížení - Zatížení teplotou.* Praha : ÚNMZ, 2005.

3. CHYTRÝ, Milan. Physical Geography of the Czech Republic. *Flora and Vegetation of the Czech Republic.* Cham : Springer, 2017.

4. CHMI. *Climate atlas of Czechia.* Prague : CHMI, 2007. 8086690261.

5. ČHMÚ. *Měsíční a roční data dle zákona 123/1998 Sb.* [Online] [Citace: 27. October 2020.] http://portal.chmi.cz/historicka-data/pocasi/mesicni-data/mesicni-data-dle-z.-123-1998-Sb#.

6. ŘSD ČR. *Projektová dokumentace mostu ev.č. 27-117*. Plzeň, 2019.

7. ŠAFÁŘ, Roman. *Betonové mosty 2: přednášky.* Praha : České vysoké učení technické, 2014.

8. Czech Geological Survey. *Geological map 1:25.000*. [Online] [Cited: 29 October 2020.] http://mapy.geology.cz/geocr_25/.

9. Thermometrics. *PT1000 Sensor.* [Online] Thermometrics Corporation. [Cited: 7 10 2020.] https://www.thermometricscorp.com/pt1000.

10. HTH8. MTR 12. *ODPOROVÝ SNÍMAČ TEPLOTY KABELOVÝ.* Polička, 2014.

11. REISSMANN Sensortechnik GmbH. *Product Information Pt100, Pt500, Pt1000*. [Online] [Cited: 7 10 2020.] https://m.reissmann.com/fileadmin/templates/_media/produkte/pdf/st_pt_100_en.pdf.

12. TECHNETEA. *Temperature measurement with a Pt100 (or Pt1000) sensor.* [Online] 12 4 2019. [Cited: 8 10 2020.] https://www.technetea.com/eng_PT100.html.

13. NACHAZEL, Ted. Michigan Scientific Corporation. *What is a Strain Gauge and How Does it Work?* [Online] 13 08 2020. [Cited: 14 10 2020.] https://www.michsci.com/what-is-a-strain-gauge/.

14. HBM GmbH. *Strain Gages and Accessories*. [Online] [Cited: 14 10 2020.] http://www.hbm.ru/pic/pdf/1176378299.pdf.

15. NATIONAL INSTRUMENTS CORP. *Measuring Strain with Strain Gages*. [Online] 15 July 2020. [Cited: 14 October 2020.] https://www.ni.com/cs-cz/innovations/white-papers/07/measuring-strain-with-strain-gages.html.

16. PLACIDI, Pisana, et al. Characterization of Low-Cost Capacitive Soil Moisture Sensors for IoT Networks. *sensors.* 2020.

17. SwitchDoc Labs. *Tutorial – Using Capacitive Soil Moisture Sensors on the Raspberry Pi.* [Online] 17 June 2020. [Cited: 15 October 2020.] https://www.switchdoc.com/2020/06/tutorial-capacitive-moisture-sensor-grove/.

18. NAJEEB, Mansoor Ani, AHMAD, Zubair and SHAKOOR, Rana A. Organic thin-film capacitive and resistive humidity sensors: a focus review. *Advanced Materials Interfaces.* 5.21: 1800969, 2018.

19. LEE, Chia-Yen and LEE, Gwo-Bin. Humidity sensors: a review. Sensor Letters. *Sensor Letters.* 3, 2005, Vols. 1-2, 1-15.

20. KOVALČÍKOVÁ, Hana. Vliv změn v pórové struktuře betonu na aktuální trvanlivost ŽB a předpjatých konstrukcí. *Diplomová práce.* Brno : VUT, 2012.

21. Vogtländisches Kabelwerk GmbH. *J-Y(St)Y Lg Eca. VOKA.* [Online] 2019. [Cited: 26 November 2020.] https://www.voka.de/cms/upload/3_produktkatalog_neu/1/366/pdf/jysty_lg_eca_de_web_1579519565.pdf.

22. BAŽANTOVÁ, Z., KOLÁŘ, K., KONVALINKA, P.,LITOŠ, J., REITERMAN, P. Multifunkční silikátový kompozit programovatelných vlastností nejen pro rychlé opravy cementobetonových konstrukcí. *iMateriály.* [Online] 1. June 2017. [Citace: 26. November 2020.] https://www.imaterialy.cz/rubriky/materialy/multifunkcni-silikatovy-

kompozit-programovatelnych-vlastnosti-nejen-pro-rychle-opravy-cementobetonovych-konstrukci__44766.html.

23. PATZÁK, B. *OOFEM - an object-oriented simulation tool for advanced modeling of materials and structures.* Acta Polytechnica 2012. 52(6):59–66.

24. RIBES, A., CAREMOLI, C. Salome platform component model for numerical simulation. *COMPSAC 07: Proceeding of the 31st Annual International Computer Software and Applications Conference.* Washington, DC : IEEE Computer Society, 2007.

25. Kitware. *ParaView*. [software], 2013. https://www.paraview.org/download/.

26. SLÁNSKÝ, B., a další. Opatření pro vyšší životnost CBK – výsledky pilotního projektu. *Sborník Betonové vozovky 2020.* p. 32-48, 2020, Sv. 1, ISBN 978-80-906541-5-0.

27. Engineering ToolBox. *Material Properties*. [Online] [Cited: 30 November 2020.] https://www.engineeringtoolbox.com/material-properties-t__24.html.

28. SCIA nv. *Scia Engineer 19.1.* [software], 2019. https://www.scia.net/cs/support/downloads.

29. PAJDUČÁK, Jaroslav. Rekonstrukce železničního mostu v Chomutově. *Bakalářská práce*. Praha : ČVUT, 2020.

30. ENGLAND, George L., TSANG, Neil CM and BUSH, David I. *Integral bridges: a fundamental approach to the time–temperature loading problem. s.l.* : Thomas Telford, 2000.

31. KELLENERS, T. J., et al. Calibration of capacitance probe sensors using electric circuit theory. *Soil Science Society of America Journal.* 68.2: 430-439, 2004.

# List of figures

Figure 1 Diagrammatic representation of constituent components of a temperature profile (1) ..... 4

Figure 2 Correlation between minimum/maximum shade air temperature ($T_{min}/T_{max}$) and minimum/maximum uniform bridge temperature component ($T_{e.min}/T_{e.max}$) (1) ..... 5

Figure 3 Temperature differences for bridge decks Type 1: Steel Decks (1) ..... 7

Figure 4 Temperature differences for bridge decks -Type 2: Composite Decks (1) ..... 8

Figure 5 Temperature differences for bridge decks -Type 3: Concrete Decks (1) ..... 8

Figure 6 Map of maximal shade temperature, which is exceeded by annual maximum with probability of 0,02 (2) ..... 10

Figure 7 Map of minimal shade air temperature, which is exceeded by annual minimum with probability of 0,02 (2) ..... 10

Figure 8 Location of bridge in Czech Republic (background map from www.freevectormaps.com/czech-republic/CZ-EPS-01-0003) ..... 11

Figure 9 Location of bridge in Železná Ruda (background map from www.openstreetmap.org) ..... 12

Figure 10 Großer Arber, 1456 m, from Bayerisch Eisenstein ..... 12

Figure 11 Annual mean air temperature in Czech Republic CHMI, Průměrná roční teplota vzduchu za období 1981-2010 [online]. [image]. [Accessed 27 October 2020]. Available from: http://portal.chmi.cz/files/portal/docs/meteo/ok/images/T8110.gif ..... 13

Figure 12 Side view from north (6) ..... 14

Figure 13 Cross-section of bridge deck (6) ..... 14

Figure 14 Bridge No. 27-117 under construction (picture: P. Švecová) ..... 15

Figure 15 Static scheme of integral bridge with concrete hinges with 1D elements ..... 15

Figure 16 Cross-section of sensor probe (10) ..... 16

Figure 17 2-wire configuration of PT 1000 sensor ..... 16

Figure 18 PT1000 Thermometer used in measurement system ..... 17

Figure 19 Scheme of resistive strain gauge parts. NATIONAL INSTRUMENTS, 2020, Resistance strain gauge [online]. [image]. 2020. [Accessed 14 October 2020]. Available from: https://ni.scene7.com/is/image/ni/Strain_Gauge_Diagram2?scl=1 ..... 18

Figure 20 Strain Gauge HBM LY11-10/120 ..... 19

Figure 21 Capacitive moisture sensor ..... 20

Figure 22 Resistive soil moisture sensor ..... 21

Figure 23 Position of measured spots in cross-section of bridge deck ..... 23

Figure 24 Horizontal position of measured spots in abutment ..... 23

Figure 25 Division of sensors in deck at spot under cornice, 7 sensors in concrete, 6 sensors on steel ..... 24

Figure 26 Division of sensors in deck at spot under traffic lane, 6 sensors in concrete, 7 sensors on steel ..... 24

Figure 27 Horizontal position of sensors in abutment shaft, all three spots are identic. Ambient air is in the top, concrete abutment shaft in mid and soil in the bottom of figure. ..... 25

Figure 28 Technique of sensor fixation and insulation from concrete used in bridge deck ..... 27

Figure 29 Technique of thermometers deployment into concrete slab ..... 28

Figure 30 Mounting of beam with thermometers into abutment shaft. On the left side is contact with the soil, on the right side contact with ambient air. . 29

Figure 31 Technique of strain gauges deployment. Strain gauges are stuck to plate of spreading rod, which is fastened to reinforcement rods. ..... 30

Figure 32 Humidity sensors deployment technique, branch box is fastened to filler beam ..... 30

Figure 33 Deployment of sensors in bridge structure marked in ground plan ..... 32

Figure 34 Deployment of sensors in bridge structure marked in cross-sections ..... 33

Figure 35 Solution of sensor connection with collecting cable ..... 34

Figure 36 Example of wire connection between sensors and collecting cable, placed in branch box. Red-black pairs of wires with orange marking are wires from sensors. ..... 34

Figure 37 Solution of thermometers connection to connecting cable in case of concrete casing beams ..... 35

Figure 38 Connection of thermometers monitoring temperature of beam into branch box ..... 35

Figure 39 Connection of moisture meters and strain gauges into branch box ..... 36

Figure 40 Schematic plan of cable routes ..... 36

Figure 41 Scheme of switchboard. Sensors on the right side, grey are thermometers, brown are strain gauges and violet are moisture meters ..... 38

Figure 42 Sketch of thermometer HPC shell ..... 39

Figure 43 Preparation of HPC thermometer shells (picture: J. Zatloukal) ..... 40

Figure 44 Finished thermometers suitable for insertion into casing beams (picture: J. Zatloukal) ..... 40

Figure 45 Example of designed reinforcement of casing beam ..... 41

Figure 46 Padded forms with prepared reinforcement (picture: J. Zatloukal) 41

Figure 47 Reinforcement with bound sensors (picture: J. Zatloukal) ..... 42

Figure 48 Casing beam ready for concreting, plastic ring protects wires and secures exhaustion position (picture: J. Zatloukal) ..... 42

Figure 49 Finished concrete beams after concreting and cavern filling (might be seen on central beam, as darker stain on edge in back) (picture: J. Zatloukal) ..... 43

Figure 50 Strain gauges on spreading rods. Making of protective cap on the left, hot glue framing works as formwork for epoxide. (picture: J. Zatloukal) . 44

Figure 51 Example of connection between sensor wires and collecting cable through conductive plate. Branch box filled with epoxide on the right side. 45

Figure 52 Connection of moisture meters into branch box (picture: J. Zatloukal) ..... 45

Figure 53 Beams ready for installation into structure (picture: J. Zatloukal) ... 45

Figure 54 Installed casing beam with thermometers in abutment shaft. Branch box is placed on the bottom side of beam. Cables are led along reinforcement rods. (picture: P. Švecová) ..... 46

Figure 55 Casing beam inserted into bridge deck (picture: J. Zatloukalová) .. 47

Figure 56 Bunch of thermometers on filler beam, covered by XPS insulation. Casing beam is behind the filler beam. (picture: J. Zatloukalová) ..... 47

Figure 57 Strain gauges on installed spreading rods (picture: J. Zatloukalová) ..... 48

Figure 58 Branch box attachment to filler beam. Probes of moisture meters are led out from branch box. (picture: J. Zatloukalová) ..... 48

Figure 59 Bridge No. 27-117 with installed switchboard box on the left abutment (picture: J. Zatloukal) ..... 49

Figure 60 Illustration of uniform temperature evaluation ..... 50

Figure 61 Possible extreme temperature profiles ..... 51

Figure 62 Example of maximal linear vertical temperature difference ..... 51

Figure 63 Example of humidity measurement development. Rising humidity value from resistive humidity meter might indicate rising content of ions. ... 52

Figure 64 Model of abutment shaft with quadrangle mesh, contact with ambient air on the top, contact with soil at the bottom of figure. Finest and mid-fine mesh represents layer of concrete and coarse mesh represents soil layer. ..... 55

Figure 65 Maximal vertical temperature difference reached at t=28 h ..... 56

Figure 66 Cooling of external edge, when ambient air temperature falls down in night, t=87h ..... 56

Figure 67 Temperature development in sensor spots, surface is represented by blue line (600 > 600 mm from contact soil-concrete), contact with soil by dark red line ..... 57

Figure 68 Five maximal temperature vertical differences during loading period ..... 57

Figure 69 Maximal vertical temperature difference occurs in t=16,5h ..... 58

Figure 70 Cooling of concrete surface in the night in t=171,5h ..... 58

Figure 71 Temperature development in sensor spots, surface is represented by dark red line (600 > 600 mm from contact soil-concrete), contact with soil by blue line ..... 59

Figure 72 Five maximal temperature vertical differences during loading period ..... 59

Figure 73 Maximal vertical temperature difference occurs in t=16,5h ..... 60

Figure 74 Surface cooling in t=171h ..... 60

Figure 75 Temperature development in sensor spots, surface is represented by dark red line (600 > 600 mm from contact soil-concrete), contact with soil by blue line ..... 61

Figure 76 Five maximal temperature vertical differences during loading period ..... 61

Figure 77 Model of spot in bridge deck under traffic lane with created mesh ..... 62

Figure 78 Maximal vertical temperature difference occurs in t=28h ..... 63

Figure 79 Heating of both surfaces in t=183 h ..... 64

Figure 80 Temperature development in sensor spots, bottom is represented by blue line (0 > 0 mm from contact CETRIS-concrete), contact with asphalt insulation by red line ..... 64

Figure 81 Concrete - five maximal temperature vertical differences during loading period ..... 65

Figure 82 Temperature development in sensor spots, bottom is represented by dark red line (0 > 0 mm from bottom surface of steel), bottom surface of top flange by dark blue line ..... 65

Figure 83 Steel - five maximal temperature vertical differences during loading period ..... 66

Figure 84 Cooling of both surfaces during the night in t=146,5 h ..... 67

Figure 85 Relatively balanced temperature both in steel and concrete in t=67,5 h ..... 67

Figure 86 Temperature development in sensor spots, bottom is represented by blue line (0 > 0 mm from contact CETRIS-concrete), contact with asphalt insulation by red line ..... 67

Figure 87 Concrete - five maximal temperature vertical differences during loading period ..... 68

Figure 88 Temperature development in sensor spots, bottom is represented by dark red line (0 > 0 mm from bottom surface of steel), bottom surface of top flange by dark blue line ..... 68

Figure 89 Steel - five maximal temperature vertical differences during loading period ..... 69

Figure 90 Cooling of both surfaces during the night in t=170,5 h ..... 69

Figure 91 Heating of both surfaces with significant effect of glare in t=65,5 h ....70

Figure 92 Temperature development in sensor spots, bottom is represented by blue line (0 > 0 mm from contact CETRIS-concrete), contact with asphalt insulation by red line ....70

Figure 93 Concrete - five maximal temperature vertical differences during loading period ....71

Figure 94 Temperature development in sensor spots, bottom is represented by dark red line (0 > 0 mm from bottom surface of steel), bottom surface of top flange by dark blue line ....71

Figure 95 Steel - five maximal temperature vertical differences during loading period ....72

Figure 96 Model of spot in bridge deck under pavement with created mesh 73

Figure 97 Cooling of both surfaces during the night in t=75,5 h ....74

Figure 98 Heating of both surfaces during the day in t=134,5 h ....74

Figure 99 Temperature development in sensor spots, bottom is represented by blue line (0 > 0 mm from contact CETRIS-concrete), contact with pavement layers by red line ....75

Figure 100 Concrete - five maximal temperature vertical differences during loading period ....75

Figure 101 Temperature development in sensor spots, bottom is represented by dark red line (0 > 0 mm from bottom surface of steel), bottom surface of top flange by dark blue line ....76

Figure 102 Steel - five maximal temperature vertical differences during loading period ....76

Figure 103 Cooling of both surfaces during the night in t=171,5 h ....77

Figure 104 Heating of both surfaces during the day in t=136 h ....78

Figure 105 Temperature development in sensor spots, bottom is represented by dark red line (0 > 0 mm from contact CETRIS-concrete), contact with pavement layers by dark blue line ....78

Figure 106 Concrete - five maximal temperature vertical differences during loading period ....79

Figure 107 Temperature development in sensor spots, bottom is represented by dark blue line (0 > 0 mm from bottom surface of steel), bottom surface of top flange by dark red line ....79

Figure 108 Steel - five maximal temperature vertical differences during loading period ....80

Figure 109 Cooling of both surfaces during the night in t=75 h ....80

Figure 110 Heating of both surfaces during the day in t=111 h ....81

Figure 111 Temperature development in sensor spots, bottom is represented by dark red line (0 > 0 mm from contact CETRIS-concrete), contact with pavement layers by dark blue line ....81

Figure 112 Concrete - five maximal temperature vertical differences during loading period....82

Figure 113 Temperature development in sensor spots, bottom is represented by dark blue line (0 > 0 mm from bottom surface of steel), bottom surface of top flange by dark red line....82

Figure 114 Steel - five maximal temperature vertical differences during loading period....83

Figure 115 Spatial view of model....84

Figure 116 Side view of model showing individual slabs with filler beams....84

Figure 117 Temperature profile used for loading....85

Figure 118 Bending moments based on loading according to standard....85

Figure 119 Bending moments after loading by combination of standard and computed values. Significant difference might be seen....86

Figure 120 Temperature profile used for loading....86

Figure 121 Bending moments based on loading according to standard....87

Figure 122 Bending moments after loading by combination of standard and computed values. Significant difference between this and previous figure might be seen....87

# List of charts

Table 1 Recommended values of linear temperature difference component for different types of bridge decks for road, foot and railway bridges (1)....6

Table 2 Recommended values of $k_{sur}$ to account for different surfacing thickness (1)....7

Table 3 Additional resistance $R_{add}$ for all bunches of sensors....37

Table 4 Measured and used average parameters of concrete used in casing beams....54